2016

Estimation Of The Quantum Effects Of Nuclei in Large Molecular Systems

Bing Gu
University of South Carolina

Estimation of the quantum effects of nuclei in large molecular systems

by

Bing Gu

Bachelor of Science
University of Science and Technology of China 2011

Submitted in Partial Fulfillment of the Requirements

for the Degree of Doctor of Philosophy in

Chemistry

College of Arts and Sciences

University of South Carolina

2016

Accepted by:

Sophya Garashchuk, Major Professor

Vitaly Rassolov, Committee Member

Qi Wang, Committee Member

John Lavigne, Committe Member

Lacy Ford, Senior Vice Provost and Dean of Graduate Studies

Acknowledgments

I am very grateful to my Ph.D. advisor Prof. Sophya Garashchuk for the privilege of dong research in her group for the past five years. No achievements is possible without her expertise in the field of theoretical chemistry and patience while teaching me the necessary knowledge to solve scientific problems. It is not just the knowledge that she teaches me that is important to me, what is more important is the right way to think while facing a challenge.

I would like to thank Prof. Vitaly Rassolov for many constructive discussions on various topics including chemistry, physics and especially quantum chemistry computation. His advice is always valuable and always gives me new ideas to solve problems. Thanks to my group members Dr. James Mazzuca, Dr. Lei Wang, Dr. David Dell'Angelo, Bryan Nichols and Dr. Brett Cagg for all the discussions and advices. I would like to thank my parents for the encouragement and support.

Finally, a special thanks to my friend Dr. Xiaohong Wang, her encouragement is instrumental to the completion of this work.

Abstract

Chemical dynamics, in principle, should be understood by solving the time-dependent Schrödinger equation for a molecular system, describing motion of the nuclei and electrons. However, the computational efforts to solve this partial second-order differential equation scales exponentially with the system size, which prevents us from getting exact numerical solutions for systems larger than 4-5 atoms. Thus, approximations simplifying the picture are necessary. The so-called Born-Oppenheimer approximation, separating motion of the electrons and nuclei is the central one: solution to the electronic Schrödinger equation defines the potential energy surface on which the nuclear motion unfolds, and there are standard quantum chemistry software packages for solving the electronic Schrödinger equation. For the nuclear Schrödinger equation, however, there are no widely applicable quantum-mechanical approaches, and most simulations are performed using classical Newtonian mechanics which is often adequate due to large nuclear masses. However, the nuclear quantum effects are significant for chemical processes involving light nuclei at low energies, and including these effects into simulation, even approximately, is highly desirable. In this dissertation, an approximate methodology of including quantum-mechanical effects within the quantum trajectory or the de Broglie-Bohm formulation of the Schrödinger equations is developed. Use of the trajectory framework makes the approach scalable to hundreds of degrees of freedom. The methodology is applied to study high-dimensional systems (solid He4 and others) relevant to chemistry.

Table of Contents

List of Tables

List of Figures

Chapter 1

Introduction

Since the discovery of quantum mechanics, chemical dynamics, in principle, can be understood by solving the time-dependent Schrödinger equation (SE) for any quantum system, which involves motion of the nuclei and electrons. However, the computational efforts to solve the equation scales exponentially with the system size, which prevents us from getting exact numerical solutions for all but simplest systems. Theoretical chemists are searching for approximations to help simplify the picture. The most basic approximation, called the Born-Oppenheimer approximation, assumes that the total wavefunction can be written as a product of the electronic wavefunction parametrically dependent on the nuclear position, and the nuclear wavefunction.

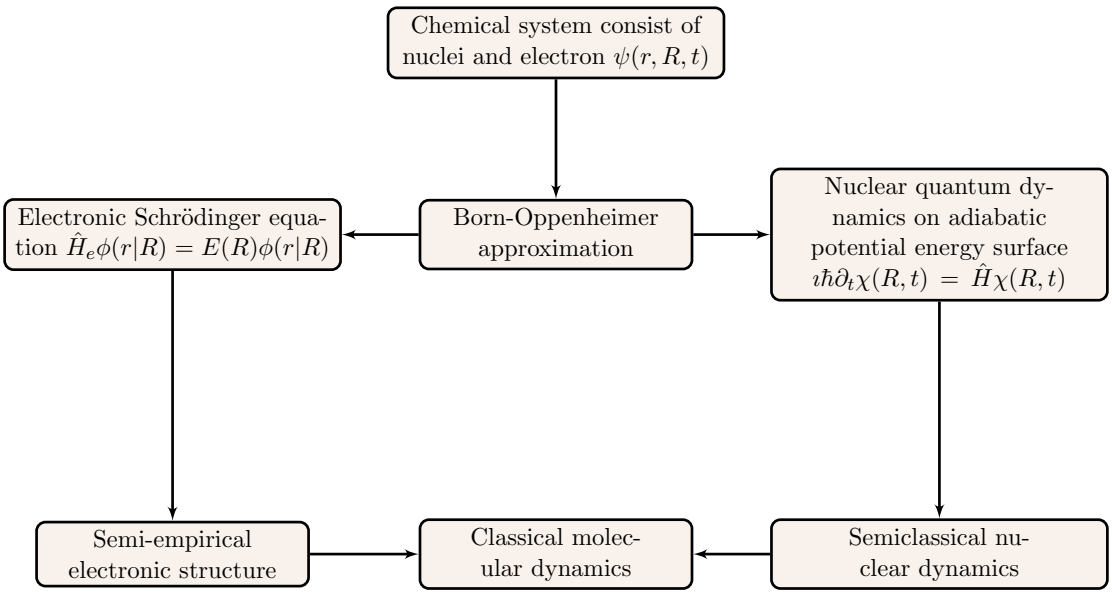

Figure 1.1: Scheme for molecular quantum dynamics

Such an approximation greatly simplifies the whole dynamic picture ignoring the "dynamic" correlation between the nuclei and electrons. Electronically non-adiabatic and electron dynamics are reviewed here [86] and are not discussed in this thesis.

The electronic SE serves as a background for the nuclear wavefunction, by providing the potential energy surface (PES). There are standard quantum chemistry software packages such as *QChem* [83], for solving the electronic Schrödinger equation using wavefunction methods or density functional theory. For the nuclear SE, there are no standard widely applicable QM tools. Due to the heavy mass of nuclei, the classical limit of the TDSE is often useful, yielding the Newtonian mechanics of the nuclei. Each nuclear configuration is represented by a classical trajectory evolving on the PES.

The Born-Oppenheimer approximation and classical treatment of constitute nuclei make the molecular dynamics method. Fig. 1.1 gives a schematic view of the approximations mentioned above.

In most cases, molecular dynamics simulations are adequate for experimentally relevant quantities. However, there are experimental results where quantum-mechanical effects of nuclear motion are important, and they cannot be reproduced using classical trajectories. QM effects in molecular dynamics, including zero-point energy, tunneling effects, non-adiabatic effects are often needed for accurate description of reactions in complex systems, such as biological environments, liquids, materials and photochemistry. For example, Schreiner reported a tunneling controlled reaction of methylhydroxycarbene in 2011 [80]. The reaction has two reaction pathways, one with a lower energy barrier but large barrier width, the other with a higher but thiner barrier. The reaction is dominated by the latter reaction pathway revealing that the tunneling effects may define the reactivity at low temperature, because the tunneling rate is very sensitive to the width of the energy barrier. Another example of nuclear quantum effects comes from water and aqueous systems due to the large zero

point energy (ZPE) contained in the O-H bond. The ZPE is the energy difference between the ground state energy and the minimum of the potential. Ref. [15] gives a comprehensive review the current status of including nuclear quantum effects in the simulation of water systems. Analysis of Bowman and coworkers [19]' simulation for a water dimer based on quasi-classical trajectories clearly showed the problem of the so-called zero-point energy leakage (ZPEL). The ZPEL is associated with incorrect energy flow of high-frequency intramolecular vibration to the low-frequency intermolecular vibration; initially the correct quantized energy drops below the ZPE value and leaks into the reactive motion of monomers. ZPEL dissociates the dimer which is incorrect and does not happen in QM. To include the QM effects into reactive dynamics we have to solve TDSE for the nuclei. Due to exponential scaling of the exact quantum dynamics, further approximations (semiclassical [39] and quasi-classical methods [70]) are required to treat large molecular systems (of more than 4-5 atoms).

The Approximate Quantum Potential (AQP) method developed in our group gives a cheap way of incorporation QM effects of nuclei into trajectory dynamics. The method is based on the de Broglie-Bohm formulation of quantum mechanics, where the wavefunction is represented by an ensemble of quantum trajectories.

The equations of motion for quantum trajectories differ from classical trajectories by an extra potential, the so-called quantum potential. This quantum potential produces all quantum effects in the trajectory framework, but is difficult to compute exactly. Thus various approximations have been developed in our group. Chapter 2 introduces the basics of the theory and numerical implementations, used to simulate a chemical reaction, including the approximate quantum potential method which is at the core of the following chapters. The time-dependent Schrödinger equation describes the evolution of a pure quantum state. In reality, most quantum systems are in contact with an environment or bath, manifested as dissipation and fluctuation

effects on the dynamics of the system that we are interested in.

To describe the energy dissipation, phenomenological friction is introduced into the QT framework, which can be used to describe the irreversible energy flow from the system to the bath. Moreover, dynamics with friction is an efficient method to obtain the ground-state, which is often the dominant QM effect, of a large quantum system. Chapter 3 gives a detailed description of the method and applications to model systems and atomic solids, specifically solid He.

For the simulation of atomic solids, we did not take the quantum statistics into account. In rigorous quantum description, the wavefunction of solid helium-4 has to satisfy the exchange symmetry. For electronic calculation, such condition is fulfilled by the use of Slater determinant, constructed out of simple particle functions. The same approach is not appropriate for nuclear system with large inter-particle correlation. Thus we developed an approximate method to estimate the exchange effects from a non-symmetric wavefunction. The method, which is based on the quantum trajectory method, is described in Chapter 5 and results for some model systems is given.

Though the quantum trajectory method gives us a convenient way to simulate quantum dynamics, there are still challenges associated with approximations for the quantum potential. The most notorious one is the singularity of the quantum potential, when interference is present. For problems where interference effects is important, a method based on basis function is often more convenient. For such purpose, we describe a method which combines the advantages of the trajectory representation and basis representation, which is called the quantum trajectory Gaussian bases (QTGB). The essence of the method is that a superposition of Gaussian wavepackets (GWP) is used to represent the wavefunction and the centers of the GWPs is guided by the quantum trajectory.

Chapter 6 will give a detailed description of the method in the content of other

Gaussian-basis methods. Chapter 8 concludes.

Chapter 2

Theory of quantum molecular dynamics

2.1 Born-Oppenhermer approximation

In principle, the behavior of electrons and nuclei can be completely understood by solving time-dependent Schrödinger equation (TDSE) ,

$$\imath\hbar\frac{\partial}{\partial t}\Psi(\boldsymbol{r},\boldsymbol{R},t)=\hat{H}\Psi(\boldsymbol{r},\boldsymbol{R},t), \tag{2.1}$$

where the Hamiltonian operator can be written as

$$H=T_e+T_N+V_e+V_N+V_{eN}.$$

T_e and T_N are the kinetic energy operator for electrons and nuclei, V_e represents the Coulomb interaction between electrons and V_N interaction for nuclei. V_{Ne} is the interaction between nuclei and electrons. Under Born-Oppenheimer (BO) approximation, the total wavefunction is written as a product form

$$\Psi(\boldsymbol{r},\boldsymbol{R},t)=\phi(\boldsymbol{r}|\boldsymbol{R})\psi(\boldsymbol{R},t)$$

where we use $\boldsymbol{r}$ for electronic coordinates and $\boldsymbol{R}$ for nuclei.

Substitute into the TDSE, we obtain

$$\imath\hbar\partial_t\psi(\boldsymbol{R},t)\phi(\boldsymbol{r}|\boldsymbol{R})=(T_N+V_N+H_e)\phi(\boldsymbol{r}|\boldsymbol{R})\chi(\boldsymbol{R},t) \tag{2.2}$$

For simplicity, assume there is only one nuclear degree of freedom (DOF), the kinetic energy is written as

$$T_N=-\frac{\hbar^2}{2M}\nabla_R^2,$$

put into the last equation we obtain,

$$\begin{aligned}\imath\hbar\partial_t\psi(\boldsymbol{R},t)\phi(\boldsymbol{r}|R) =&(T_N\phi(\boldsymbol{r}|R))\psi(R,t) + \phi(\boldsymbol{r}|R)T_N\psi(R,t) + H_e\phi(\boldsymbol{r}|R)\psi(R,t)\\ &- \frac{\hbar^2}{M}\nabla_R\phi(\boldsymbol{r}|R)\nabla_R\psi(R,t)\end{aligned} \tag{2.3}$$

Multiply both sides by $\phi(\boldsymbol{r}|R)$ and integration over electronic coordinates, we obtain

$$\imath\hbar\partial_t\psi(R,t) = D^{(1)}(R,t) + D^{(2)}(R,t) + (T_N + V_N)\psi(R,t) + E_n(R)\psi(R,t) \tag{2.4}$$

where $U(R) = \langle\phi(\boldsymbol{r}|R)|H_e|\phi(\boldsymbol{r}|R)\rangle$ and

$$D^{(1)}(R,t) = \langle\phi|\frac{-\hbar^2}{M}\nabla_R|\phi\rangle\,\nabla_R\chi(R,t) \tag{2.5}$$

$$D^{(2)}(R,t) = \langle\phi|\frac{-\hbar^2}{2M}\nabla_R^2|\phi\rangle\,\chi(R,t) \tag{2.6}$$

Due to the nuclei are much heavier than electrons and the electronic transition requires much energy than normal temperature, it is reasonable to assume the electrons always stay in the ground electronic state $n = 0$ for particular nuclear configuration R, i.e.

$$H_e\phi(r|R) = E_0(R)\phi(r|R).$$

$D^{(1)}(R,t)$ and $D^{(2)}(R,t)$ are so-called *non-adiabatic coupling* terms, which can be ignored for most applications. If we ignore the non-adiabatic coupling, we obtain the nuclear Schrödinger equation

$$\imath\hbar\partial_t\psi(R,t) = (T_N + V_N + E_0(R))\psi(R,t) \equiv (T_N + U(R))\psi(R,t).$$

$U(R)$ is the ground potential energy surface (PES), consist of the electronic energy and nuclear repulsion.

There are standard quantum chemistry packages that can be used to solve the electronic Schrödinger equation . There are also standard numerical methods to solve the nuclear Schrödinger equation , but suffers from the problem that the numerical

cost scales exponentially with system size. Thus exact methods is limited to systems consist of few particles.

Theoretical studies of chemical dynamics are typically based on classical trajectories that represent moving nuclei, since the cost of conventional quantum propagation methods scales exponentially with the number of degree of freedoms. In most cases, the classical trajectory results are often adequate for experimentally relevant quantities.

Nevertheless, quantum mechanical (QM) effects in molecular dynamics, including zero-point energy, tunneling effects, non-adiabatic effects are often needed for accurate description of reactions in complex systems, such as biological environments, liquids, materials and photochemistry.

The Approximate Quantum Potential (AQP) Methodology developed in our group gives a cheap way of incorporation QM effects into trajectory dynamics and we will introduce it in following sections.

Several theoretical methods (quantum, semiclassical and classical) is introduced in this chapter. And also a formal theoretical development of the approximate quantum potential (AQP) method developed by our group is given.

Split-operator method

The most direct way to molecular quantum dynamics is to solve the time-dependent Schrödinger equation for the nuclear motion.

$$\imath\hbar\partial_t\psi(x,t) = \hat{H}\psi(x,t), \quad \hat{H} = \frac{1}{2}\boldsymbol{p}^T\mathbf{M}^{-1}\boldsymbol{p} + V(\boldsymbol{x}), \tag{2.7}$$

where $\boldsymbol{x}, \boldsymbol{p}$ are the position and momentum operators and $\mathbf{M} = diag\{m_1, m_2, \cdots\}$ is the inverse mass matrix.

The wavefunction is a complex-valued function of spacial coordinates and time, which can be represented in a convenient basis. Commonly, a set of finite basis

representation (FBR) can be used, this FBR can be transformed into an alternative discrete variable representation (DVR) through a unitary transformation, where the potential energy operator is conveniently represented by a diagonal matrix.

An exact numerical solution of quantum mechanics using this idea is called split operator method (SPO) [59, 60]. The SPO method takes advantage of the ease of treating operators in their diagonal representations. The time dependent Schrödinger equation (5.1) has the formal solution

$$\psi(t) = \hat{U}(t)\psi(0) = \exp\left(-\frac{\imath}{\hbar}\int_0^t \hat{H}(t')dt'\right)\psi(0), \tag{2.8}$$

The total evolution operator is broken into small increments of duration Δt.

$$U(t) = \prod_{n=0}^{N-1} \hat{U}((n+1)\Delta t, n\Delta t), \quad \Delta t = t/N, \tag{2.9}$$

where

$$\hat{U}(t+\Delta t, t) = \exp\left(-\frac{\imath}{\hbar}\hat{H}(t)\Delta t\right). \tag{2.10}$$

The short time propagator, $\hat{U}(\Delta t)$ can be approximated by

$$\begin{aligned}\hat{U}(\Delta t) &= \exp\left(-\frac{\imath}{\hbar}\hat{H}\Delta t\right) \\ &\approx \exp\left(-\frac{\imath}{2\hbar}\hat{K}\Delta t\right)\exp\left(-\frac{\imath}{\hbar}\hat{V}\Delta t\right)\exp\left(-\frac{\imath}{2\hbar}\hat{K}\Delta t\right) + O(\Delta t^3).\end{aligned} \tag{2.11}$$

The kinetic energy operator $\hat{K} = \hat{P}^2/2m$ is diagonal in momentum space, and the potential energy $\hat{V}$ is diagonal in coordinate space. The fast Fourier transform algorithm provides an accurate and fast unitary transformation between the two representations.

2.2 The de Broglie-Bohm formulation of TDSE

The exact numerical solution of TDSE suffers from the exponential scaling with system size, thus it is not applicable for large molecular system. Many approximate methods are developed to treat this problem and they can be mostly classified based

on the formulation of quantum mechanics they are developed. Semiclassical methods are commonly based on Feynman's path-integral formulation and parameterized wavefunction methods are usually developed directly from Schrödinger equation with time-dependent variational principle. Gaussian wavepacket is frequently employed in the latter class of methods.

The approximate quantum potential (AQP) method is based on the de Broglie-Bohm theory [7, 8]. The time-dependent Schrödinger equation (TDSE) of wavefunction has been the cornerstone of modern quantum chemistry,

$$\hat{H}\psi(\boldsymbol{x},t) = \imath\hbar\frac{\partial\psi(\boldsymbol{x},t)}{\partial t}. \tag{2.12}$$

where $\boldsymbol{x}$ is a vector of positions for all degrees of freedom.

In de Broglie-Bohm theory, the wavefunction is represented in polar form with the amplitude $A(\boldsymbol{x},t)$ and phase $S(\boldsymbol{x},t)$, which are both real functions of $\boldsymbol{x}$ and t,

$$\psi(\boldsymbol{x},t) = A(\boldsymbol{x},t)\exp\left(\frac{\imath}{\hbar}S(\boldsymbol{x},t)\right). \tag{2.13}$$

Substituting Eq. (6.10) into TDSE, one obtains

$$\frac{\partial S(x,t)}{\partial t} = \frac{\nabla S(x,t)^2}{2m} - V(x) - U(x,t), \tag{2.14}$$

$$\frac{\partial A^2(x,t)}{\partial t} = -\frac{\partial}{\partial x}\left[A^2(x,t)\cdot\frac{1}{m}\frac{\partial S(x,t)}{\partial x}\right], \tag{2.15}$$

$$\tag{2.16}$$

where

$$U(\boldsymbol{x},t) = -\frac{\hbar^2}{2m}\frac{\nabla^2 A(\boldsymbol{x},t)}{A(\boldsymbol{x},t)}.. \tag{2.17}$$

U is non-local time-dependent quantum potential, and is proportional to $\hbar^2$. It is important to note that the polar form is not useful at nodes, where $\psi = 0$. The phase is well-defined for times before and after the node passes over a fixed point in space, not at the instant that the node crosses the point. The probability density is

$$\rho(\boldsymbol{x},t) = \psi^*(\boldsymbol{x},t)\psi(\boldsymbol{x},t) = A^2(\boldsymbol{x},t). \tag{2.18}$$

The probability flux associated with $\psi(\boldsymbol{x}, t)$ is given by (assuming each DOF has the same mass m)

$$j_\mu(\boldsymbol{x}, t) = \frac{\hbar}{2mi} \left(\psi^*(\boldsymbol{x}, t)\nabla_\mu\psi(\boldsymbol{x}, t) - \psi(x, t)\nabla_\mu\psi^*(x, t)\right). \tag{2.19}$$

This quantity gives the rate at which probability flows past a fixed point. if we insert the polar form of the wave function into equation 2.19, we get the flux in terms of the density and the derivative of the action

$$j_\mu(\boldsymbol{x}, t) = \rho(\boldsymbol{x}, t) \cdot \frac{1}{m}\nabla_\mu S(x, t). \tag{2.20}$$

In classical fluid flow, the flux is given by $j_\mu = \rho(\boldsymbol{x}, t)v_\mu(\boldsymbol{x}, t)$, where $v_\mu(x, t)$ is the flow velocity of the fluid in μ direction and $\rho(\boldsymbol{x}, t)$ is the density of fluids.

In equation 2.19, we will make this association and refer to the flow velocity of the probability fluid as the function [63]

$$\boldsymbol{v} = \frac{1}{m}\boldsymbol{\nabla} S. \tag{2.21}$$

We have dropped the position and temporal dependence in the notation.

Returning to equation 2.15, the term in brackets in the right side is just the probability flux, thus, we finally obtain the standard form of the continuity equation

$$\frac{\partial\rho(x, t)}{\partial t} = -\boldsymbol{\nabla} \cdot \boldsymbol{j} = -\boldsymbol{\nabla}(\rho\boldsymbol{v}). \tag{2.22}$$

Equation 6.12 is the Eulerian version of the *quantum Hamiltion-Jacobi equation.* The wavefunction can be discretized in coordinate space by quantum trajectories (QTs) with position $\boldsymbol{x}$ and momentum $\boldsymbol{p}$,

$$\boldsymbol{p} = \nabla S. \tag{2.23}$$

When $\hbar \to 0$, U becomes negligible and all of the trajectories become independent of each other, which is the case of classical trajectories. The quantum potential U

can be considered as a nonclassical contribution to the kinetic energy. For numerical implementation, trajectories form an ensemble, representing the wavefunction, are assigned certain weights w_i, that depend on the initial probability density and the volume associated with each trajectory,

$$w_i = \psi^*(\boldsymbol{x}_i, t_0)\psi(\boldsymbol{x}_i, t_0)d\boldsymbol{x}_i(t_0) = A^2(\boldsymbol{x}_i, t_0)d\boldsymbol{x}_i(t_0) = \rho(\boldsymbol{x}_i, t_0)d\boldsymbol{x}_i(t_0). \tag{2.24}$$

Space of non-negligible density is sufficiently sampled with trajectories, so that (N_{tr} is the number of trajectories)

$$\sum_i^{N_{tr}} w_i \approx \int_{-\infty}^{+\infty} \psi^*(\boldsymbol{x}, t)\psi(\boldsymbol{x}, t)d\boldsymbol{x} = 1, \tag{2.25}$$

and their weights remain constant in the course of dynamics [29]

$$\frac{dw_i}{dt} = 0. \tag{2.26}$$

The evolution of trajectories is given by Hamilton's equations of motion,

$$\frac{d\boldsymbol{x}_i}{dt} = \frac{\boldsymbol{p}_i}{m}, \tag{2.27}$$

$$\frac{d\boldsymbol{p}_i}{dt} = -\boldsymbol{\nabla}\left(V + U\right)\big|_{\boldsymbol{x}=\boldsymbol{x}_i}. \tag{2.28}$$

The phase of wavefunction, $S(\boldsymbol{x}_i, t)$, is equal to the action function S_i of each trajectory defined (in units of $\hbar$) by

$$\frac{dS_i}{dt} = \frac{\boldsymbol{p}_i \cdot \boldsymbol{p}_i}{2m} - \left(V + U\right)\big|_{\boldsymbol{x}=\boldsymbol{x}_i}. \tag{2.29}$$

Observables and quantum mechanical operator

Consider an Hermitian operator $\hat{A}$ which is a function of the operator $\hat{x}$ and $\hat{p}$: $\hat{A} = \hat{A}(\hat{x}, \hat{p})$. In the position representation the quantum mechanical expectation value of this operator in the normalized state $\psi(x, t)$ is given by

$$\begin{aligned}\langle\hat{A}\rangle &= \langle\psi|\hat{A}|\psi\rangle \\ &= \frac{\int \psi^*(x)\left[\hat{A}(\hat{\boldsymbol{x}}, -\imath\hbar\nabla)\psi\right](x)d^3x}{\int \psi^*(x)\psi(x)d^3x}\end{aligned} \tag{2.30}$$

where

$$(\hat{A}\psi)(x) = \int \hat{A}(x,x')\psi(x')d^3x' \tag{2.31}$$

The hermiticity of $\hat{A}$ implies that only the real part of the integrand contributes to 2.30 and we can write

$$\langle\hat{A}\rangle = \int \psi^*(x)[\hat{A}(\hat{x}, -\imath\hbar\nabla)\psi](x)d^3x \tag{2.32}$$

It is then reasonable to define an expression for the 'local expectation value' of the operator $\hat{A}$ in the state $|\psi\rangle$ in the position representation:

$$A(x,t) = \psi^*(x,t)(\hat{A}\psi)(x,t) \tag{2.33}$$

For instance, for the position operator in the position representation

$$\hat{x}(x,x') = x\delta(x-x'), \tag{2.34}$$

substituting equation 2.34 into equation 2.33, we will get

$$x = \psi^* x\psi/\psi^*\psi = x(t). \tag{2.35}$$

The local expectation value of the position operator is the trajectory itself. Thus, within the trajectory representation of wavefunction, the expectation values for the position-dependent properties are easy to compute,

$$\langle\hat{\Omega}\rangle = \int_{-\infty}^{+\infty} \psi^*(\boldsymbol{x},t)\Omega\psi(\boldsymbol{x},t)d\boldsymbol{x} = \sum_{i=1}^{N_{tr}} w_i\Omega(\boldsymbol{x}_i). \tag{2.36}$$

Correlation function

Autocorrelation function can be computed directly from quantum trajectories,

$$C(2t) = \langle\psi(x,0)|\psi(x,2t)\rangle = \langle\psi*(x,t)|\psi(x,t)\rangle = \int_{-\infty}^{+\infty} dx\psi^2(x,t) \tag{2.37}$$

Computed with quantum trajectories

$$C(2t) = \sum_i w_i e^{2\imath S(x_i,t)}, \tag{2.38}$$

where w_i is the weight for i-th quantum trajectory.

The spectrum can be obtained by Fourier Transform the autocorrelation function.

$$\sigma(\omega) = \int_{-\infty}^{\infty} C(t) e^{\imath\omega t}\, dt \tag{2.39}$$

Written in the eigenfunctions of the Hamiltonian ϕ_n

$$\sigma(\omega) = \sum_n |c_n|^2 \delta(\omega - \omega_n), \quad c_n = \langle \phi_n | \psi_0 \rangle \,. \tag{2.40}$$

2.3 Approxmiate quantum potential

Quantum potential, U, is responsible for all quantum effects. We use the QT formalism as a well-defined semiclassical propagation method by making a single approximation to the quantum potential. The classical limit is defined as AQP being zero. The essential idea is to get AQP from the global linear least-squares fitting of the nonclassical component of the momentum operator [29],

$$\boldsymbol{r} = \frac{\boldsymbol{\nabla} A(\boldsymbol{x}, t)}{A(\boldsymbol{x}, t)} \approx \tilde{\boldsymbol{r}}(\boldsymbol{x}, t) \tag{2.41}$$

at each time step in small basis $\boldsymbol{f}(\boldsymbol{x})$, which is analytically determined.

$$U \approx \frac{-\hbar^2}{2m} (\tilde{\boldsymbol{r}} \cdot \tilde{\boldsymbol{r}} + \boldsymbol{\nabla} \cdot \tilde{\boldsymbol{r}}). \tag{2.42}$$

The least squares fit [76] minimizes $\langle (\boldsymbol{r} - \tilde{r})^2 \rangle$, where $\tilde{r}$ is represented in a linear basis $\boldsymbol{f}(\boldsymbol{x})$.

For instance, for a two dimensional system, $\boldsymbol{f}(\boldsymbol{x})$ can be arranged as a vector $(1, x, y)$, so the approximate nonclassical momentum component is expressed as

$$\tilde{r} = \mathbf{C}\boldsymbol{f}, \tag{2.43}$$

where $\mathbf{C}$ is a matrix of coefficients, which solves the matrix equation

$$2\ \mathbf{S}\mathbf{C} + B = 0. \tag{2.44}$$

The matrices are defined by the outer product of vectors

$$S = \langle \boldsymbol{f} \otimes \boldsymbol{f} \rangle \,, \; B = \langle \boldsymbol{\nabla} \otimes \boldsymbol{f} \rangle^T \tag{2.45}$$

which, when expanded, are

$$S = \begin{pmatrix} 1 & \langle x \rangle & \langle y \rangle \\ \langle x \rangle & \langle x^2 \rangle & \langle xy \rangle \\ \langle y \rangle & \langle xy \rangle & \langle y^2 \rangle \end{pmatrix}, \quad \mathbf{B} = \begin{pmatrix} 0 & 0 \\ 1 & 0 \\ 0 & 1 \end{pmatrix} \tag{2.46}$$

The approximate quantum potential defined by Eqs. 5.55-2.45 is simply a quadratic function of $\boldsymbol{x}$ yielding a linear quantum force (LQF) for every trajectory. This approximation rigorously conserves energy and is exact for Gaussian wavepacket, but does not presume that $\psi(\boldsymbol{x}, t)$ is necessarily a Gaussian wavefunction. Some other approximations of quantum potential can be found in Refs [42, 94, 40, 57, 64, 87]. This simple approximation gives basic QM effects, such as wavepacket bifurcation, moderate tunneling and zero-point energy [38].

2.4 Quasiclassical trajectory method

Quasi-classical trajectory (QCT) method is a widely used method for gas phase scattering simulations. It is based on dynamics of classical trajectories, whose initial conditions are quantized. A well known problem of this approach is the zero-point energy leak (ZPEL). Quantum mechanically, each vibrational mode is expected to contain certain amount of energy not lower than to ZPE of that mode. But in the classical trajectory simulation, the energy can flow among the modes without this restriction, thus yielding unphysical results. For direct reactive scattering at high energies, which is fast compared to a period of a typical vibration, ZPEL is not a big concern. However, incorrect flow of vibrational energy between the modes becomes a problem at low energies and for bond-breaking processes [73, 81]. The ZPE of a typical OH stretch is roughly 4.8 kcal/mol.

In QCT, the initial conditions for the trajectories are chosen according to semi-classical quantization rule: for diatomic molecule, the energy of each trajectory is equal to the energy of the vibrational state and the action is quantized. The final distribution of trajectories is often analyzed according to a similar quantization scheme. The trajectories evolve according to classical equations of motion

$$\frac{d\boldsymbol{x}}{dt} = \frac{\boldsymbol{p}}{m}, \tag{2.47}$$

$$\frac{d\boldsymbol{p}}{dt} = -\boldsymbol{\nabla} V(\boldsymbol{x}). \tag{2.48}$$

Experimental quantities such as angular distribution and cross sections are easily obtainable from QCT dynamics, which makes it a popular simulation tool.

Chapter 3

Estimating quantum mechanical effects of atomic solids using quantum molecular dynamics with dissipation

Solid helium-4 is a well-known quantum atomic solid, characterized by large zero-point energy that cannot be described by harmonic approximation. In this chapter, we describe how to use a quantum molecular dynamics method with friction to compute zero-point energy and pair distribution function for large-scale quantum system and use it for solid helium-4. An modified approximation is made for the quantum potential to fix the unbalance problem encountered while applying linearized quantum force to systems with large anharmonicity. It is shown that the modified fitting procedure is capable of capturing the zero-point energy for systems with large anharmonicity. Pair distribution function is also computed at various atomic mass to study the dependence on mass.

3.1 Introduction

Solid helium-4 is a well-known quantum atomic solid, characterized by large zero-point energy that cannot be described by harmonic approximation, which is a normal way to get an estimate of zero-point energy. The same system with various density and crystal structure has been studied by various authors using different methods such as variational path integral molecular dynamics and diffusion Monte Carlo method for different properties such as zero-point energy (ZPE) and pair distribution function

(PDF) [**?** 74, 46, 45]. In this article, we will describe how to use a quantum molecular dynamics method with friction to compute zero-point energy and pair distribution function for large-scale quantum system and use it for solid helium-4 with 180 atoms.

Pair distribution function, can be obtained experimentally from the powder diffraction data, describes the average structure of materiel. It contains the information of the distances between atoms [61, 16]. For a classical solid at absolute zero, it is simply some peaks of infinity intensity at values corresponding the pair distances in the system. Due to large zero-point energy, the peaks will be broadened as the wavefunction of the system spreads over space. The dependence of atomic mass for PDF is studied for solid helium-4. For the approach adopted here is a generic method to study dissipated quantum system. Including dissipation into quantum system is generally designed to study the interaction between system and environment ("bath"), which is an important phenomenon in real physical systems.. A complete discussion of various topics about dissipated quantum system can be seen in [90].

Various authors use the Hamiltonian that is written as a sum of Hamiltonian of the system H_S, "bath" Hamiltonian of the bath H_B and their interaction H_{SB},

$$H = H_S + H_B + H_{SB}. \tag{3.1}$$

This model is often referred as Caldeira-Leggett Hamiltonian in the solid-state physics community.

Zwanzig [98] generalized the approach to nonlinear potentials. Recently, Caldeira and Leggett [11] used the Hamiltonian to study strong damped systems. Predating the model, there is another model called Caldirola-Kanai model [56] that does not include the environmental degrees of freedom explicitly in the Hamiltonian. Recently, A. S. Sanz adopted this model and studied wavepacket dynamics in viscid media in the framework of Bohmian trajectories [78]. This model describes a dissipated quantum

system that the total energy is damped to zero where the system is localized to one point in configuration space, violating the Heisenberg uncertainty principle.

The model which is considered here is in analogy to Caldirola-Kanai model in the aspect that the environmental degrees of freedom is not included in the Hamiltonian, but differ in that Heisenberg uncertainly will not be contradicted. The total energy of system is dissipated to the ground state of the system at infinity time starting with a trial wavefunction.

Inclusion of friction directly into the Schrödinger equation may be viewed as a simple way to mimic the effect of energy transfer from the system to the environment while containing quantum dynamics calculations to the system degrees of freedom. In classical mechanics, the frictional force, often considered for processes happened in condensed phase, is always taken as a particle velocity proportional term in equations of motion. The equations of motion for a classical particle with mass m, position x and momentum p while a friction force exists are as follows,

$$m\ddot{x} + \gamma\dot{x} + \nabla V(x) = 0 \tag{3.2}$$

The classical trajectory evolves under the influence of an external potential $V(x)$, which is a function of the Cartesian coordinate, x, parameter γ denotes the friction coefficient.

In standard quantum mechanics, the concept of particles is missing, instead wave-function is use to represent a system. However, in de Broglie-Bohm formulation of quantum mechanics [5, 6], propagating the wavefunction is equivalent to the evolution of an ensemble of so-called quantum trajectories ("fluid elements"), which represent the wavefunction. Then it is naturally to extend the idea of friction into dynamics of quantum trajectories, resulting in a similar equation of motion except the so-called quantum potential term, which includes all the quantum effects. Except for conceptional problems, from a practical point of view, it is always difficult to find the exact

or even approximated solution for any complicated model other than some simple ones such as free propagation and harmonic oscillator. Within the quantum trajectory framework, the main challenge is the computation of quantum force, whose exact solution requires the whole wavefunction. An accurate and practical approximation called linear quantum force (LQF) [28, 27, 30] is used in [34] to obtain ground state energy of arbitrary potential. The LQF approach is exact for the simulation with a starting Gaussian wavepacket on the potential up to second order. In this article, an unbalance problem is shown while applying the same approximation for systems with large anharmonicity. A solution is proposed to fix the problem and extend the idea to large-scale quantum systems, such as solid helium-4. It is shown by an anharmonic model that the modified approximation is capable of capturing the zero-point energy for systems with large anharmonicity.

3.2 Formulation

Bohmian mechanics

For the notations used in this paper, without specified, small Arabic letters $(i, j, k...)$ are used to label trajectories and Greek letters for degree of freedom (DoF) and bold small letters for vectors and bold capital letters for matrix. Atomic units is used by default.

In de Broglie-Bohm theory, the wavefunction is represented in polar form with the amplitude $A(\boldsymbol{x}, t)$ and phase $S(\boldsymbol{x}, t)$, which are both real functions of $\boldsymbol{x}$ and t,

$$\psi(\boldsymbol{x}, t) = A(\boldsymbol{x}, t) \exp\left(\frac{\imath}{\hbar} S(\boldsymbol{x}, t)\right). \tag{3.3}$$

The probability density can be represented by

$$\rho(\boldsymbol{x}, t) = \psi^*(\boldsymbol{x}, t)\psi(\boldsymbol{x}, t) = A^2(\boldsymbol{x}, t). \tag{3.4}$$

Substituting Eq. (6.10) into TDSE, one obtains two coupled equations of amplitude and phase,

$$\frac{\partial S(\boldsymbol{x},t)}{\partial t} = \frac{\nabla S(\boldsymbol{x},t)^2}{2m} - V(\boldsymbol{x}) - U(\boldsymbol{x},t), \tag{3.5}$$

$$\frac{\partial \rho(\boldsymbol{x},t)}{\partial t} = -\nabla\left(\rho(\boldsymbol{x},t)\frac{\boldsymbol{\nabla} S}{m}\right), \tag{3.6}$$

$$\tag{3.7}$$

where

$$U(\boldsymbol{x},t) = -\frac{\hbar^2}{2m}\frac{\nabla^2 A(\boldsymbol{x},t)}{A(\boldsymbol{x},t)}. \tag{3.8}$$

$U(\boldsymbol{x},t)$ is the so-called non-local time-dependent quantum potential, and is proportional to $\hbar^2$. Without loss of generality, we assume the mass m is the same for each DoF.

$$M_{ij} = m_i\delta_{ij} \quad i,j \in [1, N_{dim}], \tag{3.9}$$

where N_{dim} is the number of DoF.

Eq. (6.12) is the Eulerian version of the *quantum Hamiltion-Jacobi equation*, differing from classical *Hamilton-Jacobi equation* by the quantum potential term. The wavefunction can be discretized in coordinate space by quantum trajectories (QTs) with position $\boldsymbol{x}$ and momentum $\boldsymbol{p}$, defined as

$$\boldsymbol{p} = \boldsymbol{\nabla} S, \tag{3.10}$$

where $\boldsymbol{\nabla}$ here represents a column vector of differential operator,

$$\boldsymbol{\nabla} = \begin{bmatrix} \partial_{x_1} \\ \partial_{x_2} \\ \vdots \\ \partial_{x_{N_{dim}}} \end{bmatrix} \tag{3.11}$$

When $\hbar \to 0$, U becomes negligible and all of the trajectories become independent of each other, which corresponds to the classical limit. The quantum potential U can

be considered as a nonclassical contribution to the kinetic energy. The ensemble of quantum trajectories, representing the wavefunction, are assigned certain weights w_i, that depends on the initial probability density and the volume associated with each trajectory,

$$w_i(t) = \psi^*(\boldsymbol{x}_i, t)\psi(\boldsymbol{x}_i, t)\, d\boldsymbol{x}_i(t) \tag{3.12}$$

Space of non-negligible density is sufficiently sampled with trajectories, N_{traj} is the number of trajectories. The normalization of the probability correspond to the following relationship

$$\sum_i^{N_{traj}} w_i \approx \int_{-\infty}^{+\infty} \psi^*(\boldsymbol{x}, t)\psi(\boldsymbol{x}, t) d\boldsymbol{x} = 1. \tag{3.13}$$

The weight for each quantum trajectory remains constant in the course of dynamics [30] in the Lagrangian frame-of-reference,

$$\frac{dw_i}{dt} = 0. \tag{3.14}$$

The Lagrangian and Eulerian frame-of-references are connected by

$$\frac{d}{dt} = \frac{\partial}{\partial t} + \boldsymbol{v} \cdot \boldsymbol{\nabla}. \tag{3.15}$$

The evolution of trajectories is given by Hamilton's equations of motion,

$$\frac{d\boldsymbol{x}_i}{dt} = \frac{\boldsymbol{p}_i}{m}, \tag{3.16}$$

$$\frac{d\boldsymbol{p}_i}{dt} = -\boldsymbol{\nabla}\,(V + U)|_{\boldsymbol{x}=\boldsymbol{x}_i}\,. \tag{3.17}$$

Here subscript i labels the trajectories. The phase of wavefunction, $S(\boldsymbol{x}_i, t)$, is equal to the action function S_i of each trajectory defined (in units of $\hbar$) by

$$\frac{dS_i}{dt} = \frac{\boldsymbol{p}_i \cdot \boldsymbol{p}_i}{2m} - (V + U)|_{\boldsymbol{x}=\boldsymbol{x}_i}\,. \tag{3.18}$$

The position-dependent observables $\hat{O}$ can be computed from the properties of each quantum trajectory,

$$\bar{O} = \int d\boldsymbol{x}\rho(\boldsymbol{x}, t)O(\boldsymbol{x}) = \sum_i^{N_{traj}} O(\boldsymbol{x}_i)w_i \tag{3.19}$$

Incorporating friction

The friction term is straightly incorporated into the equation of motion of quantum trajectories. With friction, the total energy of the system will decay to the ground state. The energy is always transferring from the system to the "environment" degree of freedom except the system gets to the ground state. The other direction, energy flowing from the environment to the system, is not allowed if we keep the friction constant as a positive constant, which is not required in general. Starting with a trial wavefunction, quantum trajectories start to lose their kinetic energy and finally drift to a region of zero net force.

This approach is firstly described in detail in [37], where some examples of computation of zero-point energy for systems up to 10 atoms are shown. Here we make an modification of the approximation of quantum potential and show its capability to simulate large-scale quantum system of atomic solid.

The friction term depends on the velocity of each quantum trajectory and the resulting TDSE is nonlinear; the time-dependent wavefunction conserves normalization, while the total energy of the wavefunction decreases with time to the zero-point energy value. The energy dissipation is proportional to the kinetic energy of quantum trajectories,

$$\frac{dE}{dt} = -2\gamma K. \tag{3.20}$$

The equations of motion for quantum trajectories with friction in the Lagrangian frame are written as follows:

$$\frac{d\boldsymbol{p}}{dt} = -\boldsymbol{\nabla}(V(\boldsymbol{x}) + U(\boldsymbol{x}, t) - \gamma \boldsymbol{p} \tag{3.21}$$

$$\frac{d\boldsymbol{x}}{dt} = -\frac{\boldsymbol{p}}{m} \tag{3.22}$$

Integrating Eq. (3.21) with respect to x, the evolution of $S(x,t)$ with friction becomes

$$-\frac{\partial S}{\partial t} = \frac{p^2}{2m} + V + U + \gamma S + C(t). \tag{3.23}$$

The constant of integration $C(t)$ is defined in [37],

$$C(t) = -\langle S(x,t)\rangle \,. \tag{3.24}$$

Together with continuity equation unchanged by friction, the conventional TDSE with friction becomes

$$\imath\hbar\frac{\partial}{\partial t}\psi(x,t) = \hat{H}\psi(x,t) + \gamma(S(x,t) - \langle S|\,(x,t)\,|\rangle)\,\psi(x,t). \tag{3.25}$$

Approximate quantum potential

The quantum potential, $U(\boldsymbol{x},t)$, is responsible for all quantum-mechanical effects, such as zero-point energy and quantum-mechanical tunneling effects. The classical limit is defined as $U \to 0$. In our previous work [37], we were using linearized quantum force method [30, 27] to get approximated quantum potential and quantum force. And this approximation has been utilized in the simulations of enzymatic reaction dynamics [68] and nano-materials such as hydrogen collision with carbon flake [36, 89].

The procedure is briefly described as follows. The essential idea is to get approximated quantum potential from the global linear least-squares fitting of the nonclassical component of the momentum operator defined as

$$r_\alpha(\boldsymbol{x},t) = \frac{\nabla_\alpha A(\boldsymbol{x},t)}{A(\boldsymbol{x},t)} \approx \tilde{r}_\alpha(\boldsymbol{x},t) \tag{3.26}$$

at each time step in small basis $\boldsymbol{f}(\boldsymbol{x})$, which is analytically determined.

$$U \approx \sum_\alpha \frac{-\hbar^2}{2m}(\tilde{r}_\alpha \cdot \tilde{r}_\alpha + \nabla_\alpha \tilde{r}_\alpha). \tag{3.27}$$

The least-squares fitting [76] minimizes $\sum_\alpha ||(r_\alpha - \tilde{r}_\alpha)||^2$, where $\tilde{r}_\alpha$ is represented in a linear basis $f(\boldsymbol{x}) = (1, x, y, z, \dots)$.

The approximated quantum potential defined above is simply a quadratic function of $\boldsymbol{x}$ yielding a linear quantum force (LQF) for every trajectory. This linear approximation rigorously conserves energy and is exact for Gaussian wavepackets, but does

not presume that $\psi(\boldsymbol{x}, t)$ is necessarily a Gaussian wavefunction. LQF captures basic QM effects, such as wavepacket bifurcation, moderate tunneling and zero-point energy [38]. Some other methods about approximations of quantum potential can be found in Refs. [42, 94, 57, 87].

In principle, the expectation value of energy will decay to the ground state as the kinetic energy of quantum trajectories decay to zero. At the ground state, the quantum force, $\nabla U(\boldsymbol{x}, t)$, will cancel the classical force so that there is no net force for quantum trajectories, i.e. trajectories stop moving.

The challenge here is for an anharmonic system, the LQF does not have the corresponding higher order terms to balance classical force, which means the trajectories will never stop. With a small friction constant, the quantum trajectories will wiggle around equilibrium position and finally become localized.

Fitting with larger basis can cause a dramatic increase in computational cost. The size of basis will be $O(N_{dim}^2)$ if we want to include all the quadratic terms into basis. Besides that, adding higher order terms is not guaranteed to give better results.

Taking all of the factors into consideration, we proposed another least-square fitting scheme to fix the unbalance problem. We add non-classical momentum into equations of motion along with position and momentum of quantum trajectories, notice that we do not need the exact values of $r(\boldsymbol{x}, t)$ in LQF approach. The whole approximation is decomposed into two steps of polynomial fitting.

- The first step is to apply a global linear basis $(1, x, y, \dots)$ to do least-square fitting of $(\boldsymbol{p}, \boldsymbol{r})$ to minimize $\{\sum_\alpha ||(r_\alpha(x,t) - \tilde{r}_\alpha(x,t)||_2, \sum_\alpha ||(p_\alpha(x,t) - \tilde{p}_\alpha(x,t)||_2\}$, this first step is similar to the LQF except now we have the exact values of non-classical momentum. The first step is necessary due to the fact that quantum potential is a non-local property, the quantum trajectories should be influenced by each other.

- The second step is to fit the remainder

$$I_r = \sum_\alpha ||r_\alpha(x,t) - \tilde{r}_\alpha(x,t) - \tilde{\tilde{r}}_\alpha(x,t)||_2$$

and

$$I_p = \sum_\alpha ||p_\alpha(x,t) - \tilde{p}_\alpha(x,t) - \tilde{\tilde{p}}_\alpha(x,t)||_2$$

with a cubic basis for each DoF/atom. This second step is based on the first step, can be taken as adding more flexibility to quantum potential to account for anharmonic terms. The basis for this second step is different for each DoF, $f_\alpha = (1, x_\alpha, x_\alpha^2, x_\alpha^3)$.

In order to do a fitting of non-classical momentum, one has to include the equation of motion for non-classical momentum. Starting from continuity equation and after some algebra, one can obtain

$$\dot{r}_\alpha = -\left(\sum_\beta \frac{\nabla_\alpha p_\beta}{m_\beta} r_\beta + \sum_\beta \frac{\nabla_\alpha \nabla_\beta p_\beta}{2m_\beta}\right) \tag{3.28}$$

Then in Lagrangian frame of reference, the exact equations of motion for (x, p, r) will be

$$\dot{x}_\alpha = \frac{p_\alpha}{m_\alpha} \tag{3.29}$$

$$\dot{p}_\alpha = -\nabla_\alpha \left(V(\boldsymbol{x}) + U(\boldsymbol{x}, t)\right) \tag{3.30}$$

$$\dot{r}_\alpha = -\left(\sum_\beta \frac{\nabla_\alpha p_\beta}{m_\beta} r_\beta + \sum_\beta \frac{\nabla_\alpha \nabla_\beta p_\beta}{2m_\beta}\right) \tag{3.31}$$

where

$$\tilde{U}(x,t) = \sum_\alpha -\frac{\hbar^2}{2m_\alpha}\left(\tilde{r}_\alpha^2(\boldsymbol{x},t) + \nabla_\alpha \tilde{r}_\alpha(\boldsymbol{x},t)\right) \tag{3.32}$$

Equation of motion for nonclassical momentum

Start with continuity equation

$$\frac{\partial \rho(\boldsymbol{x},t)}{\partial t} + \boldsymbol{\nabla}\left(\rho(\boldsymbol{x},t)\frac{\boldsymbol{p}}{m}\right) = 0 \tag{3.33}$$

substitute $\rho = A^2$ into the continuity equation, one obtains

$$2A\partial_t A + \sum_\alpha \left(2A\nabla_\alpha A m_\alpha^{-1} p_\alpha + A^2 \nabla_\alpha p_\alpha m_\alpha^{-1}\right) = 0 \tag{3.34}$$

divide by $2A^2$,

$$\partial_t \log A = -\sum_\alpha \left(\nabla_\alpha \log A p_\alpha m_\alpha^{-1} + \frac{\nabla_\alpha p_\alpha}{2m_\alpha}\right). \tag{3.35}$$

Apply partial derivative operator ∇_α on both sides of the last equality and notice $r_\alpha = \nabla_\alpha \log A$, one obtains

$$\dot{r}_\alpha = -\left(\sum_\beta \frac{\nabla_\alpha p_\beta}{m_\beta} r_\beta + \sum_\beta \frac{\nabla_\alpha \nabla_\beta p_\beta}{2m_\beta}\right) \tag{3.36}$$

If one only makes a linear approximation of momentum, the second term of the RHS of Eq. (3.36) will vanish. The modified approximation will retain the second term due to the high order term in the basis.

To specify all the terms that are fitted in the simulation, the equations of motion with fitted terms $(\tilde{p}, \tilde{r})$ in Lagrangian frame of reference, will be

$$\dot{x}_\alpha = \frac{\tilde{p}_\alpha}{m_\alpha} \tag{3.37}$$

$$\dot{p}_\alpha = -\nabla_\alpha \left(V(\boldsymbol{x}) + \tilde{U}(\boldsymbol{x}, t)\right) - \gamma p_\alpha \tag{3.38}$$

$$\dot{r}_\alpha = -\left(\sum_\beta \frac{\nabla_\alpha \tilde{p}_\beta}{m_\beta} \tilde{r}_\beta + \sum_\beta \frac{\nabla_\alpha \nabla_\beta \tilde{p}_\beta}{2m_\beta}\right) \tag{3.39}$$

3.3 System setup

Classical potential energy

Here we describe some details about how to compute classical potential and force fields.

The potential energy for each configuration is split into short-range interaction and long-range interaction, defined by cutoff distance R_{cut}.

The short-range interaction is computed by summing up all the interacting pairs (ip),

$$V(\boldsymbol{r}) = \sum_{ip(i,j)} U(|\boldsymbol{r}_{ij}|). \tag{3.40}$$

where $\boldsymbol{r}_{ij}$ is the time-dependent vector pointing from atom i to atom j, and $U(r)$ is the interaction between two helium atoms separated by distance r.

The HFD-B(He) He_2 pair interaction [2] is used to describe the inter-atomic interaction $U(r)$, shown in Fig. (3.1). Every atom $k \in [1, N_{atom}]$ in the solid has a corresponding lattice site $\boldsymbol{R}_k$, then the separation vector between atom k and atom j at lattice sites is defined $\boldsymbol{R}_{kj} = \boldsymbol{R}_j - \boldsymbol{R}_k$, periodic boundary conditions and minimum image convention is used. For atom k, when we compute the distance between atom j with it, we always choose the image of j that will give us the closed distance $\boldsymbol{R}_{kj}$. We say it is an interacting pair if the separation distance $|\boldsymbol{R}_{kj}| < R_{cut}$. We go through all the atoms in the simulation cell and build a *neighbor list* for each atom. The *neighbour list* is not updated through the simulation even if the distance between two atoms in an interacting pair get larger than R_{cut} during the simulation.

The separation vector $\boldsymbol{r}_{ij}$ between two helium atoms i, j not sitting at lattice sites is defined as:

$$\boldsymbol{r}_{ij} = -d\boldsymbol{r}_i + \boldsymbol{R}_{ij} + d\boldsymbol{r}_j, \tag{3.41}$$

where $d\boldsymbol{r}_i,\ d\boldsymbol{r}_j$ are displacement vectors for atom i and j from lattice sites respectively.

The two-body potential is computed over a fine grid of the square of the distance between two atoms, the potential is computed using linear interpolation. When the distance get too close, the potential is set to a constant. The classical force is computed in the same way as potential, where the force is defined over the same grid beforehand using finite difference method, and apply a pairwise sum to get the total force,

$$\frac{\partial V}{\partial d\boldsymbol{r}_i} = \sum_j 2(-d\boldsymbol{r}_i + \boldsymbol{R}_{ij} + d\boldsymbol{r}_j)\frac{\partial V}{\partial |\boldsymbol{r}_{ij}|^2} \tag{3.42}$$

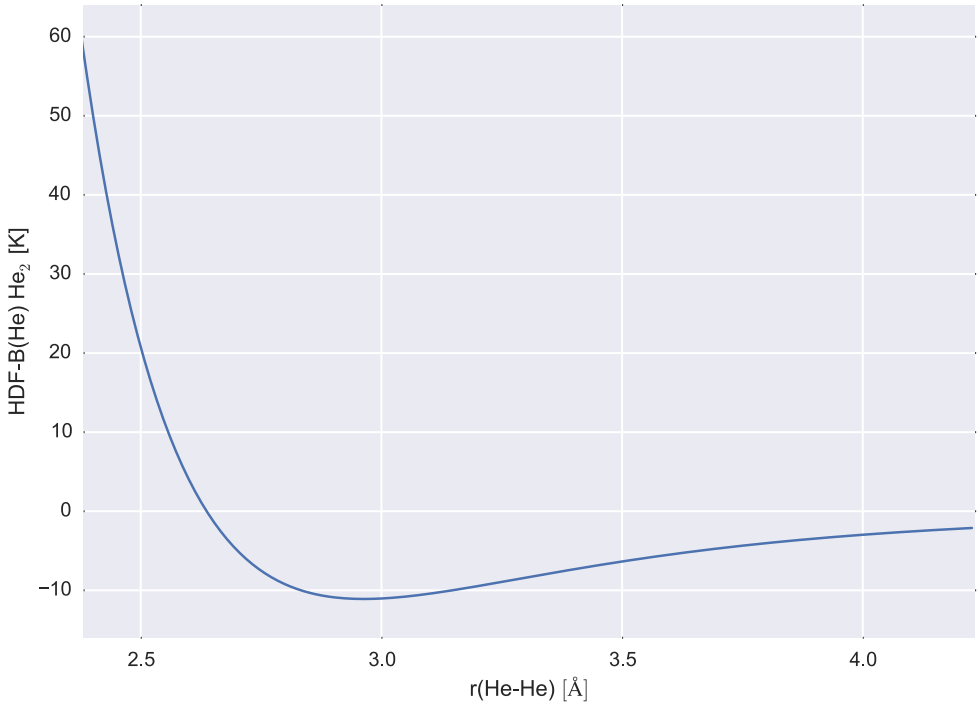

Figure 3.1: HFD-B(He) He_2 pair interaction.

For the cutoff distance R_{cut} we used in our simulation, the HFD-B(He) He_2 pair interaction has not become close enough to a negligible value. To take account of the contribution from the long-term corrections to the dynamics of quantum trajectories. the long-range interaction is pre-computed by a polynomial fitting up to second order. The fitting procedure is computed over a three-dimensional grid of the displacements of one helium atom. The potential energy for long-range interaction is get by summing up all the pair interactions between whose distance is over cutoff distance, taking into periodic boundary conditions. The system size is enlarged until the long-range potential is convergent to 10^{-8} $a.u.$. We will obtain $N_p = N_x \times N_y \times N_z$ values for potential and solve the following matrix equation to get the fitting coefficients $\boldsymbol{c} = \{c_1, c_2, ...c_{N_b}\}^T$,

$$M^T M \boldsymbol{c} = M^T \boldsymbol{V}_l, \tag{3.43}$$

where M is an $N_p \times N_b$ matrix, for each line, the elements are

$$M(i, j = 1, \ldots, N_b) = \{1, x_i, y_i, z_i, x_i^2, y_i^2, z_i^2, x_i y_i, y_i z_i, x_i z_i\}, \tag{3.44}$$

and $\boldsymbol{V}_l$ is the column vector including the long-range interaction values at all displacements,

$$V_l(i) = V_l(x_i, y_i, z_i), \ i \in [1, N_p]. \tag{3.45}$$

N_b is the number of basis terms, which in this case is 10.

The long-range force is computed analytically since we have polynomial expression for long-range potential.

3.4 Numerical implementation

The implemented code written in *Fortran* and is massively paralleled by *Message Passing Interface* (MPI), Fig. (3.2) shows the diagram of the work flow of the whole simulation. Quantum trajectories are initiated with Monte Carlo sampling in the root processor and then distributed over multiple nodes calling MPI subroutines. Each node has multi-processors, which in our case is 16. Computing expectation value of operators need the information of all the trajectories. In the first step of our approximation to quantum potential, we need to construct a big matrix S of dimensionality $(N_{dim}+1) \times (N_{dim}+1)$ as $(N_{dim}+1)$ is the number of basis used in the linear fitting, $f = (1, x_1, x_2, \ldots, x_{N_{dim}})$. It is necessary to gather all the information to compute expectation values of any operator. Each matrix element of S will be an expectation value of position operator, i.e.

$$S_{ij} = \sum_{k}^{N_{traj}} f_i^{(k)} f_j^{(k)} w_k \tag{3.46}$$

After the quantum trajectories part is paralleled, the computation of classical force which requires the program to go through all the interacting pairs is automatically paralleled, which is a general strategy for molecular dynamics simulation. The rate-limiting step then become the construction of matrix S used in the Least square

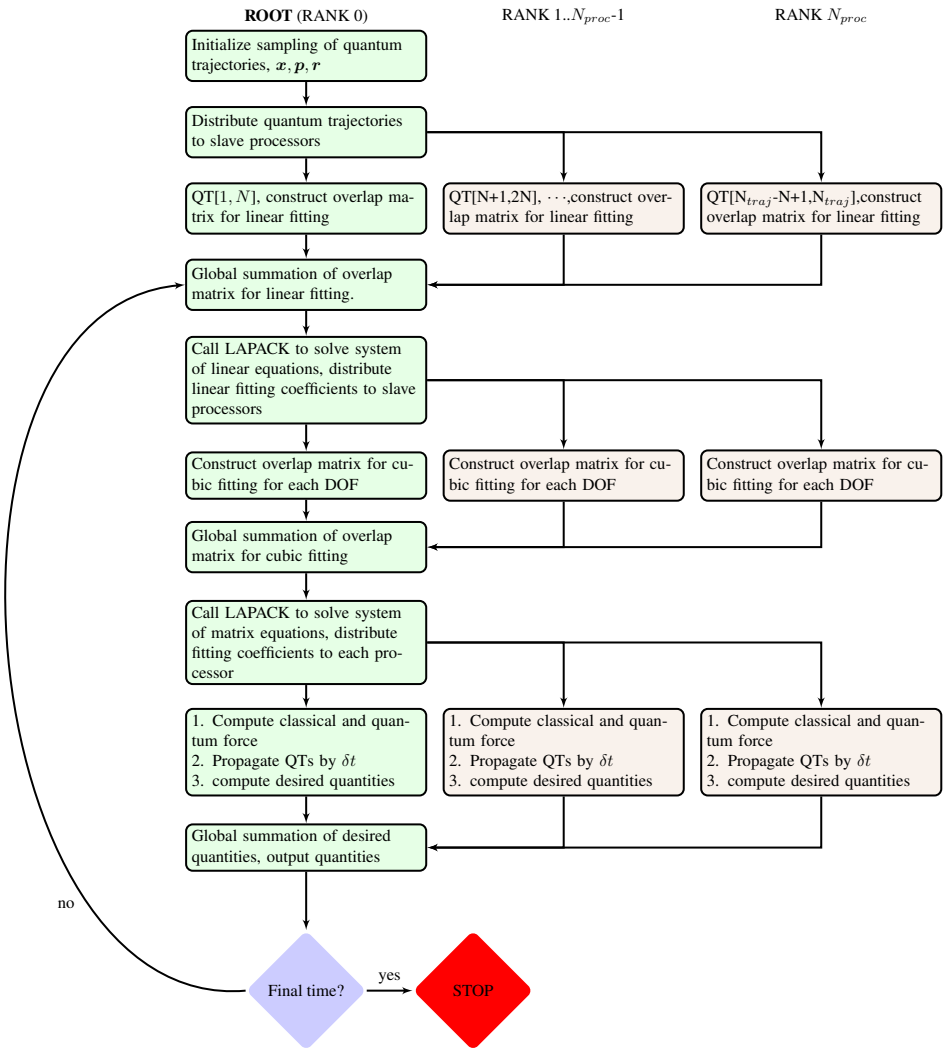

Figure 3.2: Flowchart of parallelization, quantum trajectories are distributed among processors such that the computing of classical force is paralleled.

fitting of non-classical momentum. To increase the efficiency of parallelization, the computation of matrix elements of S is distributed onto all N_{proc} processors, i.e. each processor computes a copy of S_i. One does a global sum over processors to obtain the final results at root processor, $S = \sum_i^{N_{proc}} S_i$. The same strategy is used for the second step of the fitting, where a 4×4 array is constructed for each DoF.

Coupled anharmonic oscilator

To illustrate the unbalance problem we discussed above, we choose coupled anharmonic oscillator as a model. The potential is written as

$$V(x,y) = \frac{1}{2}(x^2 + \frac{1}{2}x^4) + \frac{1}{2}(y^2 + \frac{1}{2}y^4) + \epsilon xy \tag{3.47}$$

ϵ is a parameter that can be used to control the coupling between two anharmonic oscillators. We set it to 0.5 here. We use the linear quantum force approach and modified approximation method both for this model system. Fig. (3.5) shows how total energy changes with time, it is clear to see the difference between two curves. At $t \sim 1.5$ $a.u.$, the total energy already decay to the ground state in the modified method. Fig. (3.3) shows the movement of quantum trajectories in x axis, while Fig. (3.4) is the same quantity for modified quantum force. The quantum trajectories with LQF tend to localize at the positions where the quantum force and classical force cancel each other, considering the unbalance problem, there are only at most few points in the potential energy surface that fulfill the requirement. As we can see, at long time, trajectories tend to gather at those points, which cannot be a good representation of the whole wavefunction.

Solid helium-4

For zero-point energy computation, the specific system we used in this paper is hexagonal close packed (hcp) sold ^{4}He at density $\rho = 4.61421 \times 10^{-3}\ a_0^{-3}$, corresponding to molar volume $V_{mol} = 19.34\ cm^3/mol$. The nearest-neighbor distance is 6.74223 a_0. R.J. Hinde has computed the zero-point energy for the same model using variational path integral approach in [**?**]. The initial wavefunction is chose as a product of

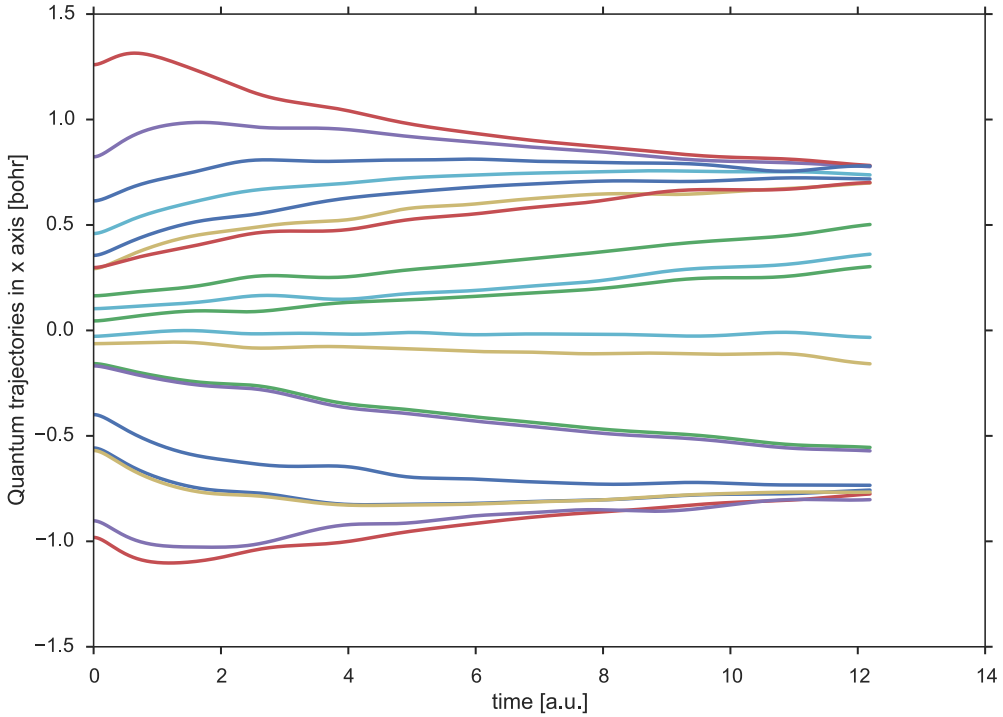

Figure 3.3: Quantum trajectories in x axis for coupled anharmonic oscillator with linear quantum force.

Crystal cell	$5 \times 3 \times 3$
R_{cut}	13.8 a_0
N_{traj}	19200
N_{dim}	3×180
m_α	4×1836
γ	8;12
δt	3
$\psi(\boldsymbol{x}, t_0)$	Gaussian
Gaussian width	0.8

Table 3.1: Simation parameters

gaussians centered at lattice sites of each atom,

$$\psi(\boldsymbol{x}, t_0) = \prod_{i=1}^{N_{dim}} \left(\frac{2\alpha_i}{\pi}\right)^{\frac{1}{4}} \exp(-\alpha_i (x_i - q_i)^2) \tag{3.48}$$

The gaussian is set to be $\alpha_i = 0.8\ a_0$ and time step $\Delta t = 3\ a.u.$. The friction constant is chosen at 8 and 12 to check convergence.

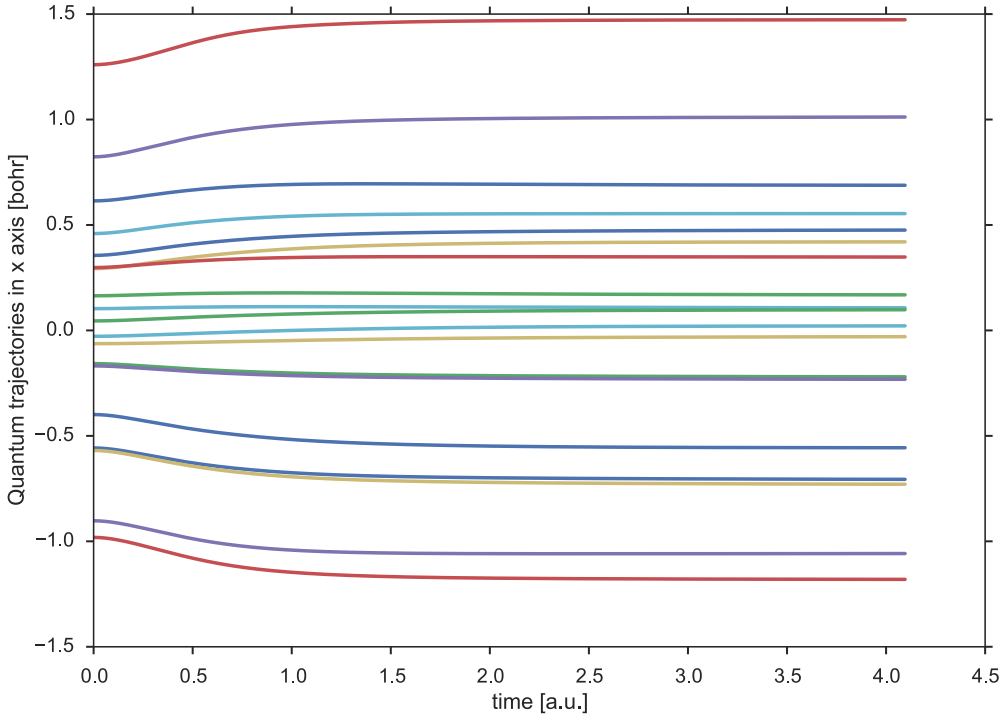

Figure 3.4: Quantum trajectories in x axis for coupled anharmonic oscillator with modified approximation to quantum potential.

γ	Fitting range $[10^4 a.u.]$	ZPE $[K/atom]$	Other work $[K/atom]$
12	9-12	-5.50	-5.48 [**?**]
40	9-12	-5.54	-5.50 [13]

Table 3.2: Zero-Point Energy Estimate for various friction constant

For numeral efficiency, the long-time $E(t)$ is fit with an exponential function

$$E = A\exp(-Bt) + ZPE,$$

, which gives ZPE estimate.

Pair distribution function

Pair distribution function $g(r)$, which represents the distance distribution between atoms, measures the disorder of a system and it is defined as

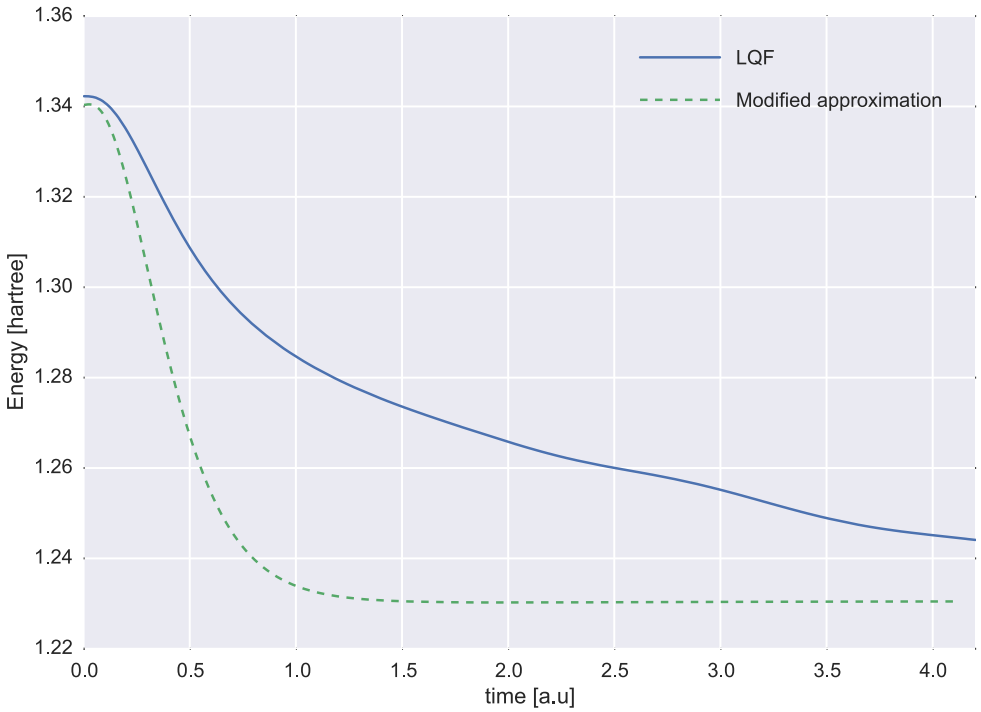

Figure 3.5: Energy components with friction coefficient $\gamma = 6$ for linearly coupled two-dimensional anharmonic oscilator. $N_{traj} = 4800,\ \Delta t = 0.002\ a.u.,\ m_x = m_y = 1\ a.u.$

$$g(\boldsymbol{r}_1, \boldsymbol{r}_2) = \frac{N(N-1)}{\rho^2}\rho(\boldsymbol{r}_1, \boldsymbol{r}_2). \tag{3.49}$$

where N is the number of particles and V is volume. $\rho = \frac{N}{V}$ is the single particle density and $\rho(\boldsymbol{r}_1, \boldsymbol{r}_2)$ is the joint probability.

$$\rho(\boldsymbol{r}_1, \boldsymbol{r}_2) = \int \cdots \int d\boldsymbol{r}_3 \cdots d\boldsymbol{r}_N\ \rho(\boldsymbol{r}_1, \cdots, \boldsymbol{r}_N) \tag{3.50}$$

where

$$\rho(\boldsymbol{r}_1, \boldsymbol{r}_2, \cdots, \boldsymbol{r}_N) = \psi^*(\boldsymbol{r}_1, \boldsymbol{r}_2, \cdots, \boldsymbol{r}_N)\psi(\boldsymbol{r}_1, \boldsymbol{r}_2, \cdots, \boldsymbol{r}_N). \tag{3.51}$$

The one-dimensional pair distribution function can be obtained by averaging $g(\boldsymbol{r}_1, \boldsymbol{r}_2)$ with the center of mass and polar angles θ and ϕ. Notice $\int d\boldsymbol{r}$ represents a three-dimensional integration.

$$g(|r_{12}|) = \frac{\int \cdots \int g(\boldsymbol{r}_1, \boldsymbol{r}_2)\, d(\frac{\boldsymbol{r}_1+\boldsymbol{r}_2}{2})\, d\phi\, d(\cos\theta)}{\int d(\frac{\boldsymbol{r}_1+\boldsymbol{r}_2}{2}) \int_0^{2\pi} d\phi \int_0^{\pi} d(\cos\theta)} \tag{3.52}$$

Since the wavefunction is represented by an ensemble of quantum trajectories, it will be convenient if we can transform the expression using terms that can be computed directly from trajectories.

$$g(r) = \int g(|\boldsymbol{r}_{12}|)\delta(r - |\boldsymbol{r}_{12}|)\, d|\boldsymbol{r}_{12}| \tag{3.53}$$

$$= \frac{N(N-1)}{\rho^2} \frac{1}{4\pi V} \int \cdots \int \rho(\boldsymbol{r}_1, \boldsymbol{r}_2)\delta(r - |\boldsymbol{r}_{12}|)\, d(\frac{\boldsymbol{r}_1 + \boldsymbol{r}_2}{2})\, d\phi\, d(\cos\theta) d|\boldsymbol{r}_{12}| \tag{3.54}$$

Notice the $d\boldsymbol{r}_{12} = |\boldsymbol{r}_{12}|^2\, d|\boldsymbol{r}_{12}| d\phi d(\cos\theta)$ and substitute into the last equation, we obtain

$$\frac{g(r) = \frac{N-1}{4\pi\rho} \langle \delta(r - |\,\boldsymbol{r}_{12}\,|\,)}{|\boldsymbol{r}_{12}|^2} \tag{3.55}$$

Here $\langle \ldots \rangle$ represents quantum ensemble average.

For numerical reason, we will plot a histogram for pair distribution function $g(r)$ over a range (R_{min}, R_{max}) split into N intervals.

Fig. (3.6) shows the pair distribution function computed at density $\rho = 5.231 \times 10^{-3}\ a_0^{-3}$. The value is chosen such that we can compare out results with make a comparison with results obtained using variational path integral molecular dynamics in S. Miura's work [74]. The results shows first two peaks in the PDF, which is in good agreement with S. Miura's work in the position of peaks and intensity, even though we are using different pair interaction. For different atomic mass, ^{3}He has a slightly wider peaks in PDF which is as expected as the wavefunction should be more spread out with lighter mass. While we change the mass to $8 \times 1836\ a.u.$, we see a much sharper peak, which is closer to a classical picture. It simply says, the system

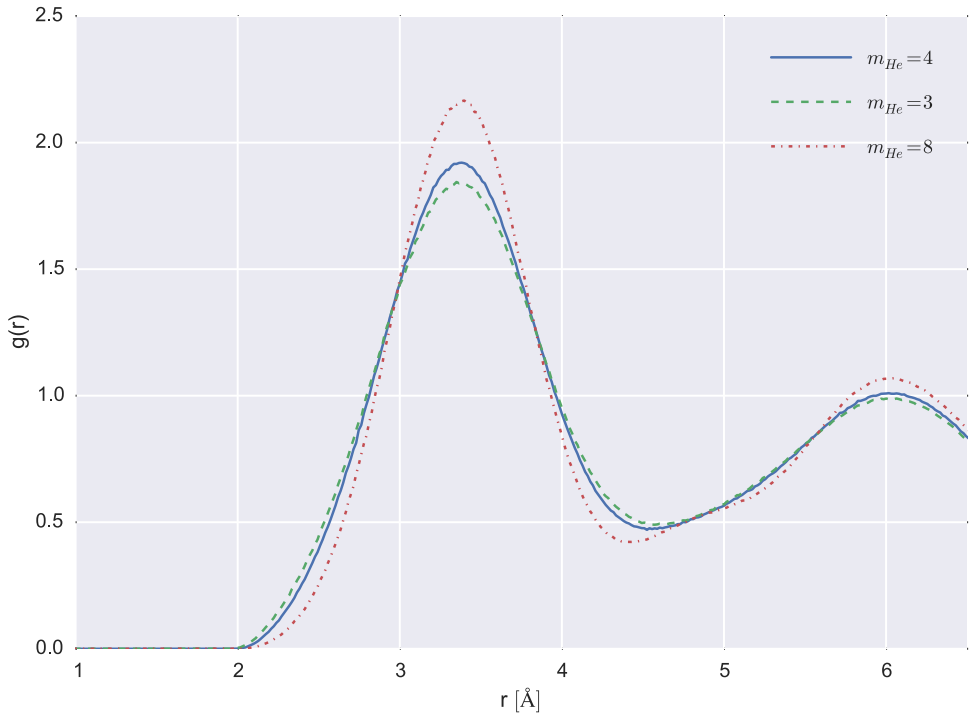

Figure 3.6: Pair distributin function $g(r)$ for various atomic mass, ^4He, ^3He, ^8He.

become more ordered while having a heavier atom and more disordered with a lighter atom, which is exactly what we would expect.

3.6 Conclusions

We describe a general approach to simulate large-scale quantum system dissipated to the ground state within the framework of quantum trajectories. Static properties such as zero-point energy and pair distribution function of quantum system can be obtained in the simulation. Specially, the simulation of quantum solid of helium-4 is represented in this paper. We showed an unbalance problem while adopting LQF to approximate quantum potential and an proposed solution is shown to be capable of capturing the zero-point energy in the model system with large anharmonicity.

We also studied how pair distribution function changes due to the change of particle mass. To conclude, with heavier mass, the disorder of quantum system at

ground state caused by zero-point motion will become less significant.

The further work will include computation of through real time quantum correlation function [67, 9] to obtain dynamic properties like diffusion constant or spectrum of vibrational modes using quantum trajectory method with approximated quantum potential [32, 22].

Chapter 4

Determination of the collective modes from the quantum-mechanical time-correlation functions

Theoretical characterization of vibrational spectra for large molecular systems often comes from the normal modes analysis derived from the quadratic approximation of the potential energy surface near its minimum. The normal modes of motion provide accurate representation of low-energy collective motion within a system near equilibrium, but they may be inadequate at high energies or for strongly anharmonic systems. In this article the collective modes of motion are examined from the time-dependent perspective. It is shown that the imaginary part of the quantum-mechanical position-position correlation functions contains all the information about the collective modes of motion without the harmonic approximation on the potential energy of a system.

4.1 Introduction

The electrons and nuclei forming a molecule are traditionally described within the Born-Oppenheimer approximation: the electronic time-independent Schrödinger equation (SE) is solved for a fixed geometry of the nuclei, and the ground state electronic energy together with the nuclear repulsion yields a single point of a potential energy surface (PES). The nuclei are routinely treated as classical particles moving on the electronic PES, but sometimes the quantum regime of nuclear behavior, character-

ized by large energy level spacing, is essential to understand processes in a molecular system. In this case the SE has to be solved for the nuclei, which is very challenging to do for a polyatomic system by traditional basis approaches of constructing and diagonalizing the Hamiltonian matrix (see Ref. [12, 10] as examples). An alternative is to use the time-evolution of wavefunctions to extract information on the energy levels, excitation energies and to get physical insight into the collective modes of motion within the system, possibly within the limited range of energies [59, 85]. For a system of N nuclei, each described in a three-dimensional space, 3 degrees of freedom (DOFs) describe the overall translation (uncoupled from the internal motion) and another 3 DOFs describe the overall rotation of a system. The remaining $3N-6$ internal DOFs ($3N-5$ for linear molecules) define the rovibrational spectrum. Often 'collective' is referred to a low-energy mode which involves large number of DOFs. We will refer to modes as being 'collective' in a more general sense of eigenmodes involving multiple DOFs describing different atoms and whose energies are isolated within the energy spectrum.

Speaking more generally, the idea of special coordinates or modes of motion characterizing a large system is widely used in physics and chemistry. Some textbook examples is the reaction coordinate describing progress of a chemical reaction or phonons in a a solid state. In theoretical chemistry, the instantaneous normal modes theories have been developed to describe short-dynamics of liquids and to give insight into their collective many-body motions [17, 1, 65]. In quasiclassical molecular dynamics, including reactive dynamics, the normal modes analysis on-the-fly has been used recently to deal with the zero-point energy leak in systems of 5-9 atoms [19, 20, 44]. In the area of the energy transfer, i. e. electronic excitations are coupled to a phonon bath representing the nuclear DOFs, Bittner, Burghard and co-workers have developed and applied a method (and its hierarchies) of identifying three phonon modes coupled to the electronic DOFs, replacing the coupling to the full high-dimensional

bath, which greatly simplifies description of electronic relaxation. [14, 41, 84, 96, 97]

Going back to the vibrational motion in a molecule, the standard eigenmode analysis of motion in a large ($N > 4$) system, often provided in the electronic structure packages, is based on the normal modes approximation: the PES as a function of coordinates is expanded through the second order near its minimum and the eigenvalues/eigenvectors of the corresponding Hessian matrix yield the energies and the coordinates defining the normal modes of motion. For a quantum system, this information gives estimates of the zero-point-energy (ZPE) and is used to interpret the vibrational infrared spectrum. This approach works in the regime of small amplitude motion and of small anharmonicity due to the underlying quadratic approximation to the PES. For more general PESs, for example, for those exhibiting the double-well character typical of reactions in condensed phase, one cannot readily extract information about the collective motion of atoms since the normal mode analysis is invalid. Below we describe how the anharmonic collective modes can be identified by analyzing the quantum dynamics of a nuclear wavefunction, namely from the position-position correlation functions. The imaginary parts of the correlation functions contain information on the excitation energies (the differences between the energy levels) and on the contributions of a particular DOF to a specific collective mode.

4.2 The formalism

Normal and collective coordinates

Let us first briefly review the normal modes analysis based on the harmonic approximation to the PES. Describing N particles in Cartesian coordinates $\boldsymbol{x}$ and denoting the total number of DOFs as $f = 3N$, the Hamiltonian can be written in mass-scaled coordinates $x'_i = \frac{x_i}{\sqrt{m_i}}$,

$$\hat{H} = \sum_{i=1}^{f} \frac{\hat{p}_i^2}{2m_i} + V(\boldsymbol{x}) = \sum_{i=1}^{f} \frac{(\hat{p}'_i)^2}{2} + V(\boldsymbol{x}'). \tag{4.1}$$

The vector $\boldsymbol{x} = (x_1, y_1, z_1, \ldots, x_N, y_N, z_N)$ lists positions of all atoms in the Cartesian space; m_i is the mass for the i^{th} DOF. For simplicity, the coordinates will always be mass-scaled ($m'_k = 1$) below and the primes will be dropped hereafter.

The potential is expanded through the second-order around an equilibrium geometry $\boldsymbol{x}_e$,

$$V(\boldsymbol{x}) = V(\boldsymbol{x}_e) + \sum_i \left.\frac{\partial V}{\partial x_i}\right|_{\boldsymbol{x}_e} (x_i - x_{ei}) + \frac{1}{2}\sum_{i,j} \left.\frac{\partial^2 V}{\partial x_i \partial x_j}\right|_{\boldsymbol{x}_e} (x_i - x_{ei})(x_j - x_{ej}),$$

where $\boldsymbol{x}_e$ is a stationary point, i.e.

$$\left.\frac{\partial V}{\partial x_i}\right|_{\boldsymbol{x}_e} = 0, \quad i = \{1, 2, \ldots, f\}$$

The Hessian matrix H is defined by the second-order derivatives of the potential energy $V(\boldsymbol{x})$,

$$H_{ij} = \frac{\partial^2 V(\boldsymbol{x})}{\partial x_i \partial x_j}$$

Setting the constant in the potential energy so that the bottom of the well is zero, and shifting the coordinates so that the minimum is at $\boldsymbol{x}_e = 0$, V becomes

$$V(\boldsymbol{x}) = \frac{1}{2}\boldsymbol{x}^T H \boldsymbol{x}.$$

If the Hessian matrix H can be diagonalized and D is the corresponding diagonal matrix with the diagonal elements $\{D_{11}, D_{22}, \ldots, D_{ff}\}$,

$$H = U^T D U, \tag{4.2}$$

then the normal mode coordinates are defined by the unitary matrix U as,

$$\boldsymbol{Q} = U\boldsymbol{x}. \tag{4.3}$$

Using these coordinates and their conjugate momentum operators,

$$\hat{P}_k = -\imath\hbar\frac{\partial}{\partial Q_k}, \tag{4.4}$$

the potential energy is written as

$$V(\boldsymbol{Q}) = \frac{1}{2}\boldsymbol{x}^T U^T D U \boldsymbol{x} = \frac{1}{2}\boldsymbol{Q}^T D \boldsymbol{Q}, \tag{4.5}$$

and the Hamiltonian of Eq. (5.2) separates into f independent harmonic-oscillator Hamiltonians with different frequencies ω_k,

$$\hat{H} = \sum_{k=1}^{f} \hat{H}_k^{HO} = \sum_{k=1}^{f} \frac{1}{2}(\hat{P}_k^2 + \omega_k^2 Q_k^2), \quad \omega_k = \sqrt{D_{kk}}. \tag{4.6}$$

Neglecting with the coupling of the overall rotation and internal motion, there are $3N-6$ frequencies (or $3N-5$ for linear molecules) relevant to the rovibrational spectrum.

The normal modes analysis is based on the transformation of coordinates, given by U, which simultaneously diagonalizes the potential V and the kinetic energy operator $\hat{K}$. Thus, the transformation of coordinates is uniquely defined by the diagonalization of the Hessian matrix. If the potential is anharmonic but separable in some unknown set of linear coordinates, then we can (i) define a general linear transformation, given by the matrix T', so that the kinetic energy operator remains diagonal, and then (ii) within those transformations search for new coordinates in which V is maximally uncoupled. Expressing the kinetic energy in the transformed coordinates $\boldsymbol{Q} = T'\boldsymbol{x}$,

$$\hat{K} = -\frac{1}{2}\sum_i \frac{\partial^2}{\partial x_i^2} = -\frac{1}{2}\sum_{jk}\left(\sum_i T'_{ji}T'_{ki}\right)\frac{\partial^2}{\partial Q_j \partial Q_k}, \tag{4.7}$$

the condition to have zero cross-terms in the operator expression is

$$\sum_i T'_{ji}T'_{ki} = \sum_i T'_{ji}(T'_{ik})^T = (T'(T')^T)_{jk} = D_{jj}\delta_{jk} \tag{4.8}$$

where D is an arbitrary diagonal matrix. The coordinates can be scaled so that this matrix becomes the identity matrix $\mathcal{I}$. This means that there is a unitary transformation described by the matrix T,

$$T = D^{-1/2}T', \quad T^T T = \mathcal{I}, \tag{4.9}$$

which transforms $\hat{K}$ into the diagonal operator. The off-diagonal elements of T, while satisfying Eq. (4.8), can be chosen to have V in separable form in the new *collective* coordinates $\boldsymbol{Q} = T\boldsymbol{x}$. These eigenmode coordinates $\boldsymbol{Q}$ can be found using the quantum-mechanical position-position correlation functions as described in the remainder of this Section.

The commutator correlation function

Consider a *commutator correlation function* defined as

$$D_{AB}(t) = \langle [\hat{A}, \hat{B}(t)] \rangle \,, \tag{4.10}$$

where $\hat{A}$ and $\hat{B}$ are two operators and $[\cdot]$ denotes a commutator,

$$[\hat{A}, \hat{B}] = \hat{A}\hat{B} - \hat{B}\hat{A}.$$

Denoting the time evolution operator as $\hat{U}(t) = e^{-\imath \hat{H} t/\hbar}$ and using

$$\begin{aligned} C_{AB}(t) = \langle \hat{A}\hat{B}(t) \rangle &= \langle \psi_0 | \hat{A}\hat{U}^\dagger(t)\hat{B}\hat{U}(t)|\psi_0\rangle = \langle \hat{U}(t)\hat{A}^\dagger\psi_0 | \hat{B}\psi(t)\rangle \\ &= \left\langle \hat{B}\psi(t) \,\middle|\, \hat{U}(t)\hat{A}^\dagger \,\middle|\, \psi_0 \right\rangle^* = \langle \psi_0 | \hat{U}^\dagger(t)\hat{B}^\dagger U(t)\hat{A}^\dagger|\psi_0\rangle^* = \langle \hat{B}^\dagger(t)\hat{A}^\dagger\rangle^* , \end{aligned} \tag{4.11}$$

one obtains the following relationship for two Hermitian operators $\hat{A}$ and $\hat{B}$,

$$C_{AB}(t) = \langle \hat{A}\hat{B}(t)\rangle = \langle \hat{B}(t)\hat{A}\rangle^* . \tag{4.12}$$

Therefore, the commutator correlation function $D_{AB}(t)$ is simply proportional to the imaginary part of the usual quantum correlation function $C_{AB}(t)$,

$$D_{AB}(t) = 2\imath\Im(\langle \hat{A}\hat{B}(t)\rangle) = 2\imath\Im\left(C_{AB}(t)\right) \tag{4.13}$$

The eigenmodes can be analyzed using correlation functions of the position operators $\hat{A} = x_i$ and $\hat{B} = x_j$. The classical position-position functions are widely used

in molecular dynamics [47]. Interpretation of the imaginary part of the QM position-position function of Eq. (4.13) as the commutator underscores the difference between the quantum and classical descriptions.

If there is a linear transformation of the coordinates which takes the Hamiltonian into a separable form, then expressing Eq. (4.13) in these transformed coordinates,

$$x_i = \sum_j T_{ij}^T Q_j = \sum_j T_{ji} Q_j, \tag{4.14}$$

choosing the operators as $\hat{A} = x_i$ and $\hat{B} = x_j$, and using the commutation relationship $[Q_j, Q_k(t)]_{k \neq j} = 0$, one obtains

$$\begin{aligned} D_{x_i x_j}(t) &= \langle [x_i, x_j(t)] \rangle = \langle [\sum_k T_{ki} Q_k, \sum_l T_{lj} Q_l(t)] \rangle \\ &= \sum_{k,l} T_{ki} T_{lj} \delta_{kl} \langle [Q_k, Q_l(t)] \rangle = \sum_k T_{ki} T_{kj} \langle [Q_k, Q_k(t)] \rangle \end{aligned} \tag{4.15}$$

Specifically, for $\hat{A} = \hat{B} = x_i$,

$$D_{x_i x_i}(t) = \sum_k T_{ki}^2 \langle [Q_k, Q_k(t)] \rangle . \tag{4.16}$$

For a fully separated Hamiltonian, the cross-correlation functions ($i \neq j$) are zeros since each DOF contributes only to a single mode, i. e. $T_{ki} T_{kj} = 0$.

The harmonic oscillator

For the harmonic oscillator the commutator correlation function $D_{AB}(t)$ of Eq. (4.15) is analytical. For each normal mode coordinate Q_k characterized by the frequency ω_k, in the Heisenberg representation the time-evolution is included in the operator Q_k (P_k is the conjugate momentum operator to Q_k)

$$\hat{Q}_k(t) = \hat{Q}_k \cos(\omega_k t) + \frac{\hat{P}_k}{\omega_k} \sin(\omega_k t). \tag{4.17}$$

Using the commutation relations between the operators in the normal coordinates

$$[\hat{Q}_k, \hat{Q}_k] = 0, \quad [\hat{Q}_k, \hat{P}_k] = \imath\hbar \tag{4.18}$$

in Eq. (4.15) one obtains the correlation function,

$$D_{x_i x_j}(t) = \imath\hbar \sum_k \omega_k^{-1} T_{ki} T_{kj} \sin(\omega_k t). \tag{4.19}$$

With Eq. (4.13), this gives

$$\Im(C_{x_i x_j}(t)) = \frac{\hbar}{2} \sum_k \omega_k^{-1} T_{ki} T_{kj} \sin(\omega_k t) \tag{4.20}$$

whose Fourier Transform (FT), in turn, yields:

$$\mathcal{F}[\Im(C_{x_i x_j})] = \frac{1}{2\pi} \int_{-\infty}^{\infty} \Im(C_{x_i x_j}(t)) e^{-\imath\omega t}\, dt \tag{4.21}$$

$$= \sum_k \frac{\hbar}{4\omega_k} T_{ki} T_{kj} \left(\delta(\omega - \omega_k) - \delta(\omega + \omega_k)\right) \tag{4.22}$$

Considering just the positive frequencies in Eq. (4.22), the FT of the auto-correlation function $C_{x_i x_i}(t)$,

$$\mathcal{F}[\Im(C_{x_i x_i})] = \frac{\hbar}{4} \sum_k \omega_k^{-1} T_{ki} T_{ki} \delta(\omega - \omega_k) \tag{4.23}$$

gives the frequencies of all the normal modes (labeled k) involving the i^{th} DOF, i.e. of the modes for which $T_{ki} \neq 0$. The quantity T_{ki}^2 measures the contribution of the i^{th} DOF to the k^{th} mode. To compensate for the ω_k^{-1} on the right-hand-side of Eq. (4.23), one can use the FT of the time-derivative of $\Im(C_{x_i x_j})$, which also corresponds to the position-momentum correlation function. Equivalently, $\mathcal{F}[\Im(C_{x_i x_i})]$ can be simply multiplied by ω to have the peaks in the FT weighted by the elements of the transformation matrix.

The relative sign of contributions from x_i and x_j to the k^{th} mode can be deduced by the sign of the corresponding peak at $\omega = \omega_k$ in the FT of the cross-correlation functions $C_{x_i x_j}(t)$. In numerical implementation the δ-function in the FT of Eq. (4.23) is represented by the Gaussian function of finite amplitude and width,

$$\delta(\omega - \omega_k) = \lim_{\epsilon \to 0} \sqrt{\frac{1}{4\pi\epsilon}} \exp\left(-\frac{(\omega - \omega_k)^2}{4\epsilon}\right). \tag{4.24}$$

The parameter ϵ defines damping of the 'signal' $\Im(C_{AB})$, multiplied by $g(t) = \exp(-\epsilon t^2)$ before the FT is performed, and is related to the temporal length of $\Im(C_{AB})$. Note,

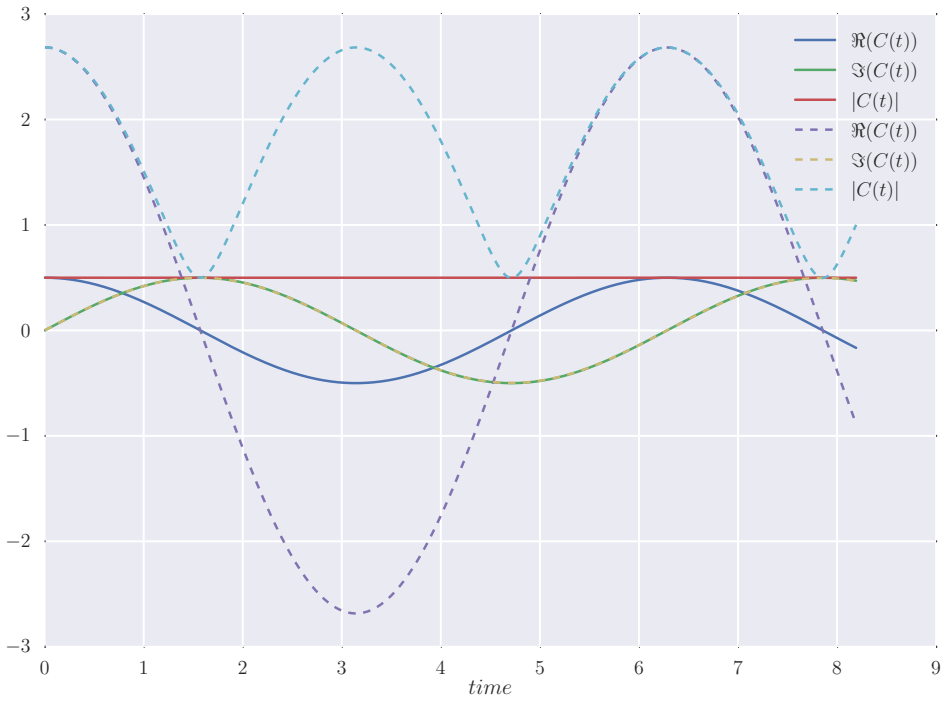

Figure 4.1: $C_{xx}(t)$ for a harmonic oscillator of frequency $\omega_1 = 1$ for two different initial wavefunctions labeled 1 and 2 and specified in Table 4.1.

that for the harmonic oscillator the commutator correlation functions are *independent* on the initial wavefunction $\psi(\boldsymbol{x}, 0)$. This fact is illustrated in Fig. 4.1 for three different Gaussian wavefunctions evolving in the harmonic potential of frequency $w = 1$. The parameters of the initial wavefunction, taken as a Gaussian,

$$\psi_0(x) = \left(\frac{2\alpha}{\pi}\right)^{1/4} e^{-\alpha(x-x_0)^2}, \tag{4.25}$$

are listed in Table 4.1.

Anharmonic systems

If the potential is anharmonic yet separable in some unknown set of linear coordinates specified by the unitary transformation matrix T, then the eigenmodes are well defined. The commutator correlation functions in terms of the elements of T are given

by Eqs (4.15) and (4.16). To analyze the correlation functions let us use a complete set of the eigenstates of the Hamiltonian:

$$\hat{H}\phi_n = \hbar\omega_n\phi_n.$$

Denoting the excitation energies ω_{kn},

$$\omega_{kn} = \omega_k - \omega_n, \tag{4.26}$$

and inserting the resolution of identity $\mathcal{I} = \sum_n |\phi_n\rangle \langle\phi_n|$ in Eq. (4.11) three times one obtains

$$\begin{aligned} C_{AB}(t) &= \sum_{m,n,k} \langle\psi_0|\phi_m\rangle \langle\phi_m|AU^\dagger(t)\phi_n\rangle \langle\phi_n BU(t)\phi_k\rangle \langle\phi_k|\psi_0\rangle \\ &= \sum_{k,n} c_k \left(\sum_m c_m^* A_{mn}\right) B_{nk} e^{-\imath\omega_{kn}t}, \end{aligned} \tag{4.27}$$

where the coefficient c_k is the projection of ψ_0 on the eigenstates ϕ_k, $c_k = \langle\phi_k|\psi_0\rangle$, and A_{mn}, B_{mn} are the matrix elements of operators $\hat{A}$ and $\hat{B}$ evaluated in the basis $\{\phi_n\}$. The FT of the correlation function (4.27) exhibits peaks at the excitation energies:

$$\mathcal{F}[C_{AB}](\omega) = \frac{1}{2\pi}\int_{-\infty}^{\infty} C_{AB}(t)e^{+\imath\omega t}\,dt = \sum_{k,n} c_k \left(\sum_m c_m^* A_{mn}\right) B_{nk}\delta(\omega - \omega_{kn}). \tag{4.28}$$

For an anharmonic system the matrix elements of the position operator are generally nonzero, $B_{nk} \neq 0$, though the largest magnitudes are expected for $B_{n,n\pm1}$. Thus, for an arbitrary initial wavefunction which is a superposition of many eigenstates, the FT gives peaks at the excitation energies. Furthermore, it is possible to identify which DOFs contribute to each mode by analyzing the relative peak heights in the FTs of the correlation functions $D_{AB}(t)$, where $\hat{A}$ and $\hat{B}$ are the position operators $\{x_1, \ldots, x_f\}$. The relative heights of the peaks depend on the matrix elements of T. For the peaks in FTs of $D_{x_ix_i}$ and $D_{x_ix_j}$ at the same ω_{kn} for any n we have:

$$\frac{\mathcal{F}[\Im(C_{x_ix_i})](\omega = \omega_{kn})}{\mathcal{F}[\Im(C_{x_jx_j})](\omega = \omega_{kn})} = \left(\frac{T_{ki}}{T_{kj}}\right)^2. \tag{4.29}$$

Therefore, for an anharmonic systems with separable potential, the anharmonicity will result in having peaks for various vibrational excitation corresponding to that anharmonic mode ($0 \to 1,\ 1 \to 2$ and so on). The peak intensities will depend on the initial wavefunction $\psi(\boldsymbol{x}, 0)$. However, the initial wavefunction has no influence on the relative peak height: in other words, for each peak belonging to anharmonic mode k, the pattern or the contribution from each DOF remains the same, as illustrated in Section 4.3 describing separable models and a weakly coupled system.

4.3 Implementation and numerical examples

Illustration of the formalism is given for model two-dimensional systems using the split-operator Fast Fourier Transform method [59, 21] to compute time-dependent QM correlation functions. To mitigate the effect of finite propagation time the correlation functions are multiplied by the damping function $g(t) = \exp(-\epsilon t^2)$,

$$\tilde{f}(\omega) = \frac{1}{2\pi} \int_{-\infty}^{\infty} f(t) e^{-\imath\omega t - \epsilon t^2} dt. \tag{4.30}$$

The parameter ϵ was set to have $g(t_f) = 10^{-4}$ at the final propagation time t_f. The damping does not shift the peak positions but somewhat affects the peak magnitudes [85]. We start with real wavefunctions ψ_0 and use symmetry in forward/backward evolution in time,

$$\psi(\boldsymbol{x}, -t) = \psi^*(\boldsymbol{x}, t), \quad C_{AB}(-t) = \langle AB(-t) \rangle = C^*_{AB}(t). \tag{4.31}$$

Then, the imaginary part of $C_{AB}(t)$ is odd with respect to time, and the FT over infinite time, $t = (-\infty, \infty)$, is reduced to

$$\mathcal{F}[f](\omega) = \frac{1}{\pi} \int_{0}^{\infty} f(t) \sin(\omega t) e^{-\epsilon t^2} dt. \tag{4.32}$$

Coupled harmonic system

Consider a system of two coupled harmonic oscillators ($f = 2$),

$$\hat{H} = \frac{1}{2}(\hat{p}_x^2 + \hat{p}_y^2) + V(x, y), \tag{4.33}$$

where

$$V = \frac{1}{2}(x^2 + y^2) + 0.4xy \tag{4.34}$$

The Hessian matrix is diagonalized, $H = U^\dagger D U$, by the unitary transformation U:

$$U = \begin{pmatrix} \frac{\sqrt{2}}{2} & -\frac{\sqrt{2}}{2} \\ \frac{\sqrt{2}}{2} & \frac{\sqrt{2}}{2} \end{pmatrix}, \quad D = \begin{pmatrix} 1.4 & 0.0 \\ 0.0 & 0.6 \end{pmatrix}$$

The initial wavefunction is chosen as a real displaced Gaussian wavepacket,

$$\psi_0(x, y) = \left(\frac{\alpha_1 \alpha_2}{\pi^2}\right)^{1/4} e^{-(\alpha_1(x-x_0)^2 + \alpha_2(y-y_0)^2)/2}, \tag{4.35}$$

where (x_0, y_0) is the center of a Gaussian and (α_1, α_2) define its dispersion.

The FTs of the imaginary parts of C_{xx}, C_{xy} and C_{yy} are shown in Fig. 4.2. The initial wavefunction is specified in Table 4.1. Due to symmetry, the results for C_{xx} and C_{yy} are superimposed on the graph. All the information about the collective motion of the system is contained in Fig. 4.2. There are two normal modes and the coordinates are making equal contribution to both modes, as seen from the ratio of peak intensities of the diagonal functions, C_{xx} and C_{yy}. The relative phase is contained in the cross-correlation function C_{xy}. The peaks near $\omega_1 = 0.78$ show that the contributions from the two DOFs are of equal magnitude and opposite sign, which corresponds to the symmetric stretch, $Q_1 = (x - y)/\sqrt{2}$. The peaks near $\omega_2 = 1.18$ are of the same magnitude and sign, corresponding to the anti-symmetric stretch $Q_2 = (x + y)/\sqrt{2}$.

Anharmonic models

In anharmonic systems the imaginary part of position-position quantum correlation depends on the initial wavefunction, but the excitation energies and relative peak

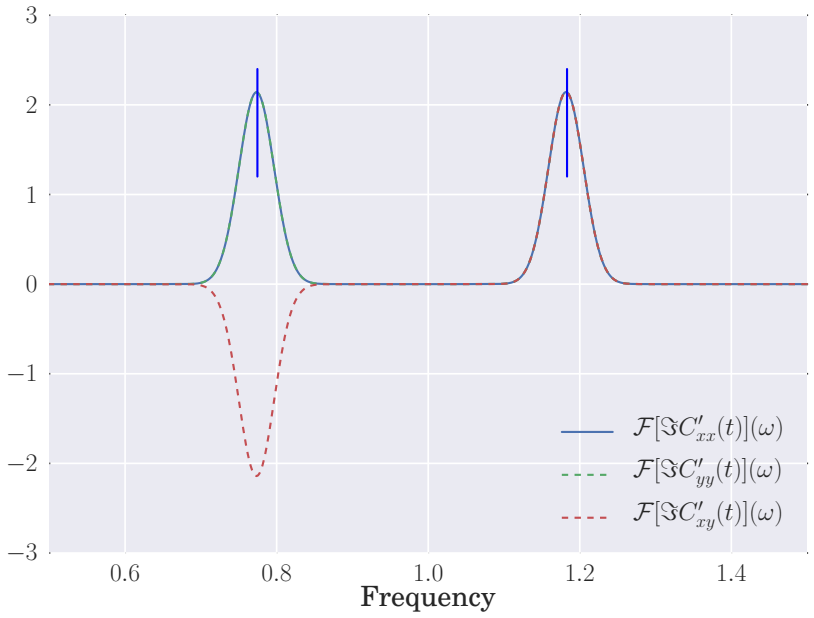

Figure 4.2: The 2D harmonic oscillator model (Eq. (4.34)). The FTs of the imaginary parts of C_{xx}, C_{yy} and C_{xy} multiplied by w. The vertical blue lines mark the analytical frequencies.

intensities in the corresponding FTs do not. To contrast with the harmonic oscillator example of Section 6.2, we examine the imaginary part of the quantum correlation function for the one-dimensional Morse potential,

$$V(x) = D_e(1 - e^{-x})^2, \quad D_e = 2\ E_h. \tag{4.36}$$

The imaginary parts of $C_{xx}(t)$ for different initial Gaussian wavefunctions, described in Table 4.1, shown in Fig 4.3, clearly depend on the initial wavefunction. (This dependence can be used to assess the anharmonicity of the potential.) Thus, the absolute intensity of the peaks of the corresponding FTs will depend on the initial wavefunction, but it is irrelevant for the analysis of the eigenmodes as illustrated below for a two-dimensional system. The relative peak intensities, i.e. the contributions of DOFs i and j to the eigen-mode k are $|T_{ki}/T_{kj}|^2$. Formally, they are independent on the chosen wavefunction, though certain peak intensities can be very small due to the particular choice of the wavefunction.

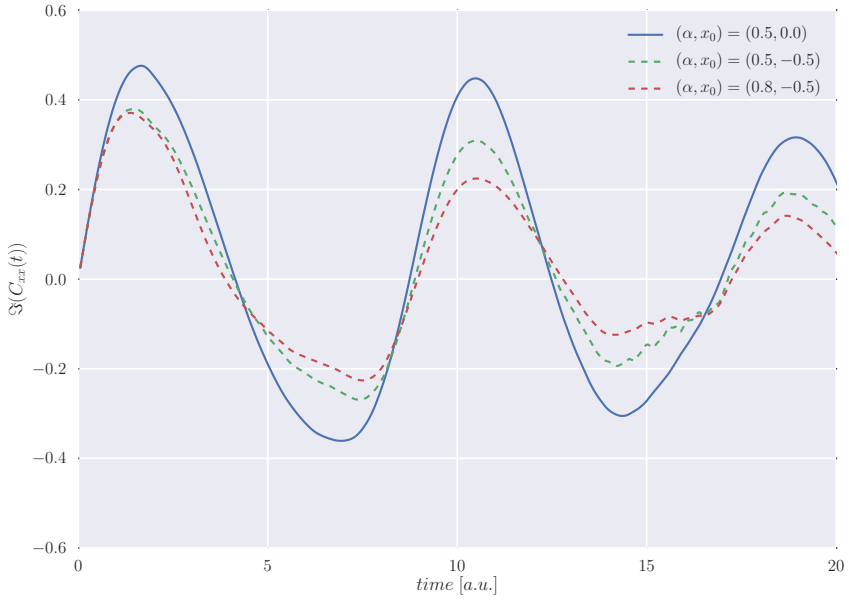

Figure 4.3: $\Im(C_{xx})$ as a function of time t for two initial wavefunctions (Table 4.1) evolving in the Morse potential of Eq. (4.36).

Let us consider a two-dimensional model potential,

$$V(x,y) = \frac{1}{6}(x^2 - 4\sqrt{2}xy - y^2) + \frac{1}{18}(x^4 - 4\sqrt{2}x^3y + 12x^2y^2 - 8\sqrt{2}xy^3 + 4y^4) - \frac{1}{8} \quad (4.37)$$

Fig. (4.4) shows the contour plot of this potential: it is a two-dimensional double well potential in the transformed coordinates, and the transformation of coordinates making the Hamiltonian separable is not apparent. To extract the anharmonic mode information from the quantum correlation functions, we start with an arbitrary chosen Gaussian wavepacket to compute C_{xx}, C_{xy} and C_{yy}. The final time of propagation was $t_f = 160$ a.u. Fig. (4.5) shows the FT of $\omega\Im(C_{\mu\nu})$. There are two distinct collective coordinates for this potential. The three positive peaks centered at the excitation energy of $w = 1$ come from the the harmonic collective coordinate. The corresponding coefficients of the transformation matrix are found from the ratio of the peaks,

$$\frac{\mathcal{F}[\Im(C_{xx})]}{\mathcal{F}[\Im(C_{yy})]} = \frac{|T_{11}|^2}{|T_{12}|^2}.$$

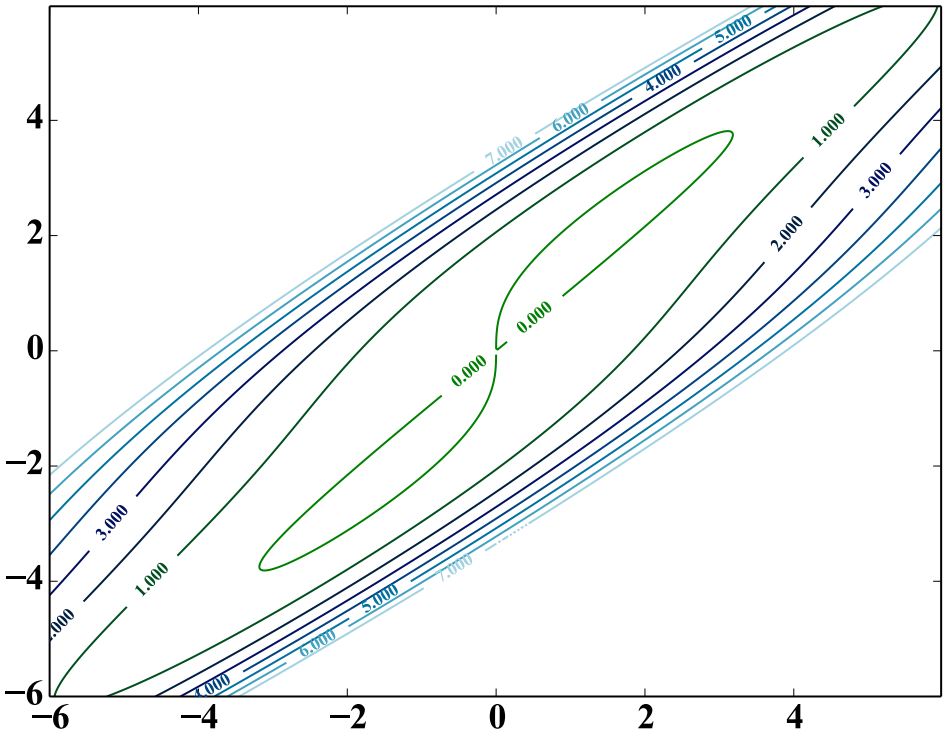

Figure 4.4: A contour plot of the two-dimensional anharmonic potential.

Figure 4.5: The Fourier Transforms of the imaginary parts of C_{xx}, C_{yy} and C_{xy} (multiplied by w) for the double-well potential as a function of frequency (energy).

After normalization condition is imposed, $|T_{11}|^2 + |T_{12}|^2 = 1$, the matrix elements are: $T_{11} \approx 0.816$, $T_{12} = 0.578$. The peaks centered near excitation frequencies $w = \{1.2,\ 1.7,\ 1.85\}$ all come from the anharmonic collective coordinate, as can be seen from the 'pattern' of the peak. The relative contributions from x and y for these two peaks are the same at the three excitation energies (Table 4.2). The negative value of the peak in $\mathcal{F}[\Im(C_{xy})]$ indicates that the contributions from x and y into this eigenmode are of opposite sign. The corresponding elements of the transformation matrix deduced from the FTs is in agreement with the analytical values listed in Table 4.3. The peaks are located at excitation energies for the $0 \rightarrow 1$, $1 \rightarrow 2$ and $2 \rightarrow 3$ transitions of the anharmonic collective coordinate.

A non-separable model

Finally, we examine a non-separable system by adding a coupling term to the previous two-dimensional potential. The coupled potential, V^c, is

$$V^c = V(x, y) + \varepsilon xy, \tag{4.38}$$

where the parameter ε controls the coupling and $V(x, y)$ is defined by Eq. (4.37). The analysis of Section 6.2 is no longer exact, however, the main eigenmode features in the Fourier Transforms of C_{xx}, C_{xy} and C_{yy} persist, at least in the weak coupling regime. The Fourier Transforms are shown in Fig. 4.6 for the three coupling values, $\varepsilon = \{0.01, 0.04, 0.08\}$. The peaks obtained from the three correlation functions line up at the frequency of the excitation energy as in the uncoupled case. The frequency positions shift according to the changes of the corresponding eigen-energies of the coupled systems. In the Figure we use the same labels – H, A, B and C – as for the peaks of the uncoupled system in Fig. 4.5. In addition we see a new peak D emerging as the coupling strength increases. We identify this peak as coming from the transition $(1, 0) \rightarrow (0, 2)$, where the pair (n_{ho}, n_{dw}) lists the quantum numbers correlating with the quantum numbers of the harmonic and the anharmonic collective coordinates of the uncoupled system, respectively. The exact excitation energies, computed as the difference of the appropriate energy levels, corresponding to the peaks in Fig. 4.6 are listed in Table 4.4. Which peaks in the FT have sizable amplitudes is understood as follows. The peaks correspond to the transitions between eigenstates contributing to the correlation functions and, thus, depend on the initial wavefunction. Without the coupling, the chosen Gaussian initial wavefunction ψ_0 (labeled '2D quartic' in Table 4.1), describes the ground state of the harmonic oscillator mode and has overlap close to 1 with the ground state of the double-well mode. Due to the structure of position-position correlation functions – $C = \langle \dots \hat{x} | \psi \rangle$ and so on – these correlation functions also capture contributions from the first excited state of both modes, and

in case of the double-mode also from the second and third excited states. Denoting the eigenfunctions of the Hamiltonian without the mode coupling as ϕ_n^{hw} and ϕ_n^{dw}, the non-zero overlaps relevant to the transitions the energy range $\omega = [0.9, 2]$ of Fig. 4.6 are:

$\langle\psi\|\phi_0^{hw}\rangle = 1$	$\langle\psi\|\phi_0^{dw}\rangle = 0.997$	$\langle\psi\|\phi_1^{dw}\rangle = 0.018$
$\langle\psi\|x\|\phi_0^{hw}\rangle = 1$	$\langle\psi\|y\|\phi_0^{dw}\rangle = 0.968$	$\langle\psi\|y\|\phi_1^{dw}\rangle = 0.181$

Without the coupling the transition $(1, 0) \rightarrow (0, 2)$ has negligible amplitude as the quantum number of the double-well mode changes by 2. With the coupling the modes are no longer separable and the amplitude of the corresponding peak D around $\omega \approx 1.75$ increases with the coupling strength.

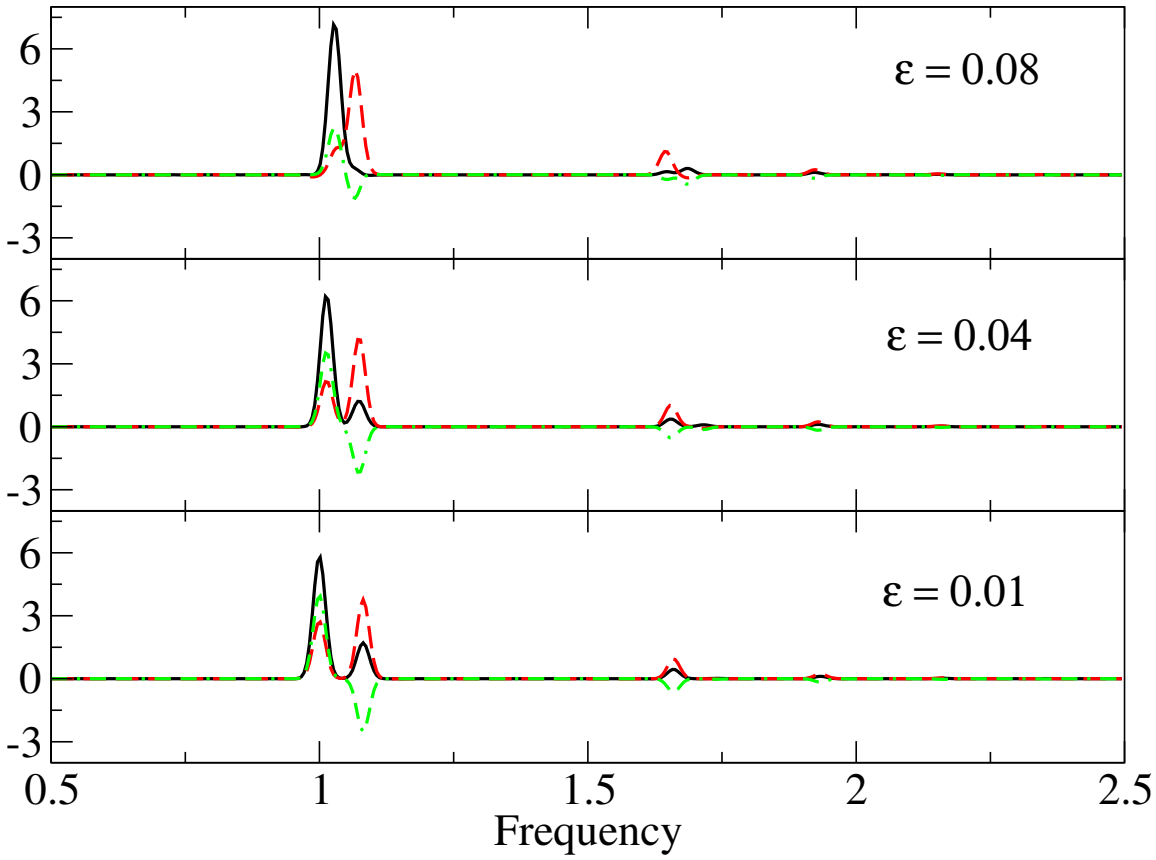

Figure 4.6: The Fourier Transforms of the imaginary parts of C_{xx}, C_{yy} and C_{xy} for the coupled anharmonic potential as a function of frequency (energy)

Overall, similar structure of the spectra in Figs 4.5 and 4.6 means that in the

regime of weak coupling there still is a transformation of coordinates which uncouples the Hamiltonian in a limited sense or, in other words, minimizes mode coupling at low energies. Since in the transformed coordinates the effects of coupling are shifted to higher energy, the analysis of position-position correlation functions may still be useful to identify the low-energy collective modes.

4.4 Conclusion

We have shown that for an anharmonic separable system information about the collective modes of motion can be extracted from the commutator correlation function given by the imaginary part of the quantum position-position correlation function. For a harmonic system the imaginary part (unlike the real part) of the quantum correlation function is independent of the wavefunction used to obtain the quantum correlation function. In other words, it contains the information about the Hamiltonian, not about the specific state of the system. For anharmonic systems, the imaginary part does depend on a wavefunction whose correlation function is computed. However, the collective or eigenmodes of the Hamiltonian, are defined by the ratio of intensities in the FT of the correlation function for each peak which is generally independent on the wavefunction choice. The relative sign of the contributions from various DOFs can be found from the cross-correlation functions of the type $\langle x(0)y(t)\rangle$. The peak positions give the excitation energies and, therefore, correspond to the peaks in a rovibrational spectrum, even though the energy levels themselves are not readily obtained from the FTs of correlation functions alone. The analysis of commutator correlation functions is exact to Hamiltonians that can be made separable by a linear transformation in a set of linear coordinates, but does not invoke the harmonic approximation of the potential as does the normal modes analysis. The the commutator-correlation approach reveals collective modes of anharmonic systems, including those with multiple minima in the potential energy surface. The approach is also applicable in the

Table 4.1: The parameters of the initial Gaussian wavepacket ψ_0 for the model systems considered. For the two-dimensional systems $\alpha_1 = \alpha_2 \equiv \alpha$.

ψ_0	Model	α [a_0^{-2}]	x_0 [a_0]	y_0 [a_0]	Model	α [a_0^{-2}]	x_0 [a_0]	y_0 [a_0]
1	1D HO	0.5	0.0		1D Morse	0.5	0.0	
2		2	-1.6			0.5	-0.5	
	2D HO	1.0	-1.6	-1.6	2D quartic	0.5	0.0	0.0

Table 4.2: Peak intensities $I_{\mu\nu}$ in the Fourier Transforms of the correlation functions, $\mathcal{F}[\Im(C_{\mu\nu})]$. The excitation energy of the harmonic mode is labeled H. The three excitation energies of the double-well mode are labeled A, B and C. Exact excitation energies are listed in the last column

Peak	ω^{FT}	I_{xx}	I_{yy}	I_{xy}	$\frac{I_{yy}}{I_{xx}}$	$\frac{I_{xy}}{I_{xx}}$	ω^{exact}
H	0.996	2.860	1.433	2.019	0.501	0.707	1.0
A	1.081	0.910	1.815	-1.280	1.995	-1.407	1.088
B	1.663	0.232	0.463	-0.328	1.996	-1.414	1.665
C	1.934	0.0563	0.113	-0.080	2.000	-1.415	1.937

Table 4.3: The transformation matrix elements obtained from the relative peak intensities listed in Table 4.2.

	Harmonic mode		Anharmonic mode	
	T_{11}	T_{12}	T_{21}	T_{22}
Numerical	0.816	0.578	0.577	-0.816
Analytical	0.816	0.577	0.577	-0.816

regime of weak mode-coupling, which is the case for most vibrational motions which, in practice, can be unraveled spectroscopically.

In the presented examples accurate quantum correlation functions have been used, which will not be a practical strategy for high-dimensional systems. The practical aspects of the collective mode analysis utilizing the quantum correlation functions for realistic molecular systems will be examined in the future.

Table 4.4: Excitation energies for the coupled system (differences between the energy levels) for various coupling parameter ε.

(n_{ho}, n_{dw})	$(0,0) \rightarrow (1,0)$	$(0,0) \rightarrow (0,1)$	$(0,1) \rightarrow (0,2)$	$(0,2) \rightarrow (0,3)$	$(1,0) \rightarrow (0,2)$
ε	peak H	peak A	peak B	peak C	peak D
0	1.000	1.088	1.665	1.937	1.7531
0.01	1.005	1.086	1.663	1.936	1.7443
0.04	1.018	1.078	1.658	1.931	1.7185
0.08	1.032	1.071	1.649	1.925	1.6876

Chapter 5

Symmetrization of the nuclear wavefunctions defined by the quantum trajectory dynamics.

n a rigorous quantum-mechanical (QM) description of indistinguishable particles the correct symmetry is often built-in into the form of an approximate wavefunction, with the electronic wavefunctions constructed as the Slater determinants of the single-particle functions being the prime example. In contrast, when evaluating QM effects for the nuclei, often described by approximate wavefunctions of full dimensionality, the wavefunction symmetry can be included directly into calculation of expectation values. The straightforward implementation, however, may be impractical for a large system due to factorial scaling of particle permutations. In this work the leading correction due to the wavefunction symmetrization within the quantum trajectory (QT) framework is presented. The correction is based on the non-symmetrized wavefunction evolved using QT dynamics with empirical friction, yielding the lowest energy states. Use of symmetry improves the accuracy and efficiency of this dynamics approach as shown on model systems of up to four dimensions.

5.1 Introduction

This work is motivated by a recent study of determining the ground state of solid He^4 using the approximate quantum trajectory (QT) dynamics with friction [43]. The system was represented within a simulation cell of 180 atoms; all nuclei were treated as quantum particles, but the Bose-Einstein statistics of the nuclei has not

been taken into account. While the effect of quantum statistics in this system may be small, though of interest in light of recent experiments [**? ? ? ? ? ?**], a practical approach to wavefunction symmetrization is desirable for generality of the QT-based dynamics and is essential for its possible extensions to dynamics of electrons.

The QT ensemble is a representation of a wavefunction evolving in time according to the time-dependent Schrödinger equation,

$$\hat{H}\psi = \imath\hbar\frac{\partial}{\partial t}\psi, \tag{5.1}$$

with the usual QM Hamiltonian,

$$\hat{H} = \hat{K} + V, \quad \hat{K} = -\frac{\hbar^2}{2m}\nabla^2. \tag{5.2}$$

For simplicity, all particles are considered identical of mass m, and the atomic units, i. e. $\hbar = 1$, are used henceforth. The arguments of functions are suppressed when unambiguous. Bold face variables denote vectors. The vector $\boldsymbol{x}$ is a vector of all the particle coordinates; ∇ is the vector of the spatial partial derivatives. The small case ψ denotes a wavefunction $\psi \equiv \psi(\boldsymbol{x}, t)$ of no particular symmetry, while the capital Ψ will be used for the symmetrized functions. An external classical potential $V \equiv V(\boldsymbol{x})$ is symmetric with respect to any permutation of the particles.

The complex wavefunction can be written in polar form in terms of the amplitude and phase,

$$\psi(\boldsymbol{x}, t) = |\psi(\boldsymbol{x}, t)| \exp(\imath S(\boldsymbol{x}, t)). \tag{5.3}$$

The quantum or Bohmian trajectories are defined by the following relation between their momenta and the wavefunction phase $S(\boldsymbol{x}, t)$ [7],

$$\boldsymbol{p} = \nabla S. \tag{5.4}$$

As follows from the TDSE (5.1), the time-evolution of the phase is given by the quantum Hamilton-Jacobi equation,

$$-\frac{\partial S}{\partial t} = \frac{\boldsymbol{p}\cdot\boldsymbol{p}}{2m} + V + U, \tag{5.5}$$

where U is the quantum potential,

$$U \equiv U(\boldsymbol{x}, t) = -\frac{\nabla^2|\psi|}{2m|\psi|}. \tag{5.6}$$

The QT positions, $\boldsymbol{x}_t$, and momenta, $\boldsymbol{p}_t$, evolve in time under the influence of the combined potential $V+U$, according to the usual Newton's equations of motion (see, for example, Ref. [93] for full details):

$$\frac{d\boldsymbol{x}_t}{dt} = \frac{\boldsymbol{p}_t}{m}, \quad \frac{d\boldsymbol{p}_t}{dt} = -\nabla(V+U)|_{\boldsymbol{x}=\boldsymbol{x}_t}. \tag{5.7}$$

The time-evolution of the probability density $|\psi|^2$ satisfies the continuity equation. A useful consequence of that is conservation in time of the trajectory 'weight', $w(\boldsymbol{x}_t)$, which is a probability of finding a particle within the associated volume element $\delta\boldsymbol{x}_t$,

$$w(\boldsymbol{x}_t) \equiv |\psi(\boldsymbol{x}, t)|^2 \delta\boldsymbol{x}_t = |\psi(\boldsymbol{x}, 0)|^2 \delta\boldsymbol{x}_0. \tag{5.8}$$

The quantum potential describes contribution to the kinetic energy due to the wavefunction localization, and the combined potential $U+V$ guides the motion of the QTs. Thus, in the QT framework all QM effects are formally attributed to the effect of the quantum potential. Therefore, the idea of including the effect of quantum statistics, i. e. of the wavefunction symmetry, through an additional potential is appealing. Such a potential, termed the Pauli potential, has been introduced in nuclear physics [**?**].

The Pauli potential arises from the symmetrized form of a wavefunction describing identical particles [4], and is interpreted as a correction to the kinetic energy operator. (To simplify notations we will consider one-dimensional particles described by the Cartesian coordinates (x, y) until Section 6.2.) In the case of two fermions, each described by a single-particle function, specifically by a one-dimensional Gaussian function,

$$g_a(x) = \exp\left(-\frac{\alpha}{2}(x-q_a)^2 + \imath p_a(x-q_a)\right)\left(\frac{\alpha}{\pi}\right)^{1/4}, \tag{5.9}$$

the two-dimensional wavefunction $\psi(x, y)$ written as the Slater determinant is:

$$\Psi_g(x,y) = \mathcal{N}(g_a(x)g_b(y) - g_b(x)g_a(y)), \quad \mathcal{N} = \langle |g_a(x)g_b(y) - g_b(x)g_a(y)|^2 \rangle^{-1/2}. \tag{5.10}$$

The kinetic energy of the particles described by the wavefunction (5.10) becomes:

$$\hat{K}_g = \frac{p_a^2 + p_b^2}{2m} + \frac{\alpha}{2m} + \bar{P}, \tag{5.11}$$

where the last right-hand-side (RHS) term $\bar{P}$ labels the Pauli potential. The first term in the RHS of Eq. (5.11) is the classical kinetic energy of the Gaussian centers. The middle term can be identified with the expectation value of the quantum potential of Eq. (5.6) for the two-dimensional, i. e. two-particle, system,

$$\langle \Psi_g | U | \Psi_g \rangle = \frac{\alpha}{2m}. \tag{5.12}$$

The Pauli potential is defined as:

$$\bar{P} = \frac{\alpha}{2m} \frac{X_{ab}}{\exp(X_{ab}) - 1}, \tag{5.13}$$

where the quantity X_{ab} is the phase space distance between the two particles:

$$X_{ab} = \frac{1}{2}\left(\alpha(q_a - q_b)^2 + (p_a - p_b)^2/\alpha\right). \tag{5.14}$$

The Gaussian parameters $\{p_a, p_b, q_a, q_b\}$ are, generally, functions of time, which evolve classically in many popular Gaussian-based methods, such as Thawed and Frozen Gaussian Wavepacket Dynamics [48, 49, 51] and numerous other approaches. Intuitively, with the symmetry these parameters are expected to evolve classically under the influence of $\bar{P} + V$, with $\bar{P}$ preventing the fermions to be close to each other in the phase space. However, as shown in Ref. [**?**], such classical treatment is, generally, incorrect and a time-dependent variational principle with constraints is employed in more rigorous methods such as Fermionic Molecular Dynamics (FMD) and Antisymmetrized MD (AMD) [**? ? ? ? ?**].

Extending the idea of the Pauli potential to the QTs, whose dynamics is modified by the potential-like term generating QM effects, seems promising. However, we note that the Pauli potential $\bar{P}$ in Eq. (5.13) comes from the constrained form of the two-dimensional wavefunction $\Psi_g(x, y)$ of Eq. (5.10). In contrast, the QT formulation of the TDSE is exact. The resulting from it quantum potential U (ignoring singularities in U for the moment) arises from the polar form of an arbitrary wavefunction. Thus, without the single-particle function approximation no modifications of the Hamiltonian are needed to evolve the full-dimensional wavefunction (regardless of its approximate form). This conclusion is consistent with the analysis of the semiclassical electron dynamics based on Gaussian wavepackets [**?**]. The symmetry of the full-dimensional wavefunction can be incorporated explicitly into (i) the initial wavefunction or into (ii) computation of the desired dynamical properties, such as expectation values and correlation functions. For example, if the property is the lowest energy state of a specific symmetry, which can be obtained either from imaginary-time [72**?**] or dissipative dynamics [35], then, both options will accelerate convergence with time. In fact, we have constructed the Pauli-type potential from the symmetrized wavefunction 'on-the-fly' and implemented it in imaginary time. However, we found that this modification introduced instability into dynamics and did not offer computational benefits compared to option (ii).

In the remainder of the paper we illustrate the symmetrization effect on simple models for the imaginary-time and dissipative dynamics (Section 5.2), and describe a practical algorithm of estimating the symmetry effect within the quantum trajectory dynamics for multidimensional systems (Sections 6.2 and 5.4). Section 5.5 offers conclusions and outlook.

The imaginary-time dynamics (relaxation)

The imaginary-time QM evolution, introduced into molecular dynamics by Miller [72] and used to simulate temperature effects or to obtain low energy states [**?**], is defined by the TDSE restated for imaginary time,

$$\hat{H}\psi = -\frac{\psi}{t}. \tag{5.15}$$

Any initial wavefunction evolves into the lowest energy state (of a certain symmetry if present) at long times, as seen from the expansion of the time-dependent wavefunction in terms of the energy eigenstates, $\hat{H}\phi_n = E_n\phi_n$ for $n = \{0, 1, \dots\}$,

$$\psi(x, y, t) = \sum_n c_n\phi_n(x, y)e^{-E_n t} \quad \text{and} \quad c_n = \langle\phi_n(x, y)|\psi(x, y, 0)\rangle. \tag{5.16}$$

The wavefunction norm depends on time; to avoid exponential growth of the wavefunction norm, the energy scale is shifted so that $E_0 > 0$. As $t \to \infty$, a wavefunction of initially undefined symmetry approaches the ground state (unless it was orthogonal to it),

$$\psi(x, y, t) \to c_0\phi_0(x, y)e^{-E_0 t}, \quad E_t \equiv \langle\psi|\hat{H}|\psi\rangle_t \to E_0 \langle\psi|\psi\rangle_t . \tag{5.17}$$

The low-lying excited states, can be obtained from the imaginary time dynamics by removing the ground state from $\psi(x, y, t)$ by projection as done, for example, in Refs [**?** 23].

For a system of identical particles using the symmetry of the eigenstates under particle permutations,

$$\phi_n(y, x) = (-1)^n\phi_n(x, y), \tag{5.18}$$

one can construct explicitly symmetrized wavefunctions,

$$\Psi_{s/a}(x, y, t) = \sum_{n=0,1\dots} c_n \left(\phi_n(x, y) \pm \phi_n(y, x)\right) e^{-E_n t}. \tag{5.19}$$

The ground and the first excited states are the lowest energy states for the symmetric and antisymmetric functions, respectively. As $t \to \infty$, the symmetrized wavefunctions converge to their respective lowest energy states faster than a function of undefined symmetry due to cancellation of contributions from the states closest in energy:

$$\Psi_s(x,y,t) \to 2c_0\phi_0 e^{-E_0 t}, \quad \Psi_a(x,y,t) \to 2c_1\phi_1 e^{-E_1 t}. \tag{5.20}$$

The convergence with time in Eqs (5.20) is fast if the lowest pair of states is well separated from the higher energy states, $E_2 - E_1 \gg E_1 - E_0$.

This point is illustrated for a two-dimensional model of Hooke's atom with the following electron-electron repulsion,

$$V(x,y) = \frac{x^2+y^2}{2} + c(|x-y| - r_0)^2 + V_0. \tag{5.21}$$

The parameter values are listed in Table 5.1 and the electron mass is $m = 1$ in atomic units. The propagation is performed on the equidistant grid using the split-operator method and the Fast Fourier Transform [59, 21] as listed in Table 5.1. The initial non-symmetrized wavefunction $\psi(x,y,0)$ is a correlated two-dimensional Gaussian,

$$\psi(x,y,0) = N\exp(-\alpha(x-q_0)^2 - \alpha(y+q_0)^2 - 2\beta(x-q_0)(y+q_0)). \tag{5.22}$$

The wavefunction parameters are given in Table 5.1. The initial wavefunction is real and is localized in the left well of the potential. Panels (a-c) of Fig. 5.1 show footprints of the evolving non-symmetrized wavefunction, at times $t = \{0, 0.8, 1.0\}$ a.u. Panel (d) shows the energy computed for the non-symmetrized wavefunction and for the generated from it symmetric and antisymmetric wavefunctions $\Psi_{s/a}(x,y,t)$ as a function of time,

$$\Psi_{s/a} = N_{s/a}(\psi(x,y,t) \pm \psi(y,x,t)), \tag{5.23}$$

where $N_{s/a}$ normalizes wavefunctions to 1. The energies of $\Psi_{s/a}$ converge to their respective lowest energy values much sooner than the energy of $\psi(x,y,t)$: at $t = 0.75$

a.u. the energies of $\Psi_{s/a}$ are converged within five digits, while the energy of $\psi(x, y, t)$ is far from converging to E_0 at $t = 2.0$ a.u. as shown in Table 5.2. Shorter imaginary-time propagation is desirable even for exact QM methods, because the wavefunction norm exponentially decays with time which may results in the loss of numerical accuracy.

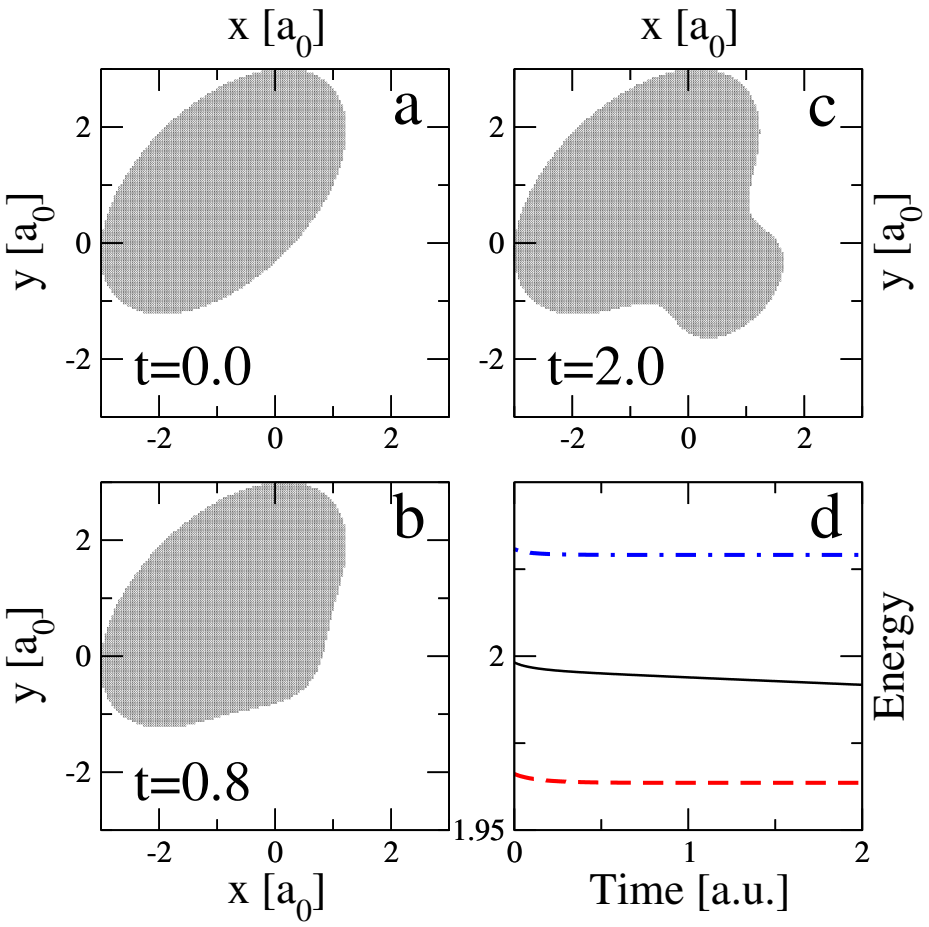

Figure 5.1: Imaginary time evolution in the two-dimensional double well. A footprint of a nonsymmetrized wavefunction for $t = \{0, 0.8, 2.0\}$ a.u. is shown on panels (a-c), respectively. The energies as functions of time for the non-symmetrized $\psi(t)$ and constructed from symmetric and antisymmetric wavefunctions are shown on panel (d) as black solid line, red dash and blue dot-dash, respectively.

Table 5.1: Parameters defining the two-dimensional double-well model and calculation of Section 5.2. The upper line lists the parameter values for the potential given by Eq. 5.21. The middle line defines the initial wavefunction $\psi(x, y, 0)$. The bottom line lists parameters of the QM propagation: N_p is the number of grid points per dimension; the grid is symmetric and x_{min} specifies its left boundary. All values are given in atomic units.

Potential V	$c = 4$	$r_0 = 2$	$V_0 = 2$
Wavefunction	$q_0 = -0.888$	$\alpha = 1$	$\beta = -0.5$
QM evolution	$dt = 0.002$	$N_p = 256$	$x_{min} = -5$

Table 5.2: Time-dependence of the energy for the non-symmetrized, symmetric and antisymmetric wavefunctions.

Time [a.u.]	E [E_h]	E^s [E_h]	E^a [E_h]
0.0	1.9982	1.9662	2.0308
0.8	1.9944	1.9636	2.0291
1.2	1.9935	1.9636	2.0291
2.0	1.9918	1.9636	2.0291

Quantum dynamics with friction (dissipation)

An alternative way of obtaining the lowest energy states is the dissipative quantum dynamics, in which the system looses energy via an empirical friction [35]. This formulation is well-suited for the trajectory-based dynamics methods as elaborated in Section 6.2. Here we only illustrate the effect of symmetry on the Gaussian dynamics in one dimension.

The energy dissipation is introduced into the conventional real-time TDSE via a non-linear term, dependent on the phase of the wavefunction S, and this empirical friction is controlled by the coefficient γ:

$$\imath \frac{\partial}{\partial t}\psi = \hat{H}\psi + \gamma \left(S - \langle S \rangle\right) \psi, . \tag{5.24}$$

The system looses energy due to friction force until the lowest energy state is reached,

$$\frac{dE}{dt} = -\frac{\gamma}{m} \langle \psi | (\nabla S)^2 | \psi \rangle. \tag{5.25}$$

The physical meaning of the dissipation term is transparent from the time-evolution

equations for QTs, following from Eq. (5.24):

$$\frac{dS}{dt} = \frac{\boldsymbol{p}\cdot\boldsymbol{p}}{2m} - V - U - \gamma(S - \langle S\rangle), \quad \frac{d\boldsymbol{x}_t}{dt} = \frac{\boldsymbol{p}_t}{m}, \quad \frac{d\boldsymbol{p}_t}{dt} = -\nabla(V+U)|_{\boldsymbol{x}=\boldsymbol{x}_t} - \gamma\boldsymbol{p}. \quad (5.26)$$

The dissipative term generates the friction force on QTs which is linear in velocity of a particle. The effect of friction vanishes once ψ evolved into an eigenstate, which is real up to an overall phase factor, because dissipation in Eq. (5.24) is defined with respect to the average phase of the wavefunction.

Unlike the imaginary-time dynamics, the dissipative TDSE is nonlinear and the eigenstate analysis is complicated. However, since the friction term is of the same spatial symmetry as the wavefunction itself, the effect of the wavefunction symmetrization on the ground state calculations is similar to the imaginary-time dynamics. The illustration below is given for a one-dimensional quadratic potential and the symmetry operation $x \to -x$. Consider dynamics with friction of a non-coherent Gaussian, describing a particle of $m = 1$ a.u.,

$$\psi(x,t) = \exp(-\alpha(t)(x - q(t))^2 + \imath p(t)(x - q(t)) + \imath s(t) + n(t)), \quad (5.27)$$

in a quadratic potential of frequency ω, $V = \omega^2 x^2/2$. Substitution of Eq. (5.27) into Eq. (5.24) determines the time-dependence of the parameters $\{\alpha, q, p, s, n\}$. Using $\alpha = \alpha_r + \imath\alpha_i$ and suppressing argument t, the evolution equations are as follows. The center of the Gaussian q moves classically under the influence of the friction force $F_{fr} = -\gamma p$:

$$\frac{dq}{dt} = p, \quad \frac{dp}{dt} = -\omega^2 q - \gamma p. \quad (5.28)$$

The action function s has classical, quantum and friction contributions:

$$\frac{ds}{dt} = \frac{p^2 - \omega^2 q^2}{2} - \alpha_r - \frac{\gamma}{4}\frac{\alpha_i}{\alpha_r}. \quad (5.29)$$

Parameter n normalizes the wavefunction:

$$\frac{dn}{dt} = \frac{1}{4\alpha_r}\frac{d\alpha_r}{dt} = \alpha_i. \quad (5.30)$$

The width parameter α evolves according to

$$\imath\frac{d\alpha}{dt} = 2\alpha^2 - \frac{\omega^2}{2} + \gamma\alpha_i. \tag{5.31}$$

Eq. (5.31) can be decomposed into real and imaginary parts, and is solvable analytically in the absence of friction, $\gamma = 0$. For the quadratic well, $\omega^2 > 0$, there is a special solution (coherent Gaussian) $\alpha_c = \omega/2$ at all times, regardless of friction. Generally, with time the width parameter converges to $\alpha = \omega/2$ for the quadratic well, and to $\alpha = 0$ in free space, $\omega = 0$, or for the parabolic barrier, $\omega^2 < 0$. Beyond the short times the convergence with time becomes exponential and the value of the exponent is inversely proportional to γ.

The effect of the wavefunction symmetrization is illustrated in Figs 5.2 and 5.3 for the value of $\omega = 1$. The symmetrized functions are simply constructed as

$$\Psi_{s/a}(x,t) = N_{s/a}\left(\psi(x,t) \pm \psi(-x,t)\right), \tag{5.32}$$

where $N_{s/a}$ is the time-dependent normalization constant. The initial wavefunction is a non-coherent Gaussian shifted from the bottom of the well: $\alpha(0) = 2.0\ \mathrm{a}_0^{-2}$, $q(0) = 1.0\ \mathrm{a}_0$, $p(0) = 0$. The wavefunction parameters are propagated in time numerically according to Eqs (5.28–5.31) and are shown in Fig. 5.2 for several values of the friction coefficient $\gamma = \{0, 1, 2, 4\}$. The symmetrized wavefunctions, constructed from evolving in time ψ, are projected onto the ground and the first excited energy eigenstates, respectively. The parameters of ψ of Eq. (5.27) converge to the ground state values faster for the larger values of γ, though larger γ is not necessarily advantageous for numerical considerations as it requires smaller time-step. The projections, $c_n = \langle\psi|\phi_n\rangle$, show similar behavior in time. The projections of $\Psi_{s/a}$ and ψ for $\gamma = 4$ onto the lowest energy eigenstates are shown in Fig. 5.3. The symmetrized wavefunctions converge to their respective lowest energy states noticeably faster than the non-symmetrized function. (The non-symmetrized function converges to the ground state $n = 0$, of course, but at short times it has non-zero projections

on multiple eigenstates.) The projections onto the second highest energy eigenstate of appropriate symmetry are also shown to illustrate the convergence properties.

Thus, we conclude that the symmetrization of the wavefunction, when evaluating expectation values and other properties, is compatible with the non-linear TDSE with friction and reduces propagation time. This should benefit calculations in general multidimensional systems, provided the symmetrization procedure can be performed efficiently. Such a procedure, which includes the leading correction on the expectation values due to particle permutations within the QT-based dynamics, is presented in the next section.

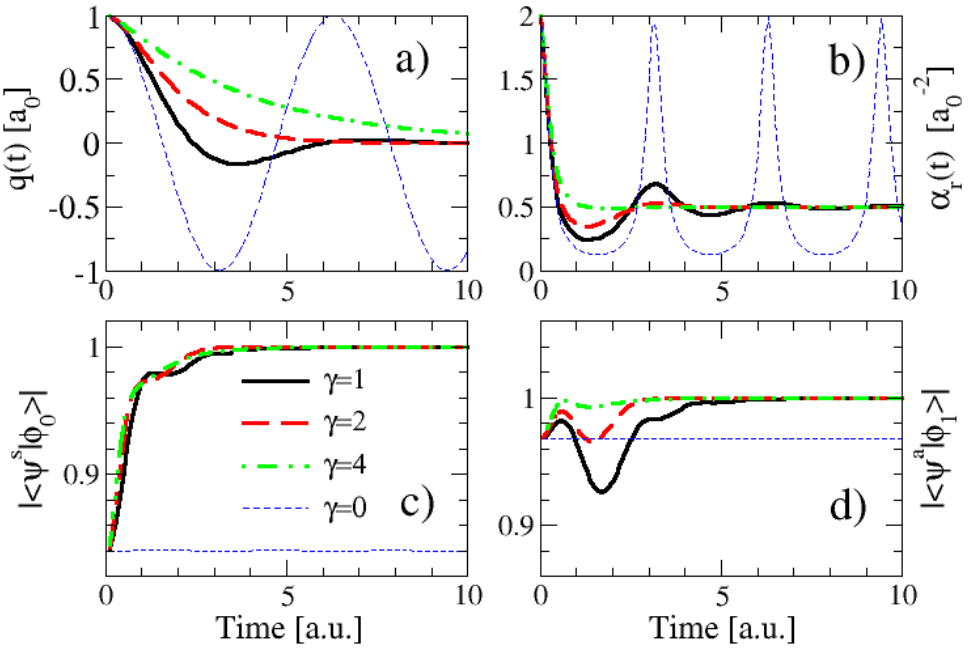

Figure 5.2: Dynamics with friction in the quadratic well. The center, $q(t)$, and the width parameter, $\alpha_r(t)$, of the Gaussian wavefunction as a function of time t are shown on panels (a) and (b). The absolute values of the projections of the symmetrized/antisymmetrized functions $\Psi_{s/a}$ onto the ground and first excited eigenstates ϕ_0 and ϕ_1 are shown on panels (c) and (d), respectively. The friction coefficient is shown on the legend (the same for all panels).

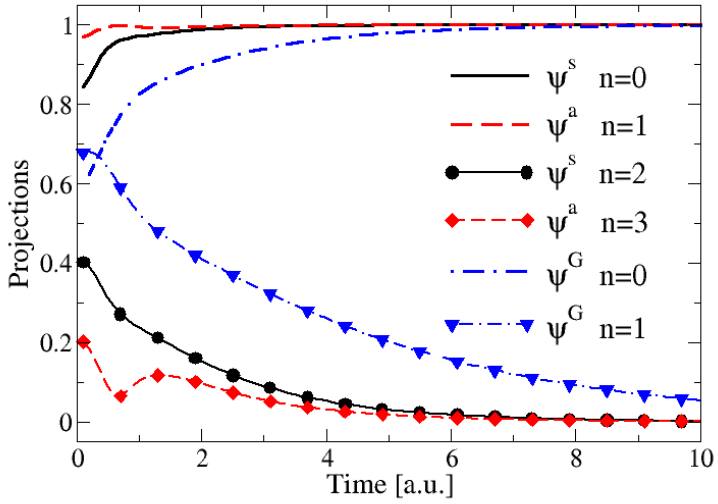

Figure 5.3: Dynamics with friction in the quadratic well. The absolute values of the projections of the symmetrized/antisymmetrized functions onto the eigenstates of the two lowest energy eigenstates of the appropriate symmetry. The quantum number and type of the wavefunction are shown on the legend.

5.3 Theory

In this section we describe a formalism of evaluating the leading correction to expectation values due to the wavefunction symmetrization compatible with the QT representation of a time-dependent full-dimensional wavefunction. In particular, in the Approximate Quantum Potential (AQP) approach [30, 31] the 'quantum' attribute of a trajectory, used to construct approximations to the quantum potential and to reconstruct a wavefunction itself, is the so-called non-classical momentum $\boldsymbol{r}$, defined as

$$\boldsymbol{r} = \frac{\nabla|\psi|}{|\psi|}. \tag{5.33}$$

The formalism presented in this Section utilizes the non-classical momentum, which in principle can be constructed from a wavefunction evolved in time with any QM method, including the imaginary time dynamics.

Formalism

In the following, we define a "configuration" as a wavefunction or a part of the wavefunction for which the list of all particle variables can be ordered, such as

$$\psi \equiv \psi(\boldsymbol{R}_1, \boldsymbol{R}_2 \cdots, \cdots, \boldsymbol{R}_N), \tag{5.34}$$

where $\boldsymbol{R}_j$ labels position of the j^{th} particle ($j = [1, N]$) in Cartesian space. Examples of configurations in the above definition are full solutions of the Schrödinger equation in coordinate space, an individual Slater determinant made of one-particle orbitals, a single product of one-electron orbitals, a quantum trajectory, or an ensemble of trajectories. Next, we act on a configuration by a permutation operator that interchanges one or more pairs of particles

$$\hat{P}_{ij}\psi(\cdots, \boldsymbol{R}_i, \cdots, \boldsymbol{R}_j, \cdots) = \psi(\cdots, \boldsymbol{R}_j, \cdots, \boldsymbol{R}_i, \cdots). \tag{5.35}$$

Note that the permutation operator is unitary

$$\hat{P}^\dagger = \hat{P}^{-1}. \tag{5.36}$$

The permuted wavefunction may or may not be identical to the original one. In further formalism development and in applications we will mostly focus on the case of permuted wavefunctions having small overlap with the original one. This is realized when individual particles in a configuration are localized in different spatial regions.

For a system of indistinguishable particles the lowest energy state wavefunction $\Psi_{s/a}$ is also the eigenstate of the permutation operator exchanging any two particles,

$$\hat{P}_{ij}\Psi_{s/a} = \pm\Psi_{s/a}$$

with $'\pm'$ signs describing the bosons/fermions. Henceforth, for convenience we will refer to symmetric wavefunction of N nuclei described in Cartesian space, though the approach is applicable to any symmetry or particles.

Now it is convenient to define one "reference" configuration with the sequentially ordered list of variables labeled 0:

$$\psi_0 = \psi(\boldsymbol{R}_{01}, \boldsymbol{R}_{02} \cdots, \cdots, \boldsymbol{R}_{0N-1}, \boldsymbol{R}_{0N}). \tag{5.37}$$

Other configurations and the permutation operators generating them from the reference configuration will be labeled as $\psi_\gamma = \hat{P}_\gamma \psi_0$, where γ enumerates sequences of the particles specified by the second subscript $j = \{1, 2, \cdots, N\}$,

$$\psi_\gamma \equiv \psi(\boldsymbol{R}_{\gamma_1}, \boldsymbol{R}_{\gamma_2}, \ldots, \boldsymbol{R}_{\gamma_N}). \tag{5.38}$$

For a system of N particles there are $N!$ unique sequences γ. Note that the product of any two permutation operators is a permutation operator, $\hat{P}_\gamma \hat{P}_{\gamma'} = \hat{P}_{\gamma''}$. It is convenient to classify permutation operators by the minimum number of permuted particles, such as two particle $\hat{P}_{ij}$, three particle $\hat{P}_{ij,jk} = \hat{P}_{ij}\hat{P}_{jk}$, linked and unlinked four particle $\hat{P}_{ij,jk,il}$ and $\hat{P}_{ij,kl}$, etc.

The symmetrized wavefunction of N particles is written as

$$\Psi_s = \mathcal{N} \sum_\gamma \psi_\gamma, \tag{5.39}$$

where $\mathcal{N}$ is the overall normalization constant of the symmetrized wavefunction.

The expectation value of any operator $\hat{O}$ is given by

$$\bar{O} = \langle \Psi_s | \hat{O} | \Psi_s \rangle = \mathcal{N}^2 \sum_{\gamma,\gamma'} \langle \psi_\gamma | \hat{O} | \psi_{\gamma'} \rangle . \tag{5.40}$$

We will consider the local or semi-local operator $\hat{O}$, invariant under any permutation, i.e.

$$[\hat{O}, \hat{P}_\gamma] = 0. \tag{5.41}$$

Then,

$$\langle \psi_\gamma | \hat{O} | \psi_\gamma \rangle = \langle \hat{P}_\gamma \psi_0 | \hat{O} | \hat{P}_\gamma \psi_0 \rangle = \langle \psi_0 | \hat{P}_\gamma^\dagger \hat{O} \hat{P}_\gamma | \psi_0 \rangle = \langle \psi_0 | \hat{O} \hat{P}_\gamma^{-1} \hat{P}_\gamma | \psi_0 \rangle = \langle \psi_0 | \hat{O} | \psi_0 \rangle . \tag{5.42}$$

With the above property, Eq. (5.40) becomes,

$$\begin{aligned}\langle\Psi_s|\hat{O}|\Psi_s\rangle =&\mathcal{N}^2\left(\sum_{\gamma}\langle\psi_\gamma|\hat{O}|\psi_\gamma\rangle+\sum_{\gamma,\gamma'\neq\gamma}\langle\psi_\gamma|\hat{O}|\psi_{\gamma'}\rangle\right)\\ =&\mathcal{N}^2\left(N!\,\langle\psi_0|\hat{O}|\psi_0\rangle+\langle\psi_0|\hat{O}|\sum_{\gamma,\gamma'\neq\gamma}\hat{P}_\gamma^{-1}\hat{P}_{\gamma'}\psi_0\rangle\right).\end{aligned}\tag{5.43}$$

The first term of the last equality in Eq. (5.43) is simplified since the total number of arrangements of N enumerated particles is $N!$. The last term can be separated according to the number of particle permutations in $\hat{P}_\gamma^{-1}\hat{P}_{\gamma'}$ as

$$\langle\psi_0|\hat{O}|\sum_{\gamma,\gamma'\neq\gamma}\hat{P}_\gamma^{-1}\hat{P}_{\gamma'}\psi_0\rangle=\frac{N!}{2}\langle\psi_0|\hat{O}|\sum_{i\neq j}\hat{P}_{ij}\psi_0\rangle+\frac{N!}{3}\langle\psi_0|\hat{O}|\sum_{i\neq j\neq k}\hat{P}_{ij,ik}\psi_0\rangle+\cdots\tag{5.44}$$

This sequence should rapidly converge for the local or semi-local operators $\hat{O}$ evaluated over wavefunctions describing particles sufficiently localized in different regions of space. In this case Eq. (5.44) is dominated by the leading terms, yielding

$$\bar{O}=\mathcal{N}^2N!\,\langle\psi_0|\hat{O}\left(1+\sum_{i>j}\hat{P}_{ij}\right)|\psi_0\rangle\,.\tag{5.45}$$

Setting $\hat{O}=1$ determines the normalization constant of the symmetrized wavefunction,

$$\mathcal{N}^{-2}=N!\left(1+\sum_{i>j}\langle\psi_0|\hat{P}_{ij}\psi_0\rangle\right).\tag{5.46}$$

Thus, our working expression for an expectation value in the first-order approximation due to symmetrization is

$$\bar{O}=\frac{\langle\psi_0|\hat{O}|\psi_0\rangle+\langle\psi_0|\hat{O}|\sum_{i>j}\hat{P}_{ij}\psi_0\rangle}{1+\langle\psi_0|\sum_{i>j}\hat{P}_{ij}|\psi_0\rangle}.\tag{5.47}$$

Implementation in the QT framework

The potential energy operator in coordinate space is local and is straightforwardly computed using Eq. (5.47). The kinetic energy operator involving derivatives is semi-local,

$$\hat{K}=\sum_{k,\sigma}-\frac{\hbar^2}{2m_k}\nabla^2_{k\sigma},$$

where m_k is the mass for k^{th} particle; $\sigma = \{x, y, z\}$ labels the Cartesian axes. To compute the expectation of the kinetic energy in the QT formulation we use the nonclassical momentum $\boldsymbol{r}$ of the reference wavefunction ψ_0 as defined in Eq. (5.33). Each component of the vector is labeled by the subscript $k\sigma$. The effect of permuting ψ_0 is expressed by the function χ_{ij},

$$\chi_{ij} \equiv \psi_0^{-1} \hat{P}_{ij} \psi_0. \tag{5.48}$$

Then the normalization is expressed as,

$$\mathcal{N}^{-2} = 1 + \sum_{i>j} \langle \psi_0 | \chi_{ij} | \psi_0 \rangle \,. \tag{5.49}$$

and the kinetic energy is given by

$$\langle K \rangle = \mathcal{N}^2 \sum_{k,\sigma} \frac{1}{2m_k} \left(\langle \psi_0 | r_{k_\sigma}^2 | \psi_0 \rangle + \sum_{i>j} \left(\langle \psi_0 | r_{k_\sigma}^2 \chi_{ij} | \psi_0 \rangle + \langle \psi_0 | r_{k_\sigma} \nabla_{k_\sigma} \chi_{ij} | \psi_0 \rangle \right) \right), \tag{5.50}$$

where k labels nuclei, σ labels Cartesian components of each nuclei, i and j label the exchanged particles.

Considering systems with well-separated local energy minima, the overlap between the reference wavefunction ψ_0 and the permuted wavefunction $\chi_{ij}\psi_0$ strongly depends on the spatial distance of the exchanged particles and, in the simplest form, only the near-neighbor permutations can be considered in summation over i, j in Eq. (5.50). If all atoms are within the same chemical environment (for instance atomic solid), then all the near-neighbor matrix elements of the type $\langle \psi_0 | \ldots \chi_{ij} | \psi_0 \rangle$ are the same and we only have to compute one element for each term in Eq. (5.50),

$$O_{ij} = \langle \psi_0 | \hat{O} \chi_{12} | \psi_0 \rangle \,. \tag{5.51}$$

The ground state calculations using the approximate QT dynamics with friction are described in Ref. [**?**] and the approach itself is not repeated here. The important result is that the quantum correction on dynamics is obtained by expanding the

non-classical momentum in the Taylor basis. Each component $r_{k\sigma}$ is fit by a cubic polynomial in (x, y, z) coordinates of k^{th} particle and by a monomial with respect to the coordinates of all other particles. The matrix elements of Eq. (5.51) can be related to the non-classical momentum already available from the approximate QT dynamics through

$$\nabla_{k_\sigma} Q_{ij} = \hat{P}_{ij} r_{k_\sigma} - r_{k_\sigma}, \quad Q_{ij} \equiv \ln \chi_{ij}, \tag{5.52}$$

as described in Section 5.4.

The expectation value of potential energy is:

$$\langle V \rangle = \mathcal{N}^2 \left(\langle \psi_0 | V | \psi_0 \rangle + \sum_{i>j} \langle \psi_0 | V \chi_{ij} | \psi_0 \rangle \right), \tag{5.53}$$

where $\mathcal{N}$ is defined by Eq. (5.49). The summation over j in Eqs (5.49), (5.50) and (5.53) includes just the near-neighbor particles. The 'near-neighbor' lists will depend on specific systems and interactions. For the ground state calculations, the lists can be precomputed and stored for each particle, since the particles are not expected to exhibit large amplitude motion, provided a reasonable initial wavefunction.

5.4 Models and implementation

In principle, an evolving non-symmetrized wavefunction $\psi(\boldsymbol{x}, t)$ can be used to estimate the ground state energy at any finite time t, whether during the imaginary or dissipative dynamics, as long as ψ has some extend into the barrier region separating equivalent minima of the potential, as illustrated in Section 5.2. In the QT implementation, any observables can be simply computed by the summation over the QT ensemble of N_{traj} trajectories discretizing the initial wavefunction,

$$\langle \hat{O} \rangle = \sum_{i=1}^{N_{traj}} O(\boldsymbol{x}_i) w_i, \tag{5.54}$$

where the trajectory weight is defined in Eq. (5.8). However for the permutation operator, $\hat{O} = \hat{P}$, the contribution to the integral comes from the barrier region, while,

generally, only small fraction of QTs will end up there. Therefore, such integrals are performed by Monte Carlo as described in Section 5.4, followed by the model applications of Section 5.4.

Evaluation of integrals involving particle permutations

To start a QT simulation an initial wavefunction, often of the Gaussian form, is represented in terms of the QT ensemble. The trajectory positions are chosen randomly using normal deviates [76]. All average quantities needed to evolve the QTs are computed according to Eq. (5.54). To efficiently evaluate expectation values involving particle permutations of Eq. (5.51), which is needed to analyze – not to perform – the dynamics, we re-sample the probability density $|\psi|^2$ in the barrier region using Monte Carlo techniques. The approximate analytical function for the probability density is available (up to a normalization constant) from the fitted nonclassical momentum. The non-linear approximation to $\boldsymbol{r}$ [**?**] is given in Appendix 5.6 for completeness,

$$r_\mu \approx a_\mu + \sum_\nu b_{\mu\nu} x_\nu + c_\mu x_\mu^2 + d_\mu x_\mu^3, \tag{5.55}$$

where μ labels the degrees of freedom (DOF), $\mu = [1, f]$, and represent the two indices of atoms in three-dimensional Cartesian space, $\mu \equiv k\sigma$. Eq. (5.55) yields the following unnormalized approximate wavefunction amplitude:

$$|\tilde{\psi}_0| = \exp\left(\sum_{\mu=1}^{f}\left(a_\mu x_\mu + \frac{b_{\mu\mu}}{2}x_\mu^2 + \frac{c_\mu}{3}x_\mu^3 + \frac{d_\mu}{4}x_\mu^4\right) + \frac{1}{2}\sum_{\mu\neq\nu} b_{\mu\nu}x_\mu x_\nu\right). \tag{5.56}$$

The normalization constant for $\tilde{\psi}_0$ can be obtained by straightforward Monte Carlo evaluation of $\langle|\tilde{\psi}_0|^2\rangle$ but it is not required, since this constant cancels in the expression for the wavefunction energy,

$$E = \frac{\langle\tilde{\psi}_0|\sum_\mu \frac{r_\mu^2}{2m_\mu}(1+e^Q) + \sum_\mu \frac{r_\mu \nabla_\mu Q}{2m_\mu}e^Q + V(\boldsymbol{x})(1+e^Q)|\psi_0\rangle}{\langle\tilde{\psi}_0|1+e^Q|\tilde{\psi}_0\rangle}. \tag{5.57}$$

For simplicity we have dropped the explicit spacial and temporal dependence. All the necessary quantities in Eq. (5.57) can be written as

$$\langle O \rangle = \int_{-\infty}^{\infty} O(\boldsymbol{x}) \mathcal{P}(\boldsymbol{x})\, d^f \boldsymbol{x}$$

with the probability function for the Monte Carlo integration, $\mathcal{P}(\boldsymbol{x}) = |\tilde{\psi}_0|^2 / \langle |\tilde{\psi}_0|^2 \rangle$. We use the Metropolis algorithm to sample $\mathcal{P}(\boldsymbol{x})$, as it is based on the relative probabilities, $\mathcal{P}(\boldsymbol{x})/\mathcal{P}(\boldsymbol{x}')$. Therefore, the normalization constant is not needed and just the barrier region is sampled to evaluate Eq. (5.57). In the numerical implementation of the Metropolis sampling, initially N_w walkers are randomly chosen. Then, the Metropolis algorithm is used to update the position of each walker; 20% of the total Monte Carlo steps is used to thermalize the walkers.

Implementation and examples

To illustrate the QT-based symmetry, or particle exchanges, correction and its range of validity, we consider three and four-dimensional models, for which the exact ground state energies were obtained using imaginary time dynamics on a grid using the split-operator method/Fast Fourier Transform [59, 21]. The potential energy V includes pairwise interactions and a quadratic in $\boldsymbol{x}$ term holding the center of mass of a system at zero:

$$V(\boldsymbol{x}) = \frac{K}{2} x_{cm}^2 + \sum_{i,j>i} \frac{k}{2}((|x_i - x_j| - R_0)^2, \quad x_{cm} = \sum_i x_i / N \tag{5.58}$$

The models represent a chain of one-dimensional atoms kept at R_0 distance apart by harmonic springs. The analytical form of Q defined by Eq. (5.52) is:

$$\begin{aligned} Q_{ij}(\boldsymbol{x}) &= \sum_{k=1}^{N} \Delta a_{ij}(x_j - x_i) + \sum_{k \neq i,j} (b_{ik} - b_{jk})(x_j - x_i) x_k \\ &+ \frac{b_{ii} - b_{jj}}{2}(x_j^2 - x_i^2) + \frac{\Delta c_{ij}}{3}(x_j^3 - x_i^3) + \frac{\Delta d_{ij}}{4}(x_j^4 - x_i^4) \end{aligned} \tag{5.59}$$

where $\Delta h_{ij} = h_i - h_j,\ h = \{a, b, c, d\}$. The kinetic energy simplifies to

$$\langle K \rangle = \frac{\mathcal{N}^2}{2m} \left(\langle \psi_0 | \sum_\mu r_\mu^2 | \psi_0 \rangle + n \langle \psi_0 | \sum_\mu r_\mu^2 \chi_{12} | \psi_0 \rangle + n \langle \psi_0 | \sum_\mu r_\mu \nabla_\mu \chi_{12} | \psi_0 \rangle \right) \tag{5.60}$$

where n is the number of nearest-neighbor permutations we have to consider. The first and second terms in Eq. (5.60) are simply related to the fitted form of $\boldsymbol{r}(\boldsymbol{x})$. The analytical form for the third term containing $\nabla_\mu \chi_{12} = e^{Q_{12}(\boldsymbol{x})} \nabla_\mu Q_{12}(\boldsymbol{x})$ is:

$$\nabla_\mu Q_{12} = \begin{cases} -\Delta a_{12} - (b_{11} - b_{22}) x_1 - \Delta c_{12} x_1^2 - \Delta d_{12} x_1^3, \\ \Delta a_{12} + (b_{11} - b_{22}) x_2 + \Delta c_{12} x_2^2 - \Delta d_{12} x_2^3, \\ (b_{1\mu} - b_{2\mu})(x_2 - x_1), \quad \mu \geq 3 \end{cases} \tag{5.61}$$

The parameters of the models are given in Table 5.3 and details of the QT dynamics and sampling are given in Table 5.4.

For $N = 3$ atoms the equilibrium geometry is $\boldsymbol{x}_0 = (-\frac{2R_0}{3}, 0, \frac{2R_0}{3})$ and its permutations, yielding a total of $3! = 6$ minima of the potential energy. Figure 5.4 shows the computed energy values in comparison with the QM results and wit the normal modes value. (The latter does not depend on R_0.) Clearly, the exchange effect lowers the energy value computed without the permutational symmetry. The exchange increases the uncertainty in the position space and decreases the uncertainty in the momentum space, which lowers the kinetic energy. There is a slight increase in the potential energy due to exchange, since there is more probability density in the barrier region. From the figure, it is clear that the exchange effect gives a noticeable contribution to the ground state energy at $R_0 < 5\ a_0$. The ground state energies with exchange corrections are in good agreement for $R_0 = [2.4, 5.0]$ a_0. Even when $R_0 = 2$ a_0, the exchange correction still captures significant portion of the energy decrease. At short inter-particle distance the nearest-neighbor approximation is poor as expected. For example, within the nearest-neighbor approximation the denominator of Eq. (5.47) the summation over permutations is:

$$\sum_{i \neq j} \langle \psi_0 | P_{ij} | \psi_0 \rangle = 2 \langle \psi_0 | P_{12} | \psi_0 \rangle + \langle \psi_0 | P_{13} | \psi_0 \rangle \approx 2 \langle \psi_0 | P_{12} | \psi_0 \rangle$$

The inter-particle distance (atom 1 and 2) is $\frac{2}{3} R_0$; for $R_0 = 1.0$ a_0 the expectation

Table 5.3: Parameters for the model systems.

Model, N	K $[E_h \cdot a_0^{-2}]$	k $[E_h \cdot a_0^{-2}]$	R_0 $[a_0]$	m $[a.u.]$
3	10	1	$[1.0, 5.0]$	1
4	16	1	$[1.0, 5.0]$	1

Table 5.4: Parameters for quantum trajectory dynamics simulation and Monte Carlo computation. N_t is the number of time steps; N_{traj} is the number of trajectories; γ is the friction constant; dt is the time step. For the Monte Carlo integration: N_w is number of walkers; N_m is the number of Monte Carlo steps; N_{th} is the number of thermalization steps.

Model, N	N_{traj}	dt $[a.u.]$	N_t	γ $[a.u.]$	N_w	N_m	N_{th}/N_m
3 & 4	12800	0.001	4000	8	20	10^6	20%

value is $\langle P_{12} \rangle \approx 0.68$. The distance between atoms 1 and 3 is $\frac{4}{3}R_0$, thus the contribution due to permutation of atoms 1 and 3 should not be ignored.

For the case of $N = 4$ atoms, the nearest-neighbor inter-particle distance is $R_0/2$ (and the next nearest distance is R_0). The trends in the ground state energy and accuracy are similar to the three-dimensional case as shown in Fig. 5.5. The exact QM calculations are limited to short distances due to the size of the required four-dimensional grid. For a condensed phase system with periodic boundary conditions a general setup of computing the exchange corrections is outlined in Appendix 5.7.

5.5 Discussion and summary

We have formulated an estimate of the permutational symmetry (exchange) effects for a quantum system consisting of indistinguishable particles. The estimate includes only two-particle permutations in the nearest-neighbor approximation, i. e. exchanges of the neighboring atoms. For a crystal structure, it means considering just the first shell. As has been demonstrated for the three- and four-particle models, the exchange correction is accurate in the regime of $\langle \psi_0 | \hat{P}_{ij} | \psi_0 \rangle \ll 1$, and may even give a useful estimate beyond this regime.

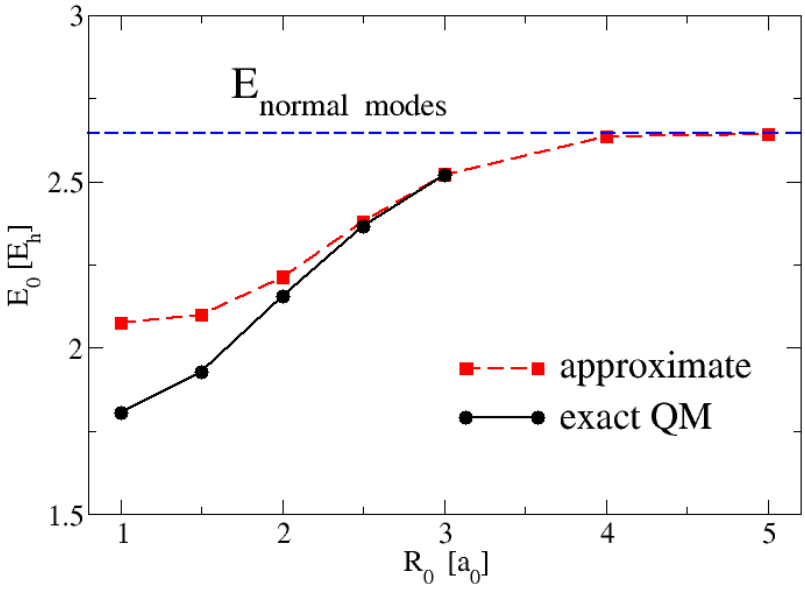

Figure 5.4: The ground-state energy for the three-particle model system as a function of the equilibrium distance. Red dash shows estimates obtained from the approximate QT dynamics and black solid line gives the exact values. The results approach the normal modes value at large R_0.

To make the estimates numerically more efficient we have implemented the "importance" sampling of the barrier regions (between the equivalent minima) which avoids explicit calculation of the wavefunction normalization (which would scale quadratically with the number of the Monte Carlo points). This allowed us to use the normal deviates sampling of the initial wavefunction with QT positions as needed for the QT dynamics. Further improvement of the Monte Carlo integration in the barrier region can be achieved if the probability function $\mathcal{P}(\boldsymbol{x})$ is sampled over the barrier region instead over the "local" solution ψ_0, in which case the integration becomes,

$$\int_{-\infty}^{\infty} e^{Q(\boldsymbol{x})}|\psi_0|^2\, d^f\boldsymbol{x} = \int_{-\infty}^{\infty} e^{Q(\boldsymbol{x})}|\psi_0|^2\mathcal{P}^{-1}(\boldsymbol{x})\mathcal{P}(\boldsymbol{x})\, d^f\boldsymbol{x} = \sum_{k=1}^{N_s} e^{Q(\boldsymbol{x}^{(k)})}\mathcal{P}^{-1}(\boldsymbol{x}^{(k)})$$

In this case, ψ_0 has to be normalized explicitly which can be accomplished by sampling the probability density function, $\mathcal{P}_0(\boldsymbol{x})$, taken for convenience to be a multivariate normal sampling after ignoring the higher-order terms in the exponent of

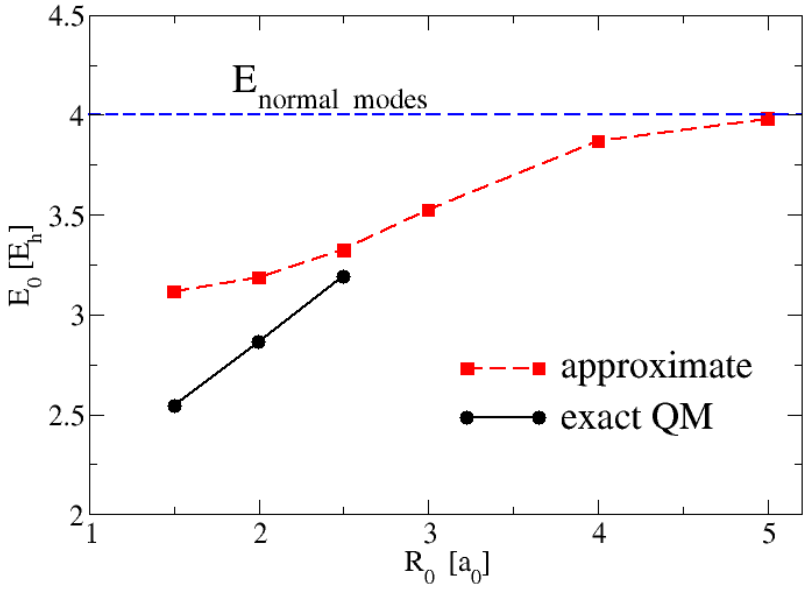

Figure 5.5: The ground-state energy for the four-particle model system as a function of the equilibrium distance. Red dash shows estimates obtained from the approximate QT dynamics and black solid line gives the exact values. The estimates approach the normal modes value at large R_0.

$|\psi_0|^2$. Alternatively, the description of the barrier region can be improved by taking an additional symmetric Gaussian basis function, Ψ_1, which would satisfy the permutational symmetry. Then, the ground-state energy can be obtained by diagonalizing a 'minimalistic' Hamiltonian matrix defined by the basis $\{\Psi_s, \Psi_1\}$, where Ψ_s is the symmetrized local ground state wavefunction. The parameters in the added basis function can be determined variationally. In the future we will explore these options of boosting the numerical efficiency and estimate the exchange effect in solid ^{4}He.

As a general conclusion, the Pauli potential is an artifact of the single-particle wavefunction representation or use of other low-dimensional functions such as the reduced density to describe the many-body system. If a full-dimensional wavefunction is available, incorporation of symmetry is cost-effective in calculations of the lowest energy states using the imaginary-time dynamics or other methods. The real-time

dynamics with friction converges to the ground energy state of the appropriate symmetry. Estimation of the symmetry effect for the ground state energy can be made using the 'nonclassical' momentum, $\boldsymbol{r} = \psi^{-1}\nabla\psi$, available from the approximate QT dynamics. Other dynamics approaches (including the imaginary-time evolution) yielding a full-dimensional time-dependent wavefunction could be used to define $\boldsymbol{r}$ as well.

5.6 Approximation to the non-classical momentum

In the QT dynamics formulation of the TDSE all quantum-mechanical effects are generated by the quantum potential U (Eq. (5.6)), which being inversely proportional on the particle mass, can be viewed as a correction to the classical dynamics of the nuclei. For a practical high-dimensional implementation in this regime, U is computed approximately from a global Least Squares Fit of the nonclassical momentum (Eq. 5.33)) [30, 31], which is exact for harmonic systems. The fitting in terms of monomials in $\boldsymbol{x}$ have been used to study QM behavior of a proton in an enzymatic environment and interacting with a carbon flake [25**?**]. For strongly anharmonic systems the non-linear approximation has been developed allowing better balance of the classical and quantum forces [**?**]. We briefly review this non-linear approximation since the fitting coefficients are used to estimate the symmetrization effects as well as the quantum effects on dynamics. The components of the non-classical momentum are evolved along each QT according to

$$\frac{r_\alpha}{dt} = -\left(\sum_\beta \frac{\nabla_\alpha p_\beta}{m_\beta} r_\beta + \sum_\beta \frac{\nabla_\alpha \nabla_\beta p_\beta}{2m_\beta}\right), \tag{5.62}$$

with the gradients in the RHS found approximately in a two-step fitting procedure:

1. Minimize $I^r = \langle \sum_\alpha (r_\alpha(x,t) - \tilde{r}_\alpha(x,t))^2 \rangle$ and $I^p = \langle \sum_\alpha (p_\alpha(x,t) - \tilde{p}_\alpha(x,t))^2 \rangle$ expanding $\tilde{r}$ and $\tilde{p}$ with a global linear basis $\boldsymbol{f} = (1, \boldsymbol{x})$.

2. Fit the residual for each atom or DOF, $I_\alpha^r = \langle (r_\alpha(x,t) - \tilde{r}_\alpha(x,t) - \tilde{\tilde{r}}_\alpha(x,t))^2 \rangle$ and $I_\alpha^p = \langle (p_\alpha(x,t) - \tilde{p}_\alpha(x,t) - \tilde{\tilde{p}}_\alpha(x,t))^2 \rangle$ using a higher-order basis, for instance, the cubic polynomials $f_\alpha = (1, x_\alpha, x_\alpha^2, x_\alpha^3)$. This second step leads to a more flexible quantum force under the assumption that the correlation between the particles of DOFs (or group of particles/DOFs) is captured by the linear terms.

The analytical fitting functions for r_α and p_α are used to compute corrections due to symmetry in terms of $Q_{ij} = \ln \chi_{ij}$,

$$\nabla_\alpha Q_{ij} = \frac{\nabla \chi_{ij}}{\chi_{ij}} = \hat{P}_{ij} r_\alpha - r_\alpha \tag{5.63}$$

to obtain the analytical expression for $Q_{ij}(\boldsymbol{x})$ as we have an approximated analytical wavefunction for ψ up to a normalization constant.

5.7 Implementation with periodic boundary conditions

For large quantum systems, such as solid ^{4}He, the general setup of computing the exchange corrections is as follows. The potential is a sum of pairwise interactions,

$$V = \frac{1}{2} \sum_{i,j \neq i} V_{ij}(R_{ij}), \quad R_{ij} = |\boldsymbol{R}_j - \boldsymbol{R}_i|, \tag{5.64}$$

where R_{ij} is the distance between the atoms i and j. For periodic condensed phase systems the periodic boundary conditions (PBC) is usually employed. After the simulation cell of length L is defined the PBC is set up by employing the minimum image convention [54]. For each atom i, the interaction with the atoms j is computed if the following condition is fulfilled,

$$R_{ij} = \min\{|\boldsymbol{R}_j - \boldsymbol{R}_i|, |\boldsymbol{R}_j - \boldsymbol{R}_i \pm L/2|\} < R_{cut}$$

is computed, where R_{cut} is a cutoff distance defining the interacting radius. The neighbor list is built for each atom once, at the beginning without updating in the

dynamics even the distance of two atoms may become larger than R_{cut}. The general steps for the complete computation is as follows

1. Set up the periodic boundary potential and compute the neighbor-list.

2. Define an initial wavefunction as the product of Gaussian wavefunctions in terms of QTs.

3. Perform dissipative QT dynamics for a predefined time interval T.

4. Output all fitting coefficients in the last time step. If displaced coordinates are used, perform coordinates transformation to regular Cartesian coordinates as described in Appendix **??**.

5. Estimate the ground state energy including the exchange effect using Monte Carlo. If the estimate if not sufficiently close to the previous value, repeat steps $3-5$.

Chapter 6

Quantum-mechanical evolution with Gaussian bases defined by the quantum trajectories

Development of a general approach to construction of efficient high-dimensional bases is an outstanding challenge in quantum dynamics describing large amplitude motion of molecules and fragments. A number of approaches, proposed over the years, utilize Gaussian bases whose parameters are somehow – usually by propagating classical trajectories or by solving coupled variational equations – tailored to the shape of a wavefunction evolving in time. In this chapter, we define the time-dependent Gaussian bases through an ensemble of quantum or Bohmian trajectories, known to provide a very compact representation of a wavefunction due to conservation of the probability density associated with each trajectory. While the exact numerical implementation of the quantum trajectory dynamics itself is generally impractical, these trajectories are well suited to guide the Gaussian basis functions as illustrated on several model problems.

6.1 Introduction

Importance of the quantum-mechanical effects associated with the nuclei is gaining recognition in chemistry and physics, as researchers now manipulate matter, light, electric and magnetic fields at the atomistic level to develop advanced materials and molecular structures with desired properties. Some examples are quantum sieving, i. e. hydrogen/deuterium isotope separation, based of the zero-point-energy dif-

ference, dependence of optoelectronic properties of P3HT/PCBM heterojunction on the hydrogen/deuterium substitution of the polymer P3HT, proton conductance in low-dimensional boron nitrides and silicon-based structures.

Quantum-mechanical effects are expected to be the most pronounced for light nuclei at low temperatures when a typical energy of a process is comparable to the separation between rovibrational energy levels for the nuclei. For a rigorous description, one has to solve the time-dependent Schrödinger equation for the nuclei evolving on a single or multiple electronic potential energy surfaces. The traditional exact approaches based on direct-product bases or discrete variable representation (DVR) of nuclear wavefunctions are practical to systems of 4-5 atoms (about 12 degree of freedoms) due to exponential scaling of the basis size with dimensionality of a system.

The largest reactive system that has been stuied with a full-dimensional quantum treatment is a collision of hydrogen and methane [79].

Over the years many efforts went into the development of more efficient adaptive bases for exact time-evolution methods and of approximate and semiclassical dynamics methods. The most well-developed exact method balancing computational cost and accuracy is the multi-configuration time-dependent Hartree method [71], MCTDH, based on contraction of a general basis to single (or a few) particle functions. This method and its extensions such as multilayer MCTDH [88] have been very useful and successful in studies of bound high-dimensional molecular systems with PES of polynomial (in coordinates) form. The variational multi-configuration Gaussian [91] vMCG version of the MCTDH is most closely related to this work.

For approximated methods employing basis functions, the wavefunction is usually represented by a linear combination of many stationary or dynamics basis functions. The evolution of time-dependent parameters (including expansion coefficients and also parameters defining the basis function) can be determined from Dirac-Frenkel variational principle [**?** 69]. A full variational approach usually ends up with coupled

equations for all the time-dependent parameters. Alternatively, one can specify the motion of part of the parameters and use TDVP for the rest, which can be considered as variational principle with constraints.

An example will be for Gaussian wavepacket, the central position and momentum can be associated with classical trajectories in phase space, the remaining parameters are the linear expansion coefficients. The idea of using Gaussian functions to represent nuclear time-dependent wavefunctions in chemistry goes back to Heller [50, 52]. On the one hand Gaussian functions exactly describe evolution of an initially Gaussian wavefunction (or wavepacket) in a time-dependent parabolic potential, which is a highly useful model of molecular vibrations. On the other hand GWP dynamics is easily connected to classical mechanics, which is adequate to describe nuclear motion in many situations and is widely used to simulate molecular systems: in a parabolic potential the center of the GWP moves classically. Finally, Gaussian functions are convenient to work with in numerical implementation, because many integrals can be performed analytically. While using a single Gaussian to approximate a wavefunction has an obvious limitation – a Gaussian is a localized wavefunction and thus cannot describe a process involving bifurcation of the probability density, the idea of using multiple Gaussians to represent a wavefunction have been used to develop a number of exact and approximate methods. Some of the exact methods are coupled coherent Gaussians [82, 77] with the GWP moving along the classical or multiple Ehrenfest trajectories, matching pursuit [92] with GWPs found through a re-expansion procedure, ab initio multiple spawning (AIMS) [55] for non-adiabatic dynamics based on classically evolving position and momentum of the Gaussian centers and vMCG, where Gaussian parameters are determined variationally. The latter has the advantage of rigorously conserving the wavefunction energy, but the resulting coupled equations are very tedious to implement numerically and the Gaussian parameters loose their physical meaning, compared to the GWPs centered on classical trajectories. In the

area of semiclassical Gaussian-based dynamics the thawed and frozen Gaussians and the initial value representation Herman-Kluk method [53, 58] are the most popular. One important conclusion emerging from the semiclassical work is: while a single thawed Gaussian, i. e. a Gaussian with the complex time-dependent width parameter, is an exact general solution of the quantum harmonic oscillator model, use of multiple thawed Gaussians in a basis representation of a wavefunction is numerically tedious and unstable. Thus, in our approach described below, we limit ourselves to the 'frozen' Gaussian basis of constant-in-time width. We note at this point, that in the area of time-independent rovibrational calculations, it has been demonstrated that Gaussian bases whose width parameters have been adapted to the potential can be very efficient [24]. Therefore, in the context of time-dependent bases, a middle ground between frozen and thawed Gaussian bases may be found. However, this line of research is not part this work.

Generally speaking, the problem of using stationary basis for dynamics is similar to the grid-based methods that the entire configuration space of polyatomic system has to be covered, which leads to exponential scaling problem. The time-dependent basis approach reduce the redundancy of the static basis, thus avoiding the exponential scaling problem. However, the problem of this is that the energy is usually not conserved through dynamics while it is always conserved while using static basis. The energy is only conserved when employing a full variational treatment without specifying the equations of motion for any parameters or in a complete basis, which is seldom achieved in practice. And also severe numerical problem (basically the ill-conditioning of the overlap matrix) can arise due to the linear dependence of the basis functions. This problem is discussed and some methods have been proposed in literature [**?**].

Besides methods using basis functions, various researchers[3, 95, 26, 27] have taken a different route to solve TDSE in the framework of de Broglie-Bohm mechanics

[7, 8]. In this theory, the wavefunction is represented by an ensemble of quantum trajectories, which is evolved under the classical force together with so-called quantum force. The motion of quantum trajectories represents the flow of probability. The challenge in these methods is the computation of quantum force,

$$U = -\frac{\hbar^2}{2m}|\psi|^{-1}\nabla^2|\psi|, \tag{6.1}$$

which can be extremely complicated while the wavefunction has singular points and ripples.

Here, we propose a method which combines the two approaches and test it with several one-dimensional and two-dimensional models. We use the time-dependent Gaussian wavepacket to represent the wavefunction and the motion of the central position is guided by quantum trajectories. The main advantage of the proposed method is the capability to treat quantum-mechanical tunneling, which is difficult if using classical trajectory guided GWP or Ehrenfest type average. Also due to the nature of quantum trajectories, the basis is always evolved in the region where the density is non-negligible.

6.2 Formalism

Atomic units is used if not stated explicitly. One possible way to solve time-dependent Schrödinger equation (TDSE) is to use time-dependent variational principle with a set of basis functions $\phi_k(t), k = 1, \ldots, N_b$, characterized by a set of time-dependent parameters $z_{k\mu}(t),\ n = 1, \ldots, N_p$, where N_b is the number of basis used to represent the wavefunction and N_p is the number of parameters for each basis.
$z_{k\mu}$ labels the μ-th parameter in k-th basis. Normalization of the wavepacket is conserved in the course of dynamics.

The wavefunction at any time can be projected onto the subspace spanned the

set of basis as

$$\psi(x,t) = \sum_{k=1}^{N_b} c_k(t)\phi_k(t), \tag{6.2}$$

where c_k are the expansion coefficient. Assume the basis functions have no explicit time-dependence but instead depend on the time-dependent parameters,

$$\phi_k(t) \equiv \phi(z_{k\mu}(t), \mu = 1, \ldots, N_p). \tag{6.3}$$

Thus take the derivative with time of the last equation yields

$$\dot{\phi_k} = \sum_{\mu} \dot{z}_{k\mu} \frac{\partial \phi_k}{\partial z_{k\mu}}. \tag{6.4}$$

Substitute Eq. (6.2) into TDSE and assume the equations of motion for the parameters characterizing the basis function has been pre-determined yields

$$\imath\hbar \sum_k \left(\dot{c}_k(t) \left|\phi_k\right\rangle + \sum_{\mu} c_k(t) \dot{z}_{k\mu} \left| \frac{\partial \phi_k}{\partial z_{k\mu}} \right\rangle \right) = \sum_k c_k(t) \hat{H} \left|\phi_k\right\rangle \tag{6.5}$$

Multiply both sides by $\langle\phi_j|$ yields

$$\imath M \dot{c} = (H - \imath D)\boldsymbol{c}, \tag{6.6}$$

where

$$M_{mn} = \left\langle \phi_m \,|\, \phi_n \right\rangle, \quad D_{mn} = \left\langle \phi_m \left| \sum_{\mu} \dot{z}_{m\mu} \right| \frac{\partial \phi_n}{\partial z_{n\mu}} \right\rangle \tag{6.7}$$

and H is the hamiltonian matrix,

$$H_{mn} = K_{mn} + V_{mn}, \tag{6.8}$$

$$K_{mn} = \left\langle \phi_m \left| \sum_k -\frac{\hbar^2}{2m} \frac{\partial^2}{\partial x_k^2} \right| \phi_n \right\rangle, \quad V_{mn} = \left\langle \phi_m \,|\, V(\boldsymbol{x}) \,|\, \phi_n \right\rangle. \tag{6.9}$$

This is the general equation to solve TDSE with basis sets characterized by time-dependent parameters.

Eq. 6.6 together with the pre-determined equations of motion for the parameters can completely solve the TDSE under the variational approximation.

Since the concept of quantum trajectory is going to be used in specifying the equations of motion for the parameters, we will briefly review the de Broglie-Bohm mechanics where it is defined.

Bohmian mechanics

In de Broglie-Bohm theory, the wavefunction is represented in polar form with the amplitude $A(\boldsymbol{x},t)$ and phase $S(\boldsymbol{x},t)$, which are both real functions of $\boldsymbol{x}$ and t,

$$\psi(\boldsymbol{x},t) = A(\boldsymbol{x},t)\exp\left(\frac{\imath}{\hbar}S(\boldsymbol{x},t)\right). \tag{6.10}$$

The probability density can be represented by

$$\rho(\boldsymbol{x},t) = \psi^*(\boldsymbol{x},t)\psi(\boldsymbol{x},t) = A^2(\boldsymbol{x},t). \tag{6.11}$$

Substituting Eq. (6.10) into TDSE, one obtains two coupled equations of amplitude and phase,

$$\frac{\partial S(\boldsymbol{x},t)}{\partial t} = \frac{\nabla S(\boldsymbol{x},t)^2}{2m} - V(\boldsymbol{x}) - U(\boldsymbol{x},t), \tag{6.12}$$

$$\frac{\partial \rho(\boldsymbol{x},t)}{\partial t} = -\nabla\left(\rho(\boldsymbol{x},t)\frac{\boldsymbol{\nabla}S}{m}\right), \tag{6.13}$$

$$\tag{6.14}$$

where

$$U(\boldsymbol{x},t) = -\frac{\hbar^2}{2m}\frac{\nabla^2 A(\boldsymbol{x},t)}{A(\boldsymbol{x},t)}. \tag{6.15}$$

$U(\boldsymbol{x},t)$ is the so-called non-local time-dependent quantum potential, and is proportional to $\hbar^2$. Without loss of generality, we assume the mass m is the same for each DoF.

Eq. (6.12) is the Eulerian version of the *quantum Hamiltion-Jacobi equation*, differing from classical *Hamilton-Jacobi equation* by the quantum potential term. The wavefunction can be discretized in coordinate space by quantum trajectories (QTs) with position $\boldsymbol{x}$ and momentum $\boldsymbol{p}$, defined as

$$\boldsymbol{p} = \boldsymbol{\nabla}S, \tag{6.16}$$

where $\boldsymbol{\nabla}$ here represents a column vector of differential operator,

$$\boldsymbol{\nabla} = \begin{bmatrix} \partial_{x_1} \\ \partial_{x_2} \\ \vdots \\ \partial_{x_{N_{dim}}} \end{bmatrix}, \tag{6.17}$$

where N_{dim} is the number of DoF.

Substitute the velocity $\boldsymbol{v} = \frac{\boldsymbol{p}}{m}$ into 6.13 yeilds

$$\frac{\partial \rho}{\partial t} + \nabla \cdot (\rho \boldsymbol{v}) = 0, \tag{6.18}$$

which turns out to be the continuity equation for the probability density.

When $\hbar \to 0$, U becomes negligible and all of the trajectories become independent of each other, which corresponds to the classical limit. The ensemble of quantum trajectories, representing the wavefunction, are assigned certain weights w_i, that depends on the initial probability density and the volume element associated with each trajectory,

$$w_i(t) = \psi^*(\boldsymbol{x}_i, t)\psi(\boldsymbol{x}_i, t)\, d\boldsymbol{x}_i(t) \tag{6.19}$$

Space of non-negligible density is sufficiently sampled with trajectories, let N_{traj} be the number of trajectories. The normalization of the probability correspond to the following relationship

$$\sum_{i}^{N_{traj}} w_i \approx \int_{-\infty}^{+\infty} \psi^*(\boldsymbol{x}, t)\psi(\boldsymbol{x}, t) d\boldsymbol{x} = 1. \tag{6.20}$$

The weight for each quantum trajectory remains constant in the course of dynamics [30] in the Lagrangian frame-of-reference,

$$\frac{dw_i}{dt} = 0. \tag{6.21}$$

The evolution of quantum trajectories is given by Hamilton's equations of motion,

$$\frac{d\boldsymbol{x}_i}{dt} = \frac{\boldsymbol{p}_i}{m}, \tag{6.22}$$

$$\frac{d\boldsymbol{p}_i}{dt} = -\boldsymbol{\nabla}\,(V + U)|_{\boldsymbol{x}=\boldsymbol{x}_i}\,. \tag{6.23}$$

Here subscript i labels the trajectories. The phase of wavefunction, $S(\boldsymbol{x}_i, t)$, is equal to the action function S_i of each trajectory defined (in units of $\hbar$) by

$$\frac{dS_i}{dt} = \frac{\boldsymbol{p}_i \cdot \boldsymbol{p}_i}{2m} - (V+U)|_{\boldsymbol{x}=\boldsymbol{x}_i}\,. \tag{6.24}$$

The position-dependent observables $\hat{O}$ can be computed from the properties of each quantum trajectory,

$$\langle \hat{O} \rangle = \int d\boldsymbol{x} \rho(\boldsymbol{x}, t) O(\boldsymbol{x}) = \sum_i^{N_{traj}} O(\boldsymbol{x}_i) w_i \tag{6.25}$$

Frozen Gaussian wavepackets

Despite the numerical advantages of using Gaussian wavepackets, it also has the property that the uncertainty in position and momentum is exactly equal to $\hbar$. The GWPs are extensively used in semiclassical methods.

A real multi-dimensional Gaussian wavepacket is

$$g_k = \sqrt[4]{\frac{detA}{\pi^n}} \exp\left(-\frac{1}{2}\sum_{\mu\nu}(x_\mu - q_{k\mu}(t))A_{\mu\nu}(x_\nu - q_{k\nu}(t)) + \imath\gamma_k(t)/\hbar\right). \tag{6.26}$$

f refers to the number of DOF and the Greek letters $\mu, \nu = 1, \ldots, f$ labels the DOF. The wavefunction is expanded as a linear combination of GWPs with complex coefficients $c_k, k = 1, N_b$, N_b is the number of basis function,

$$\psi(\boldsymbol{x}, t) = \sum_k c_k(t) g_k. \tag{6.27}$$

For simplicity, assume the matrix $A_{\mu\nu}$ is a diagnol matrix and $A_{\mu\mu} = \alpha_\mu$. The overlap matrix in the EOM for the coefficients can be expressed as

$$M_{jk} = \langle g_j | g_k \rangle = \Pi_{\mu=1}^f \exp\left(-\frac{\alpha_\mu}{4}(q_{j\mu} - q_{k\mu})^2\right) \exp\left(\imath(\gamma_k - \gamma_j)/\hbar\right). \tag{6.28}$$

We drop the explicit time-depdendence of the parameters characterizing the wavefunction for notational simplicity.

For numerical efficiency, here we use the forzen Gaussian approximation , i.e., $A_{\mu\nu}$ is a constant matrix.

We asssocaite the phase term $S(t)$ to the action function of the trajectory, i.e.

$$\dot{\gamma_k} = \sum_\mu \frac{p_{k\mu}^2}{2m_\mu} - V(\boldsymbol{q}). \tag{6.29}$$

This term is not affecting the dynamics, since it can be absorbed in the complex coefficients.

Instead of using classical trajectories for the center of GWP or using time-dependent variational principle to obtain EOM, we adopt the EOM for quantum trajectory, which is

$$\dot{q}_{k\mu} = \frac{\partial_\mu S}{m_\mu}. \tag{6.30}$$

The matrix element for kinetic energy operator is given by

$$K_{jk} = \sum_\mu \frac{\alpha_\mu}{4m_\mu}(1 - \frac{\alpha}{2}\left((q_{j\mu} - q_{k\mu})^2\right) M_{jk}. \tag{6.31}$$

Taylor expand the potential energy at the center of two Gaussian basis $\bar{\boldsymbol{q}} = \frac{1}{2}(\boldsymbol{q}_j + \boldsymbol{q}_k)$ yields

$$V = V_0(\bar{\boldsymbol{q}}) + \sum_\mu \partial_u V(\bar{\boldsymbol{q}})(x_\mu - \bar{q}_\mu) + \frac{1}{2}\sum_{\mu\nu} \partial_\mu\partial_\nu V(\bar{\boldsymbol{q}})(x_\mu - \bar{q}_\mu)(x_\nu - \bar{q}_\nu) + \cdots \tag{6.32}$$

Thus the matrix element of potential energy turns out to be

$$V_{jk} = \left(V_0 + \sum_\mu \frac{\partial_\mu^2 V}{4\alpha_\mu}\right) M_{jk} \tag{6.33}$$

And also

$$D_{jk} = \langle g_j \,|\, -\imath\partial_t \,|\, g_k\rangle = \sum_\mu \imath\frac{\alpha_\mu}{2m_\mu} p_{k\mu}(q_{k\mu} - q_{j\mu}) M_{jk} \tag{6.34}$$

Thus the methods start with a sampling of intial configurations (trajectories), obtain the expansion coefficients by minimizing the error with chosen intial wavefunction and compute the spacial derivative of the phase of the wavefunction, the following is simply numerically integrating the coupled equations of motion for the coefficients and quantum trajectories. All the matrix elements with Gaussian wavepacket as basis which is needed to propagte the EOM has been given in this section.

Gaussian integrals

Computing the matrix element mainly involves Gaussian integrals, here we derive some useful Gaussian integrals. Assume

$$|z_k\rangle = \left(\frac{\gamma_k}{\pi}\right)^{1/4} e^{-\frac{\gamma}{2}(x-q_k)^2+\imath p_k(x-q_k)/\hbar} \tag{6.35}$$

Define

$$\Delta q = q_k - q_j, \quad \Delta p = p_k - p_j$$

thus

$$\langle z_j|z_k\rangle = (\gamma_j\gamma_k)^{1/4}\left(\frac{2}{\gamma_j+\gamma_k}\right)^{1/2}\exp\left(-\frac{\gamma_j\gamma_k}{2(\gamma_j+\gamma_k)}\left(\frac{\Delta^2 p}{\gamma_j\gamma_k}+\Delta^2 q+2\imath\left(\frac{p_k}{\gamma_k}+\frac{p_j}{\gamma_j}\right)\Delta q\right)\right)$$

The expression can be simplified while $\gamma_j = \gamma_k$.

$$\langle z_j|(x-q_k)^n|z_k\rangle = \left\langle z_j\left|\left(\frac{\hbar}{\imath}\frac{\vec{\partial}}{\partial p_k}\right)^n\right|z_k\right\rangle \tag{6.36}$$

$$\langle z_j|(x-q_j)^n|z_k\rangle = \left\langle z_j\left|\left(\imath\hbar\frac{\overleftarrow{\partial}}{\partial p_j}\right)^n\right|z_k\right\rangle \tag{6.37}$$

6.3 Numerical implementation

One of the numerical difficuties for this method is the overlap matrix can be ill-conditioned when two GWPs get too close. One of the properties of quantum trajectories is that they will never cross, the exact quantum force tends to prevent them from crossing.

In principle, the momentum computed from the wavefunction will have the exact same effects, from a practical point of view, the quantum trajectories will ocationaly cross, which renders the overlap matrix M ill-conditioned, causing a severe numerical problem as one has to inverse the overlap matrix while integrating the EOM.

To resolve this problem, a resampling method is used.

After propagating the wavefunction for certain time interval T, in order to avoid the singularity of the overlap matrix of GWP caused by unphysical behavior of quantum trajectories, we resample all the quantum trajectories under the current wavefunction.

The purpose of the resampling is to put GWP to where the wavefunction stays and reduce the redundant basis where the probability is negligible and add more basis where the wavefunction become spread out in space.

The first step of resampling is to decide the new set of parameters characterizing GWP $\{x', p', c'\}$ and decide the number of basis to describe the wavefunction.

A simple way to accomplish this is to start with an initial point x_0, at the very left, and compute the density at this point numerically, $|\psi(x_0, t)|^2 = |\sum_k c_k g_k(x_0)|^2$. Define a threshhold ϵ, if $|\psi(x_0, t)|^2 < \epsilon$, disregard the point, otherwise take the position as the center of a GWP which will be included in the new basis set. Move to the right by an interval Δx and repeat the last step until we get to the region where the density is negligible.

The number of basis decided by this procedure N' can be different from the one used in previous propagation. The advantage of this is that we have the flexibility to add or remove the number of basis. For instance, at the beginning, we may not need many basis functions to describe the wavefunction, when the wavefunction bifurcates, we may need more basis.

After we have all the postions for the new basis set, the momentum is computed by differentiating the phase of wavefuncion, $p'_k = \frac{\partial S}{\partial x}\Big|_{x=x'_k}$. We can reset $\gamma'_k = 0$, since the number can be absorbed in the new expansion coefficients, which are decided by minimizing the error between the new wavefuction constructed by the new basis can the old wavefunction,

$$I = ||\sum_k c'_k g'_k - \psi(x, t)||^2.$$

The minimization yields

$$\boldsymbol{M}'\boldsymbol{c}' = \boldsymbol{b}', \tag{6.38}$$

where

$$M'_{jk} = \langle g'_j | g'_k \rangle \,, \quad b'_k = \langle g'_k | \psi(x,t) \rangle \,. \tag{6.39}$$

Integration scheme

Another difficulty comes from the integration scheme. A first-order Euler method

$$\boldsymbol{c}(t+\Delta t) = \boldsymbol{c}(t) + \Delta t \dot{\boldsymbol{c}}(t), \quad \boldsymbol{x}(t+\Delta t) = \boldsymbol{x}(t) + \Delta t \dot{\boldsymbol{x}}(t), \tag{6.40}$$

causes numerical instabilities at long time. One has to use a extremely small time step to make the numerical integration practical and energy bound within certain range.

Instead we adopts the second-order differencing (SOD) scheme, which makes the integration more stable,

$$\dot{c}(t) \approx \frac{\boldsymbol{c}(t+\Delta t) - c(t-\Delta t)}{2\Delta t}, \quad \dot{x}(t) \approx \frac{\boldsymbol{x}(t+\Delta t) - x(t-\Delta t)}{2\Delta t} \tag{6.41}$$

Thus

$$\boldsymbol{c}(t+\Delta t) = \boldsymbol{c}(t-\Delta t) + 2\Delta t \dot{\boldsymbol{c}}(t), \quad \boldsymbol{x}(t+\Delta t) = \boldsymbol{x}(t-\Delta t) + 2\Delta t \dot{\boldsymbol{x}}(t) \tag{6.42}$$

The advantages of using SOD is discussed in detail by Leforestier et al [60].

Momentum convolution

To smooth out the momentum obtained from the spaial derivative of phase of the wavefunction, we use a Gaussian convolution

$$\psi(x) = \lim_{\beta\to\infty} \left(\frac{\beta}{2\pi}\right)^{1/2} \int_{-\infty}^{\infty} e^{-\frac{\beta}{2}(x-y)^2} \psi(y)\, dy \tag{6.43}$$

Here we use the relationship

$$\delta(x-y) = \lim_{\beta\to\infty}\left(\frac{\beta}{2\pi}\right)^{1/2} e^{-\frac{\beta}{2}(x-y)^2}.$$

Consider a one-dimensional case,

$$\psi(t) = \sum_k c_k(t) g_k \tag{6.44}$$

and using the Gaussian integral

$$\left(\frac{\beta}{2\pi}\right)^{1/2}\int_{-\infty}^{\infty} e^{-\frac{\beta}{2}(x-y)^2} e^{-\frac{\alpha}{2}(y-q_k)^2} dy = \sqrt{\frac{\beta}{\alpha+\beta}}\exp\left(-\frac{1}{2}\frac{\alpha\beta}{\alpha+\beta}(x-q_k)^2\right)$$

And the momentum will thus become

$$p = \nabla S = \Im\psi^{-1}\nabla\psi = \Im\psi^{-1}\left(\frac{\beta}{\pi}\right)^{1/4}\int_{-\infty}^{\infty}(-\beta(x-y))e^{-\frac{\beta}{2}(x-y)^2}\psi(y)\,dy \tag{6.45}$$

Let β be a finite number will smooth out the momentum at the center of GWP basis. Note that when $\beta \to 0$, all the momentum will become the averaged value, which is similar to Erhenfest approximation. When $\beta \to \infty$, the convolution has no effect on the obtained momentum.

6.4 Models

Various types of model systems including Morse oscillator representing the vibration of H_2 and double-well system and double-well coupled with a harmonic oscillator will be tested with this method, obtained results will be compared with exact quantum-mechanical results using split-operator method [59].

Morse oscilator

The first model is the Morse oscillator representing the vibration of H_2, which is a typical anharmonic potential.

$$V(x) = d\left(1-\exp(-a(x-x_0))\right)^2 \tag{6.46}$$

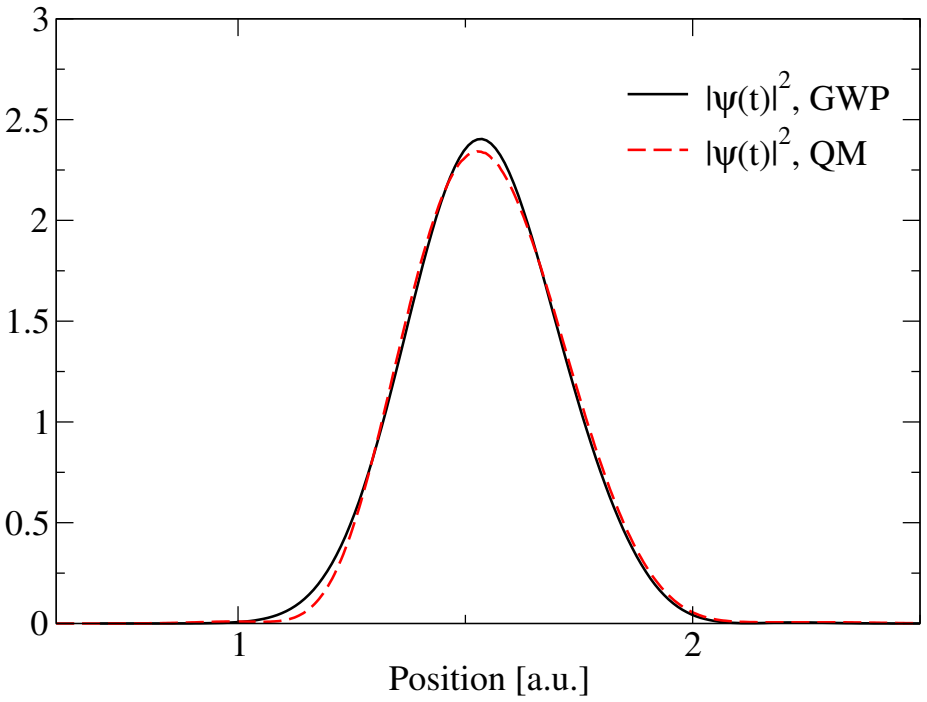

Figure 6.1: wavefunction propagation using Gaussian basis and SPO for Mose oscillator at $t = 800$ $a.u.$.

where $d = 0.176$ E_h, $a = 1.02$ a_0^{-1}, $x_0 = 1.4$ a_0.

Start with a displaced Gaussian wavepacket,

$$\psi_0 = \sqrt[4]{\frac{\alpha_0}{\pi}} \exp\left(-\alpha_0(x - x_0)^2 + \imath p_0(x - x_0)\right), \tag{6.47}$$

where $\alpha_0 = 9.16$ $a.u., p_0 = 0$ $a.u., x_0 = 1.3$ $a.u.$. 10 GWPs with width parameter $\alpha = 64$ is being used in the simulation with a time step $\Delta t = 0.2$ $a.u.$. The reduced mass of H_2 is 925 a.u..

To examine the accuracy of the wavefunction in the dynamic process, the auto-correlation function is also computed,

$$C(t) = \langle\psi_0|e^{-\imath Ht/\hbar}|\psi_0\rangle = \left\langle U^\dagger(t/2)\psi_0 \,\middle|\, U^\dagger(t/2)\psi_0 \right\rangle = \langle\psi(-t/2)\,|\,\psi(t/2)\rangle\,. \tag{6.48}$$

. If initial wavefunction is real, then

$$\psi(-t/2) = \psi^\dagger(t/2) \tag{6.49}$$

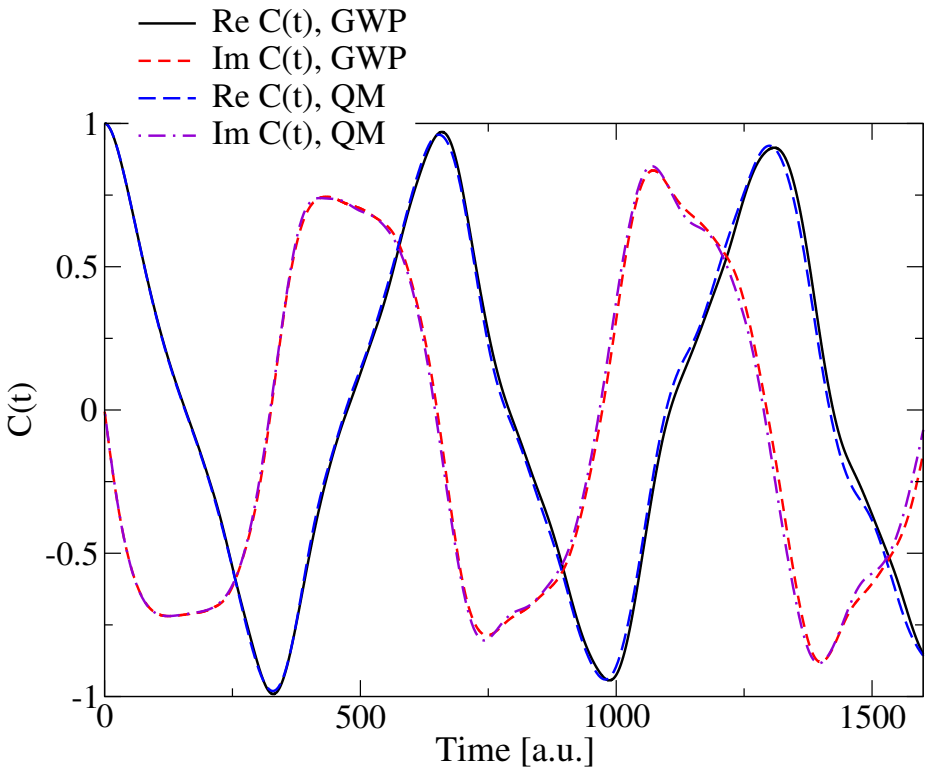

Figure 6.2: Auto-correlation function for Morse oscilator using QT guided GWPs and SPO (labelled by QM).

thus

$$C(t) = \int_{-\infty}^{\infty} \psi^2(t/2)\, dx. \tag{6.50}$$

From fig. 6.2, it is clear to see that the autocorrelation computed with GWP basis is in good agreement with exact auto-corrlation function. And we do not encounter the ill-conditioning problem of the overlap matrix for this model, thus the resampling scheme is not being used in this case.

Double well

Double well system is usually encountered in the reaction of hydrogen or electron transfer, where quantum-mechanical tunneling effects play significant roles. Deep tunneling effects cannot be described by classical trajectories as they do not have

enough energy to go across the barrier. Quantum trajectories, representing the flow of probability, can describe the tunneling effects even though they do not have enough energy at initial time moment. The quantum potential makes the quantum trajectories correlated with each other, thus the energy for each individual trajectory is not conversed. Thus some trajectories will gain enough energy to go over the barrier.

Here we choose a potential from Wu and Batista [92], which is a model system to simulate electron tunneling between disjoint classical allowed region.

$$V(x) = \frac{1}{16\eta}x^4 - \frac{1}{2}x^2, \tag{6.51}$$

where $\eta = 1.3544\ a.u.$.

A local barrier is located at $x = 0$ with barrier height $V_b = 1.3544\ a.u.$.

We choose the initial wavefunction as a Gaussian wavepacket sitting in the left well,

$$\psi_0 = \sqrt[4]{\frac{\alpha_0}{\pi}} \exp\left(-\alpha_0(x - x_0)^2 + \imath p_0(x - x_0)\right). \tag{6.52}$$

where $\alpha_0 = 0.5,\ x_0 = -2.5,\ p_0 = 0$. The mass is set to $m = 1\ a.u.$. The initial energy for this wavefunction is $E_0 = 0.9318\ a.u.$, which is about 68% of the barrier height. The feature of this model is the wide barrier width, the distance between two local minima is around 4.7 a.u., which causes difficulty for semiclassical methods [92].

10 GWPs with width parameter $\alpha = 16$ are used for the simulation and time step is set to $10^{-3}\ a.u.$.

We examine the wavefunction while the tunneling happens. Fig. 6.3 shows the wavefunction at $t = 3\ a.u.$. The results obtained with GWP is in good agreement with exact quantum mechanical result.

To further examine the accuracy of the wavefunction, Fig. 6.4 shows the auto-correlation function, very good agreement with exact quantum-mechanical results is achieved.

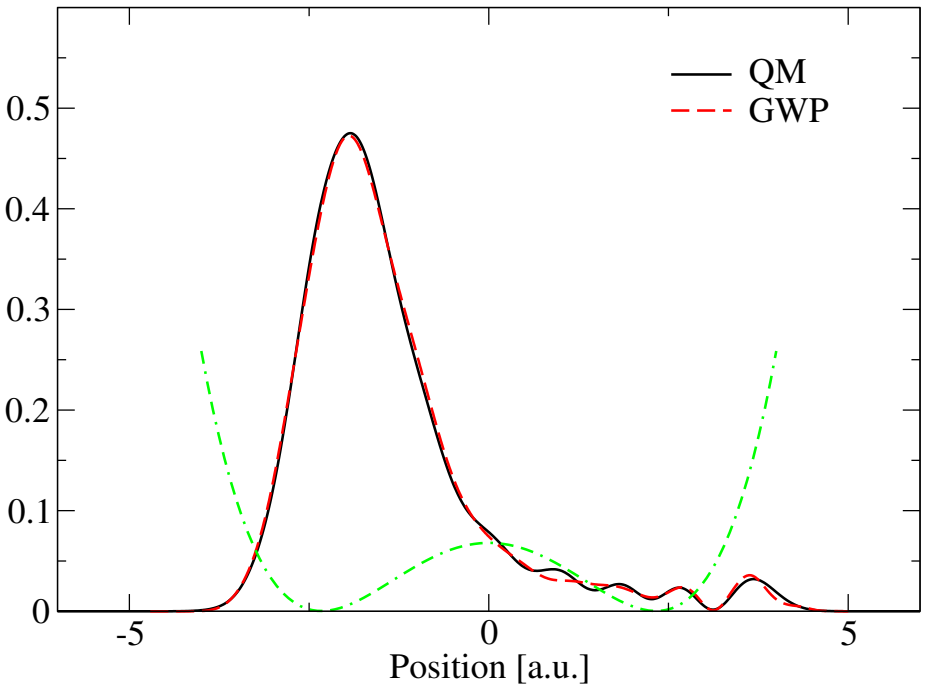

Figure 6.3: Wavefunction for double well using QT guided GWPs and SPO (labelled by QM) at $t = 3$ $a.u.$. Part of the wavefunction tunnels through th barrier located at $x = 0$. The green dot-dashed curve is the rescaled and shifted potential.

Two-dimensional double well system

The last model is a double-well system coupled with a harmonic oscillator, which is typical for reactive dynamics in condensed phase. This model is being used by Garashchuk et al [33] to study coupling between quantum DOF and classical DOF. The potential is given by

$$V(x, y) = y^2(ay^2 - b) + \frac{1}{2}c(x - y)^2 + \frac{b^2}{4a}, \tag{6.53}$$

and the parameters are set as $a = 1$, $b = 4$ $c = 4$. The particle mass are set to $m_1 = m_2 = 1$ $a.u.$. Fig. 6.5 shows the contour of the potential energy, two local minima are located at $(-\sqrt{2}, -\sqrt{2})$, $(\sqrt{2}, \sqrt{2})$. The barrier is located at $(0, 0)$ with barrier height $E_b = 4$ E_h. We examine the autocorrelation function starting with a

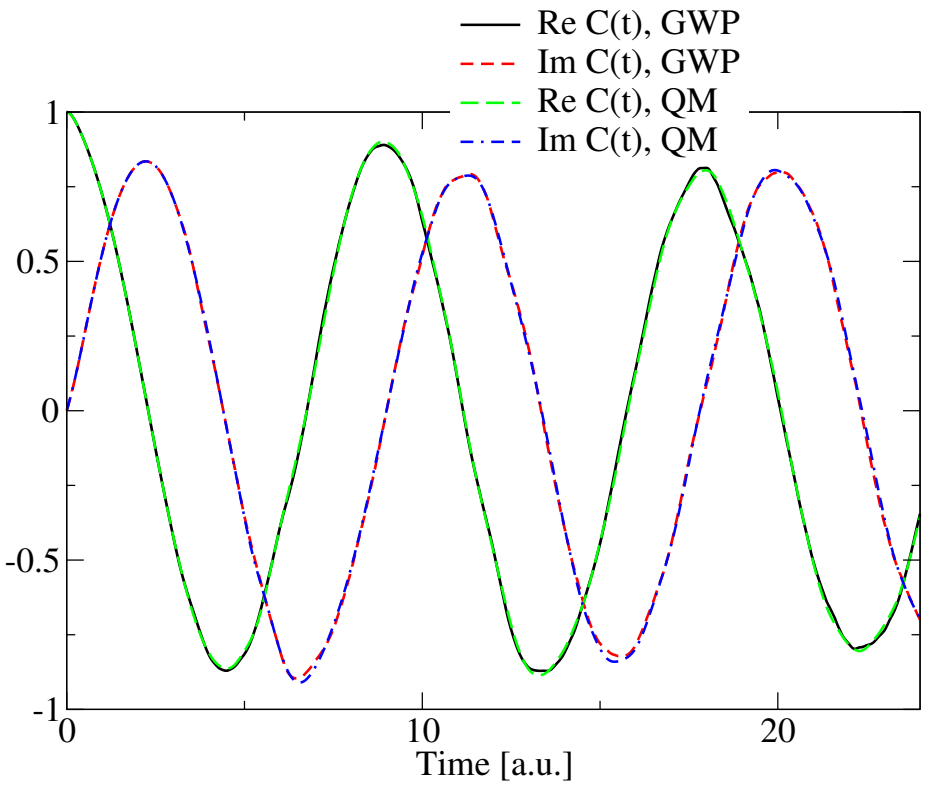

Figure 6.4: Autocorrelation function obtained with quantum trajectory guided GWPs, comparing with exact quantum-mechanical results.

Table 6.1: Parameters for the initial wavefunction used in the 2-dimensional double well system.

x_0	y_0	p_x	p_y	α_x	α_y
-1.4	-1.4	0	0	1	1

Gaussian wavefunction sitting in the left well of the potential,

$$\psi_0 = \left(\frac{\alpha_x \alpha_y}{\pi^2}\right)^{1/4} \exp\left(-\frac{\alpha_x}{2}(x-x_0)^2 - \frac{\alpha_y}{2}(y-y_0)^2 + \imath p_x(x-x_0) + \imath p_y(y-y_0)\right). \tag{6.54}$$

Parameters for the initial wavefunction is listed in Tab. 6.1. The dynamics is simulated with 10×10 Gaussian wavepacket with time step $\Delta t = 10^{-3}$ $a.u.$.

The eigenfrequency $\nu_n \equiv \frac{E_n}{2\pi\hbar}$ can be obtained by Fourier transforming the autocorrelation function. The resolution of the frequency is limited by the length of the signal. To avoid this problem , here we use the harmonic inversion method [66].

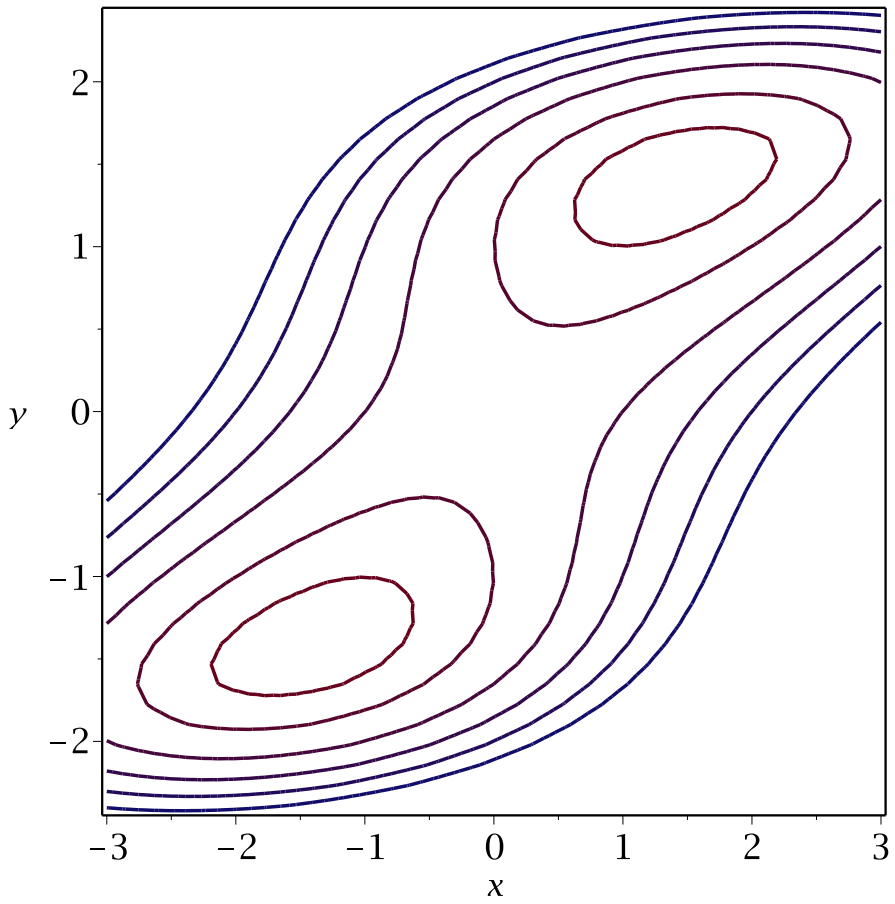

Figure 6.5: Contour plot of the two-dimensional potential. Two local minima are located at $(-\sqrt{2}, -\sqrt{2})$, $(\sqrt{2}, \sqrt{2})$.

Table 6.2 shows the eigenfrequency of the ground and one excited state obtained with harmonic inversion method using the data from GWP and exact quantum-mechanical result. The simulation is performed with several sets of parameters and clearly, the results is insensitive to parameters. In practice, the best parameters is determined by the model and initial wavefunction. The obtained energies is in good agreement which is expected since the accuracy depends on the quality of the autocorrelation function.

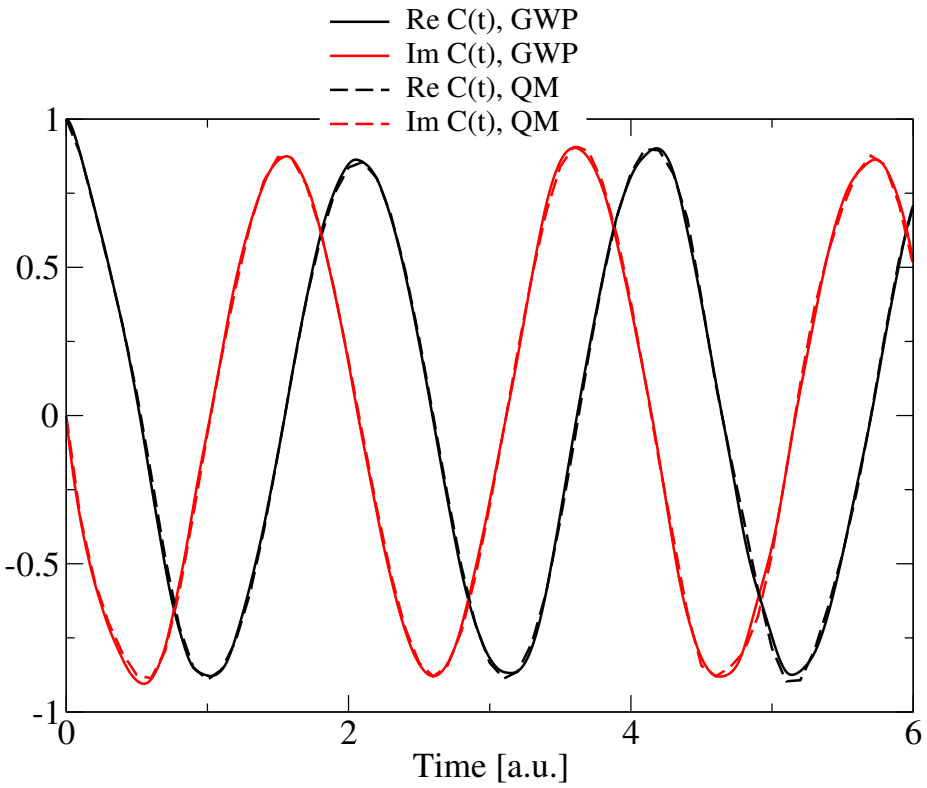

Figure 6.6: autocorrelation function computed with chosen initial wavefunction. Comparison is made with exact quantum-mechanical results.

Table 6.2: Eigenfrequency of the ground and one excited states in atomic units obtained from harmonic inversion method.

	GWP[1]	GWP[2]	GWP[3]	QM
ν_g	0.4827	0.4822	0.4830	0.4829
ν_e	0.7110	0.7180	0.7209	0.7163

[1] 10×10 GWPs with $\alpha = 16$
[2] 12×12 GWPs with $\alpha = 16$
[2] 16×16 GWPs with $\alpha = 32$

6.5 Discussions

The proposed method takes advantage of the idea of quantum trajectories representing the flow of probability defined in the de Broglie - Bohm mechanics and also the time-dependent variational principle with Gaussian-type basis. In principle, the parameters characterizing the GWPs can evolve in an arbitrary way. For instance, one can define a classical trajectory to evolve the average position and mementum of the GWP, though the quantum-mechanical tunneling effects can not be described in this way. None of the classical trajectories will have enough energy to cross the barrier if the initial energy is lower than the barrier as classical trajectories are uncoupled. A reasonable method has to cover the whole range with non-negligible density through the dynamic process. Adopting quantum trajectories will let the method be capable to describe tunneling effects. Someone may notice that we may have some redundancy to use the ensemble of quantum trajectories to represent the wavefunction as well as the Gaussian basis. Notice that by adopting the TDVP, the number of basis (QTs) that we have to use is 3-4 orders of magnitudes smaller compared to the regular quantum trajectory methods which is typically of the order of 10^4.

Strictly speaking, we can not claim that the ensemble of QTs used here represents the wavefunction, it nevertheless still represents the flow of probability. And that is what we need is to place the GWPs as the requirement for a variational approximation to work is that the wavefunction is almost in the space spanned by the basis set.

From the test of various model systems, it is clear that the proposed method can propagate an arbitrary chosen initial wavefunction accurately for the bound potential and also systems where the quantum-mechanical tunneling effects is significant.

Chapter 7

Nuclear Quantum Effects on adsorption of H_2/D_2 on metal ions

The nuclear quantum effects (NQE) on the zero-point energy, influencing adsorption of H_2 and isotopologues on metal ions, are examined from the normal modes analysis of ab initio electronic structure calculations for 17 metals and from the nuclear wavepacket dynamics on the ground state electronic potential energy surfaces (PES) in three dimensions for Li^+ and Cu^{+2}. The dynamics-based nalysis incorporates effects of the PES anharmonicity. The largest effects due to the quantum character of the metallic nuclei are observed for the lighter metals Li and Be. The largest selectivity in adsorption based on the differences of the zero-point energy of H_2 and isotopologues is predicted for Cu, Ni and Co ions. The estimates of NQEs involving dynamics of H_2 in Cartesian coordinates is extendable to the metals embedded into molecular environments such as those of metal-organic frameworks.

7.1 Introduction

The separation of hydrogen isotopologues, such as D2, HD, H2 and variants is a significant research target in the nuclear industry.1,2 Deuterium (D), a stable non-radioactive isotope of hydrogen, famous for its excellent neutron moderating properties. Moreover, deuterium is of great importance due to its wide applications in a medical treatment and a detection as a tracer element.

In nature, deuterium occurs with an average abundance of 0.015 % of the total

amount of hydrogen in the oceans, while the most common hydrogen isotope (H) accounts for more than 99.98 %. Due to its rarity, deuterium exists in the form of HDO, or the mono-deuterated water molecule. Such low deuterium abundance makes its industrial harvesting a challenging job. Luckily, deuterium is twice heavier than hydrogen and can be efficiently separated based on the mass difference. The most common industrial deuterium enrichment processes are the electrolysis, distillation, chemical exchange and Girdler-Sulphide. These processes are strait forward subject but the extremely rare deuterium abundance makes its separation quite expensive.

It has been suggested by Beenakker et al. that hydrogen isotopologues can be efficiently 5separated with nanoporous materials. Beenakker et al. purposed the Kinetic Quantum Sieving (KQS) method that occurs in the ultra-porous materials.5 The KQS is the most pronounced when the difference between a pore and molecular diameter is not much larger than the de Broglie wavelength of a molecule. Quantum sieving method appears to be the most efficient at a 6relatively low temperature, nearly cryogenic, when the quantum effects are the strongest. KQS method is only possible in the ultra-porous materials with the strict geometrical criteria and only few porous materials can satisfy its criteria.

In a different separation mechanism, called Chemical Affinity Quantum Sieving (CAQS), strongly attractive centers of porous materials may adsorb preferentially heavy isotopologues due to their smaller zero-point energy, resulting in a stronger adsorption enthalpy. This method is maximized by strong adsorption centers, which allow high selectivity at high temperatures (100K and above), and is more appropriate for the rational design of porous materials for efficient hydrogen isotopologues separation. Specifically, MOFs with open metal centers is an example of such materials, and we will examine the nuclear quantum effects underlying CAQS for a set of metal centers binding H2 and its isotopologues.

7.2 Nuclear Quantum Effects for MeH_2: the normal mode analysis

The electronic energy for MeH_2 ions is sensitive to the quality of the ab initio method. Since for comparison of the ZPEs we need to obtain the electronic potential energy surfaces of high accuracy, after trying DFT and MP2 methods, we use CCSD with G3MP2Large basis for all atoms [18] for the geometry optimization and normal modes analysis. For the quantum nuclear dynamics calculations of Section 7.3 we use the same theory level for the full PES construction of Li^+H_2 and a slightly smaller basis CCSD/G3Large for the PES construction of $Cu^{+2}H_2$. The electronic structure calculations are performed with Q-Chem4.3 [**?**].

The NQE within the normal modes analysis is performed for MeH_2, MeHD and MeD_2 where Me represents the following metal ions: Me={Li^+, Na^+, K^+, Be^+, Mg^+, Ca^+, Be^{+2}, Mg^{+2}, Ca^{+2}, B^+, Al^+, Co^+, Ni^+, Cu^+, Co^{+2}, Ni^{+2}, Cu^{+2}}. For the transition metal centers Co, Ni and Cu several spin multiplicities have been considered. To assess the importance of the quantum behavior of the metal ions we have also computed the ZPE for the triatomics assuming unphysically large mass of the metal, $m_{Me} = 10^6$ a.m.u. The optimal geometries and of the MeH_2 triatomics and all the ZPEs are summarized in Table 7.1 and the main trends are shown in Figs 7.1–7.3. Binding of H_2 to the metal center changes the ZPE which roughly correlates to the H-H distance (Fig. 7.1). The change in the ZPE compared to the free H_2 is in the range from 0.5-2.5 kcal/mol while the H-H is stretched up to 8% compared to the free H_2 value.

To assess contribution of the metal center to the ZPE, the ZPE has been also computed for the infinitely heavy Me ion bound to H_2 (labeled as 'HH*' in Table 7.1). The largest changes between these two ZPE values, indicating more 'quantum' character of the metal center, are found as expected for the lighter metal ions, namely Be^+2, Li^+, Be^+ (Fig. 7.2). The difference for these species is 0.176, 0.086 and 0.088 kcal/mol respectively. Smaller changes in the ZPE indicate less 'quantum' character

the metal nuclei, such as the fourth row metals. The difference for Cu^{+2} is 0.023 kcal/mol.

The adsorption selectivity is determined by the difference between the ZPE for MeH_2 and MeD_2, $\Delta = ZPE(MeH_2) - ZPE(MeD_2)$ shown in Fig. 7.3. The largest Δ is found for the transition metals (2.33-2.48 kcal/mol) followed by Li and Be metal centers (2.22-2.29 kcal/mol) which are also the most 'quantum' metal centers. Therefore, a more detailed dynamics study of the NQE is performed for one of the most quantum system, $Li^{+}H_2$, and for one of the most 'selective' systems, $Cu^{+2}H_2$.

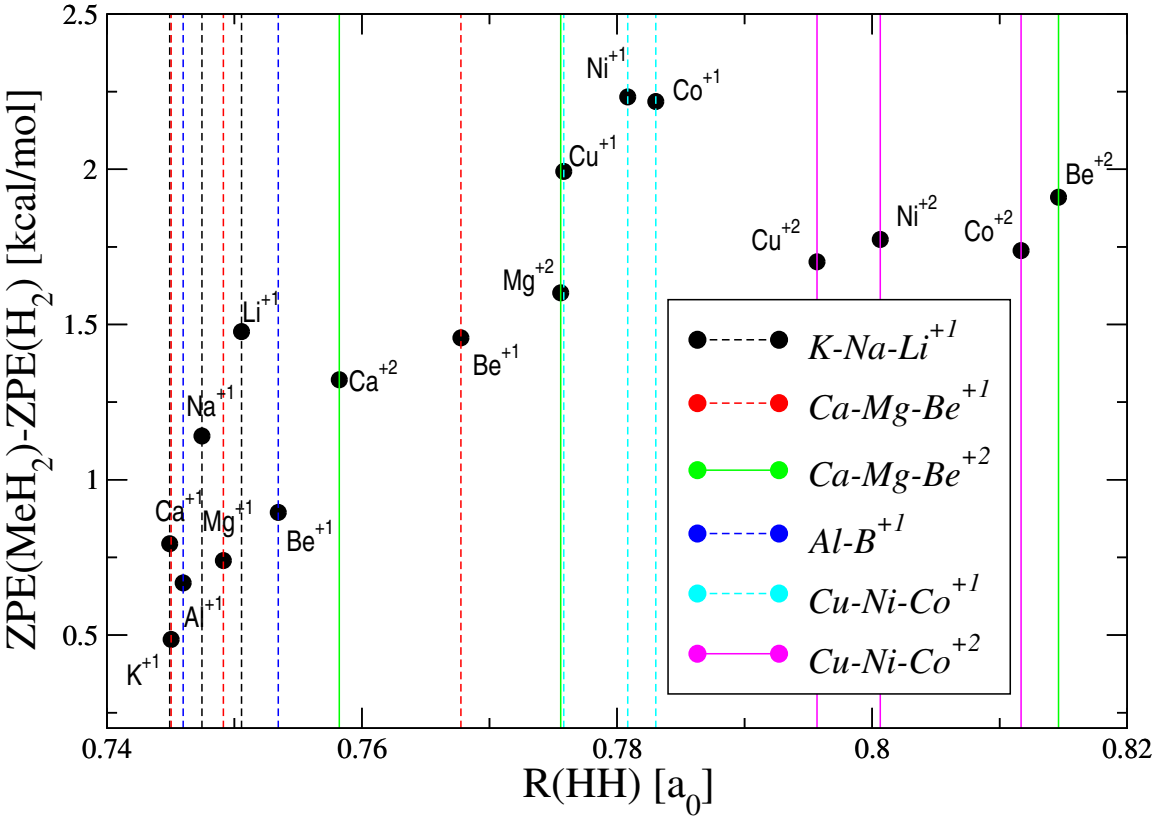

Figure 7.1: The ZPE of MeH_2 ions relative to the ZPE of H_2 molecule as a function of the HH distance. The vertical lines match the metal ions of the legend.

7.3 Nuclear Quantum Effects for MeH_2: nuclear dynamics

To go beyond the normal mode analysis and allow for the anharmonicity of PES, we have used quantum nuclear dynamics to obtain the ground states and selected

Table 7.1: Geometry and ZPE for Me-H_2 trimers and H/D isotopologues. The last ZPE column (HH*) is the value for an infinitely heavy metal. The column Δ lists the difference in ZPE of H_2 bound to the metal center of the main isotope mass and to the infinitely heavy metal. [a] CCSD/G3Large method used for the PES. [b] H_2 and isotopologues without the metal center.

Metal	Geometry			ZPE [kcal/mol]					Ion	
mass Me	Me-H [Å]	H-H [Å]	∠ HHMe°	HH	HD	DD	HH*	Δ	Charge	S^2
3 Li	2.036724	0.750560	79.382302	7.783	6.749	5.560	7.697	0.086	1	0
11 Na	2.424159	0.747456	81.131565	7.447	6.442	5.282	7.426	0.021	1	0
19 K	2.948414	0.744928	82.742672	7.100	6.142	5.028	7.092	0.008	1	0
4 Be	1.838459	0.767759	77.947716	7.763	6.729	5.549	7.675	0.178	1	
12 Mg	2.664742	0.749134	81.919707	7.046	6.097	4.992	7.033	0.046	1	
20 Ca	3.380715	0.745043	83.673734	6.792	5.879	4.807	6.789	0.019	1	
4 Be	1.620057	0.814619	75.438643	8.216	7.134	5.927	8.038	0.088	2	0.75
12 Mg	2.045225	0.775584	79.070068	7.908	6.837	5.626	7.862	0.013	2	
20 Ca	2.463211	0.758228	81.146383	7.628	6.593	5.409	7.609	0.003	2	
5 B	2.353029	0.753443	80.787395	7.201	6.236	5.119	7.163	0.038	1	
13 Al	3.076253	0.745984	83.035945	6.974	6.035	4.940	6.965	0.009	1	
27 Co	1.888585	0.795679	77.856330	8.008	6.910	5.681	7.985	0.022	2	1.7402
28 Ni	1.840668	0.800639	77.438592	8.080	6.971	5.733	8.055	0.022	2	2.0034
29 Cu	1.794757	0.811681	76.931183	8.044	6.937	5.707	8.019	0.019	2	
27 Co	1.743300	0.783037	77.022365	8.524	7.352	6.046	8.502	0.023	1	2.0080
28 Ni	1.735737	0.780840	77.001842	8.539	7.365	6.056	8.517	0.025	1	0.75
29 Cu	1.774239	0.775827	77.371155	8.299	7.161	5.884	8.280	0.025	1	
[a]29 Cu	1.812126	0.809082	77.100660	8.022	6.920	5.693	7.997		2	0.7512
[b] free		0.742119		6.306	5.462	4.461				1

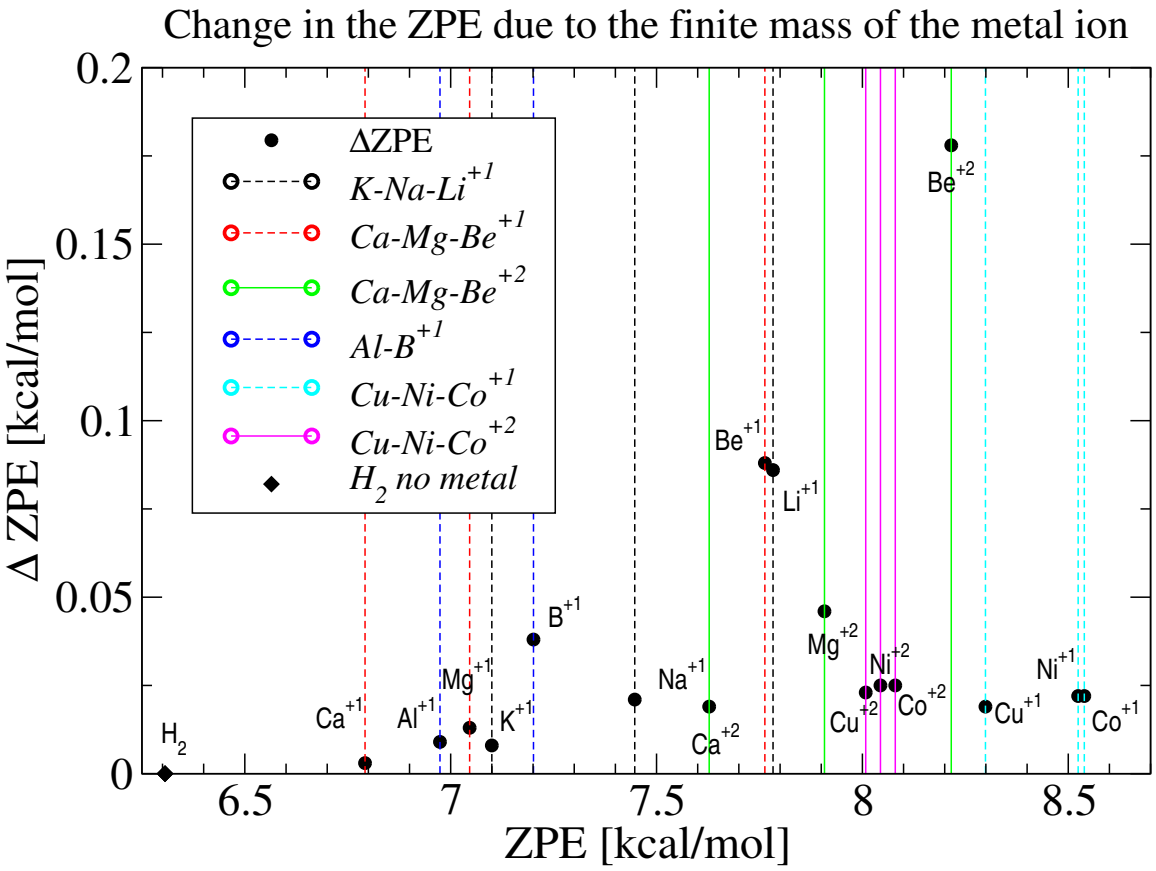

Figure 7.2: Assessing the QM character of the metallic nuclei: the difference Δ of the ZPE of MeH_2 species with the ZPE computed for infinitely heavy metal ion as a function of the ZPE. The vertical lines match the metal ions of the legend.

excited energy levels. Analysis of the free non-rotating H_2 whose PES is fitted with the Morse potential [75] shows that the anharmonicity of the H_2 vibration, $\eta_V = (E_1 - E_0)/(2E_0) - 1$ is close to 10%. The anharmonicity parameter of the Morse potential for H_2 is $\chi \equiv \omega/(4D) = 0.04$, where ω is the harmonic frequency and D is the well-depth. Our of triatomics two metal ions are considered for the dynamics investigation: Li^+H_2 and $Cu^{+2}H_2$ with H/D substitution. The former species will have the most pronounced NQE associated with the metal nucleus. The latter species is expected to have the largest selectivity in H_2/D_2 adsorption.

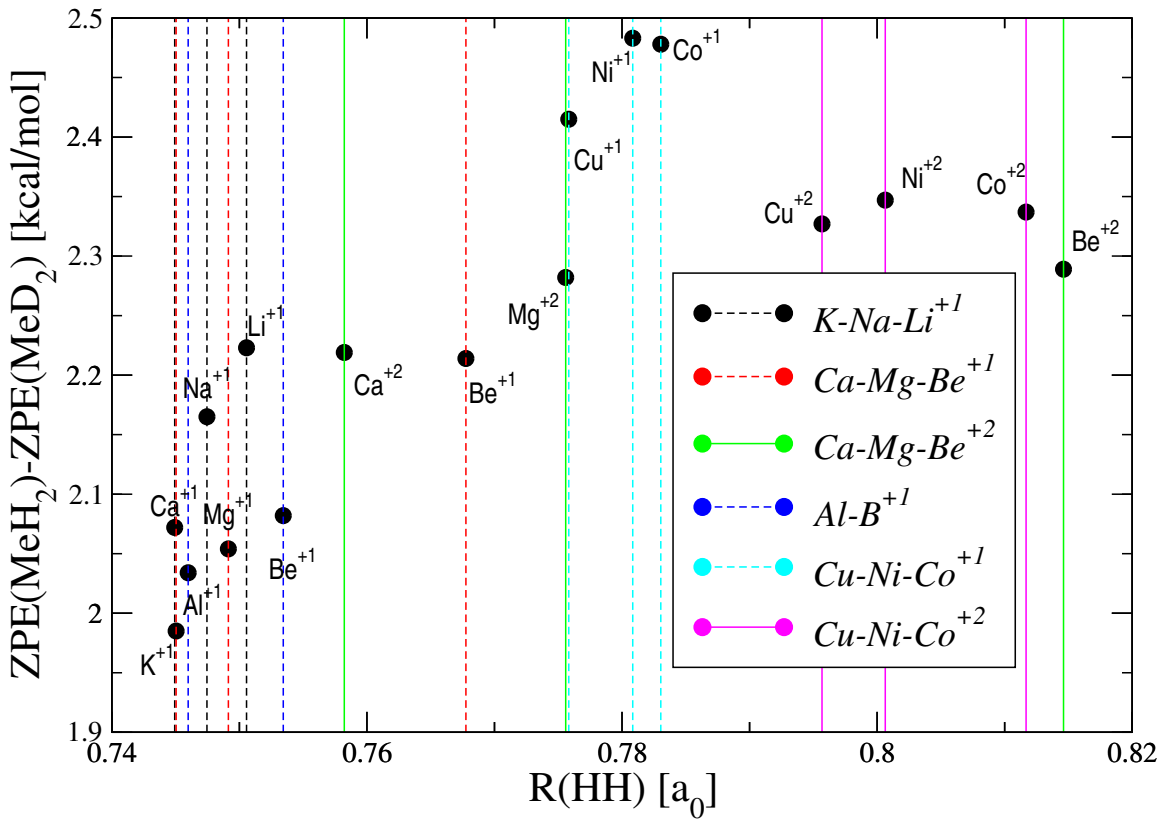

Figure 7.3: H_2/D_2 adsorption selectivity: the difference between the ZPE of MeH_2 ions with the ZPE of MeD_2. The vertical lines match the metal ions of the legend.

Li^+H_2

Li^+H_2 is the smallest triatomic from our set of Section 7.2, with just four electrons, with the 'most quantum' metal nucleus. Therefore, we construct a high-quality analytical PES for this system. A grid of ab initio points computed at the CCSD/G3MP2Large level is used to construct a spline-based analytical PES.

All three nuclei are treated as QM particles described in the Jacobi coordinates (R, r, θ) [**?**] and the molecule is non-rotating. The distances are described on an equidistant grid and the Discrete Variable Representation is used for the angle [62].

The ground state energy and a few low-lying excited energy levels are obtained from the Fourier transform of the autocorrelation function $C(t)$ of a wavefunction ψ_0, $C(t) = \langle \psi_0 | \psi_t \rangle$. The wavefunction is evolved in real time using the split operator

propagator and Fast Fourier Transform [59, 21]. The propagation parameters are given in Table 7.2. The initial wavefunction ψ_0 is set as a product of Gaussian functions in R and r, and the angular dependence is introduced to ensure that the initial wavefunction overlaps with the first few exited states:

$$\psi_0^{real}(R, r, \theta) = \sin^2\theta e^{-\alpha(R-R_e)^2-\beta(r-r_e)^2}. \tag{7.1}$$

Table 7.2: Simulation parameters for the Li^+H_2 system. N_t is the number of time-steps dt taken. N_θ is the number of the angle DVR points.

Propagation	N_t	dt [a.u.]	α [a_0^{-2}]	β [a_0^{-2}]	R_e [a_0]	r_e [a_0]	N_θ
Real time	30000	2	12	12	3.8	1.40	40

The normal modes vibrational analysis of the CCSD/G3MP2Large calculation yields three modes shown in Fig. 7.4: the relative translational mode of frequency 477.51 cm^{-1}; the diatomic rotational mode of frequency 669.54 cm^{-1}; the diatomic vibrational mode of frequency 4297.32 cm^{-1}. The lowest transition frequencies obtained from the Fourier transform of the autocorrelation functions are listed in Table 7.3. Apparently the low excitation states do not involve excitation of the diatomic vibrational mode.

The anharmonicity can be measured using the difference between two lowest excitation transition

$$\eta = \frac{\omega_{10} - \omega_{21}}{\omega_{10}}$$

Here $\omega_{mn} = (E_m - E_n)/\hbar$ is the transition frequency between states m and n. For the harmonic system $\eta = 0$. Labeling the relative translational mode as T and the diatomic rotational mode as R, one can obtain $\eta_T = 6.8\%$ and $\eta_R = 7.5\%$. Our estimate for the H-H vibration is $\eta_V = 10\%$.

$Cu^{+2}H_2$

In case of $Cu^{+2}H_2$, given its large mass and small changes in the normal modes ZPE as discussed in Section 7.2. we do not treat Cu as the quantum nucleus. The H-H is

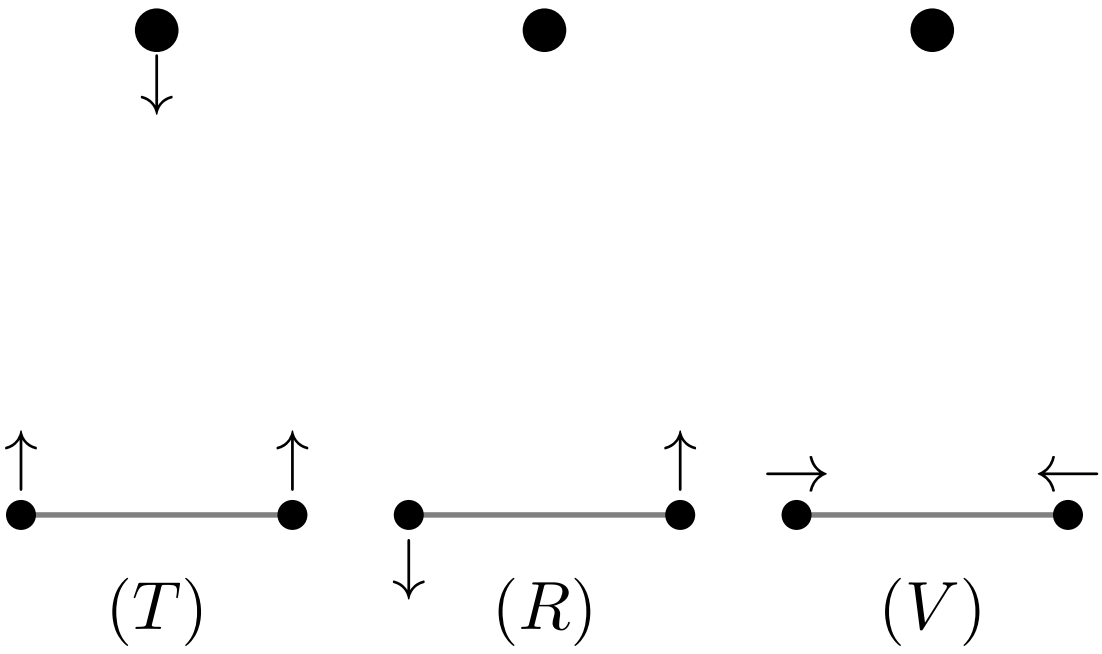

Figure 7.4: The normal modes of Li^+H_2: relative M-H_2 translation (T), H_2 rotation (R) and H_2 vibration (V).

Table 7.3: Transition frequencies and corresponding excitation energies.

Transition frequency [cm^{-1}]	Transition	Normal mode frequency [cm^{-1}]
514.8	T: $\|0\rangle \rightarrow \|1\rangle$	477.51
479.6	T: $\|1\rangle \rightarrow \|2\rangle$	
737.0	R: $\|0\rangle \rightarrow \|1\rangle$	669.54
682.0	R: $\|1\rangle \rightarrow \|2\rangle$	

described using three quantum Cartesian coordinates (x, y, z): the center of H_2 fixed at its equilibrium position with respect to Cu^{+2} and the H-H vector is defined in three Cartesian coordinates: x measures the H-H distance and y and z the orientation of H_2 with respect to the metal center. This set up can be used to MeH_2 embedded in a MOF. In the absence of the MOF environment, however, there is cylindrical symmetry of the PES with respect to rotation along the x-axis, and the z coordinate then is redundant. The PES is obtained from a six-point two-dimensional interpolation of the electronic energy values computed on the (x, y) grid $x = [-1.5, 1.5]$, $dx = 0.1$ a_0 and the same for y. The PES points are obtained using CCSD within the 6-31G*

Table 7.4: QM dynamics parameters for $Cu^{+2}H_2$. The time-step and the width parameters are rescaled by the appropriate isotope mass for HD and DD.

N_{pnts}	time step	final time	Grid start	
128	0.025	2.5	0.0	-1.575
Δx	ψ_0 width $[a_0^{-2}]$		ψ_0 center $[a_0]$	
0.025	6	2	1.53	0.0

Table 7.5: Parameters of the Morse potential fitting ab initio data (CCSD/G3Large) for H_2 stretch and $Cu^{+2}H_2$ stretch.

	HH	Cu-H
D	0.0991235	0.0714296
a	1.12074	.768744
r_0	1.53809	3.34728
x_e	0.0415367	0.01678
ZPE E_h	0.0080635	0.002377
E_0^{HH} $[kcal/mol]$	5.06	1.49
E_0^{HD} $[kcal/mol]$	4.39	1.22
E_0^{DD} $[kcal/mol]$	3.60	1.06

Table 7.6: ZPE from the fitting of the wavefunction energy decaying to the ground state. The last column, ZPE*, lists the normal modes values (CCSD/G3Large).

	E_0 [E_h]	E_0 $[\frac{kcal}{mol}]$	ZPE^{tr} $[\frac{kcal}{mol}]$	ZPE $[\frac{kcal}{mol}]$	ZPE* $[\frac{kcal}{mol}]$
H_2	0.01001	6.28	1.49	7.77	8.02
HD	0.00893	5.61	1.22	6.83	6.92
D_2	0.00764	4.80	1.06	5.86	5.69

basis for H and G3Large basis for Cu. The split-operator/Fast Fourier Transform propagation in imaginary time give estimates of the ZPE for H_2 and its isotopologues. To accelerate convergence of the imaginary time dynamics we add a simple quadratic potential $V_z = kz^2/2$. To estimate the ground state energy of the triatomic Li^+H_2 and isotopologues, the ZPE of the separable in $z-$coordinate motion is subtracted and the ZPE of the Morse potential, mimicking the translational motion of H_2 bound to Cu^{+2}, is added. The propagation parameters and the initial wavefunction ψ_0 are listed in Table 7.4.

The Morse parameters to the H_2 stretch and $Cu^{+2}H_2$ stretch, or H_2 translation, are given in Table 7.5.

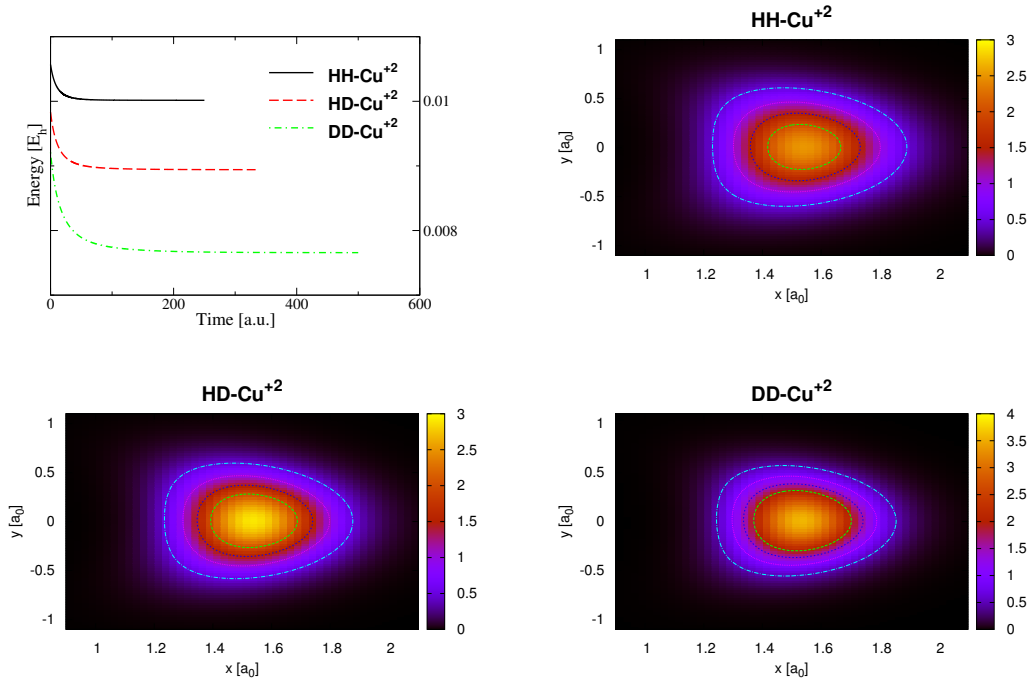

Figure 7.5: The wavefunction energy as a function of time. Contour plots of the ground state wavefunction for H_2, HD and D_2 bound to Cu^{+2}. Contours are plotted for the isodensity values of $\{0.5, 1.0, 1.5, 2.0\}$.

Chapter 8

Conclusion

The take home message is that the quantum effects of nuclei such as zero-point energy, tunneling effects can be essential for understanding of chemical processes. This is supported by some experimental results for water systems and low-temperature reactions. Exact quantum treatment is scalable to just 4-5 atoms due to exponential increase of computational resources with the system size. This motivates theoretical chemists to develop approximations to simplify the computation. Various semiclassical methods are being developed, yet currently there is no widely used general approach.

The quantum trajectory method developed in our group is based on the de Broglie-Bohm formulation of quantum mechanics. The state of a quantum system is represented by an ensemble of quantum trajectories. The equations of motion for these quantum trajectories differ from classical equations of motion by an extra potential, the so-called "quantum potential". The quantum potential has a simple and elegant mathematical expression, but poses severe numerical challenges if one wants to compute it exactly.

We have developed the *approximate quantum potential* (AQP) method and its extension describing the energy dissipation in a quantum system. This AQP dynamics with friction was used to obtain the ground state energy and wavefunction of any quantum system with large anharmonicity. After tests of low-dimensional model systems, we studied the solid helium 4 modeled with 180 nuclei. The formalism to estimate the effects of quantum statistics and to extract collective modes of motion

in a large quantum system have been developed.

The interference effects are difficult to describe within the AQP formulation. Thus, we introduce a new method, the quantum trajectory guided Gaussian bases, which is a marriage of the basis set representation with the wavefunction and trajectory representation. The set of Gaussian bases is characterized by the centers, the centers move in the same way as quantum trajectories, yielding a very compact time-dependent basis, while superposition of Gaussians describes interference. This approach is used for double well, Eckart barrier and a 2-dimensional double well coupled with harmonic oscillator model systems illustrating the concept for bound and scattering problem.

Extensions of the approach baed on adaptive-width functions and basis reexpansions are planned for the future.

Bibliography

[1] John E. Adams and Richard M Stratt. Instantaneous normal mode analysis as a probe of cluster dynamics. *Journal of Chemical Physics*, 93(2):1332, 1990.

[2] R.A. Aziz, F.R.W. McCourt, and C.C.K. Wong. *Mol. Phys.*, 61:1487, 1987.

[3] D. Babyuk and R. E. Wyatt. Multidimensional reactive scattering with quantum trajectories: Dynamics with 50-200 vibrational modes. *J. Chem. Phys.*, 124:214109(1–7), 2006.

[4] David H. Boal and James N. Glosli. Quasiparticle model for nuclear dynamics studies: Ground-state properties. *Phys. Rev. C*, 38:1870–1878, Oct 1988.

[5] D. Bohm. A Suggested Interpretatin of the Quantum Theory in Terms of "Hidden" Variables. I. *Phys. Rev.*, 85:166–179, 1952.

[6] D. Bohm. A Suggested Interpretatin of the Quantum Theory in Terms of "Hidden" Variables. II. *Phys. Rev.*, 85:180–193, 1952.

[7] David Bohm. A suggested interpretation of the quantum theory in terms of "hidden" variables. i. *Phys. Rev.*, 85:166–179, Jan 1952.

[8] David Bohm. A suggested interpretation of the quantum theory in terms of "hidden" variables. ii. *Phys. Rev.*, 85:180–193, Jan 1952.

[9] Jean-Pierre Boon and Sidney Yip. *Molecular Hydrodynamics*. New York: Dover Publications, 1991.

[10] Drew Brandon and Bill Poirier. Accurate calculations of bound rovibrational states for argon trimer. *The Journal of Chemical Physics*, 141(3), 2014.

[11] A. O. Caldeira and J. J. Leggett. *Phys. Rev. Lett.*, 46:211, 1981.

[12] S. Carter, S. J. Culik, and J. M. Bowman. Vibrational self-consistent field method for many-mode systems: A new approach and application to the vibrations of CO adsorbed on Cu(100). *J. Chem. Phys.*, 107:10458–10469, 1997.

[13] C. Cazorla and J. Boronat. *J. Phys.: Condens. Matter*, 20:015223, 2008.

[14] Lorenz S. Cederbaum, Etienne Gindensperger, and Irene Burghardt. Short-time dynamics through conical intersections in macrosystems. *Phys. Rev. Lett.*, 94:113003, Mar 2005.

[15] Michele Ceriotti, Wei Fang, Peter G. Kusalik, Ross H. McKenzie, Angelos Michaelides, Miguel A. Morales, and Thomas E. Markland. Nuclear quantum effects in water and aqueous systems: Experiment, theory, and current challenges. *Chemical Reviews*, 116(13):7529–7550, 2016. PMID: 27049513.

[16] David Chandler. *Introduction to modern statistical mechanics*. Oxford University Press, 1987.

[17] Minhaeng Cho, Graham R. Fleming, Shinji Saito, Iwao Ohmine, and Richard M. Stratt. Instantaneous normal mode analysis of liquid water. *The Journal of Chemical Physics*, 100(9):6672, 1994.

[18] Larry A. Curtiss, Paul C. Redfern, Krishnan Raghavachari, Vitaly A. Rassolov, and John A. Pople. G3 theory using reduced Møller-Plesset order. *J. Chem. Phys.*, 110(10):4703–4709, 1999.

[19] Gabor Czako, Alexey L. Kaledin, and Joel M. Bowman. A practical method to avoid zero-point leak in molecular dynamics calculations: Application to the water dimer. *J. Chem. Phys.*, 132, 2010.

[20] GÃąbor CzakÃş, Alexey L. Kaledin, and Joel M. Bowman. Zero-point energy constrained quasiclassical, classical, and exact quantum simulations of isomerizations and radial distribution functions of the water trimer using an ab initio potential energy surface. *Chemical Physics Letters*, 500(4âĂŞ6):217 – 222, 2010.

[21] M. D. Feit, J. A. Fleck Jr., and A. Steiger. Solution of the Schrödinger equation by a spectral method. *J. Comp. Phys.*, 47(3):412 – 433, 1982.

[22] S. Garashchuk. Description of bound reactive dynamics within the approximate quantum trajectory framework. *J. Phys. Chem. A*, 113:4451–4456, 2009.

[23] S. Garashchuk. Calculation of the zero-point energy from imaginary-time quantum trajectory dynamics in Cartesian coordinates. *Theoretical Chemistry Accounts*, 131:1083, 2012.

[24] S. Garashchuk and J. C. Light. Quasirandom distributed Gaussian bases for bound problems. *J. Chem. Phys.*, 114:3929–3939, 2001.

[25] S. Garashchuk, James Mazzuca, and J. Jakowski. Multidimensional quantum trajectory dynamics in imaginary time with approximate quantum potential. *J. Chem. Phys.*, 135:034104, 2011.

[26] S. Garashchuk and V. A. Rassolov. Semiclassical dynamics based on quantum trajectories. *Chem. Phys. Lett.*, 364:562–567, 2002.

[27] S. Garashchuk and V. A. Rassolov. Quantum dynamics with Bohmian trajectories: Energy conserving approximation to the quantum potential. *Chem. Phys. Lett.*, 376:358–363, 2003.

[28] S. Garashchuk and V. A. Rassolov. Semiclassical dynamics with quantum trajectories: Formulation and comparison with the semiclassical initial value representation propagator. *J. Chem. Phys.*, 118:2482–2490, 2003.

[29] S. Garashchuk and V. A. Rassolov. Energy conserving approximations to the quantum potential: Dynamics with linearized quantum force. *J. Chem. Phys.*, 120:1181–1190, 2004.

[30] S. Garashchuk and V. A. Rassolov. Energy conserving approximations to the quantum potential: Dynamics with linearized quantum force. *J. Chem. Phys.*, 120:1181–1190, 2004.

[31] S. Garashchuk and V. A. Rassolov. Stable long-time semiclassical description of zero-point energy in high-dimensional molecular systems. *J. Chem. Phys.*, 129:024109, 2008.

[32] S. Garashchuk and T. Vazhappilly. Wavepacket approach to the cumulative reaction probability within the flux operator formalism. *J. Chem. Phys.*, 131(16):164108, 2009.

[33] Sophya Garashchuk, David DellâĂŹAngelo, and Vitaly A. Rassolov. Dynamics in the quantum/classical limit based on selective use of the quantum potential. *The Journal of Chemical Physics*, 141(23), 2014.

[34] Sophya Garashchuk, V. Dixit, Bing Gu, and James Mazzuca. *J. Chem. Phys.*, 138:054107, 2013.

[35] Sophya Garashchuk, Vaibhav Dixit, Bing Gu, and James Mazzuca. The Schrödinger equation with friction from the quantum trajectory perspective The Schrödinger equation with friction from the quantum trajectory. 054107, 2013.

[36] Sophya Garashchuk, Jacek Jakowski, Lei Wang, and Bobby G. Sumpter. *J. Chem. Theory Comput.*, 9, 2013.

[37] Sophya Garashchuk and Vitaly Rassolov. Semiclassical Bohmian Dynamics. 27, 2011.

[38] Sophya Garashchuk, Vitaly Rassolov, and Oleg Prezhdo. *Reviews in Computational Chemistry*, volume 27, chapter Semiclassical Bohmian dynamics, pages 111–210. Wiley, 2011.

[39] Sophya Garashchuk and Vitaly A. Rassolov. Semiclassical dynamics with quantum trajectories: Formulation and comparison with the semiclassical initial value representation propagator. *J. Chem. Phys.*, 118(6):2482–2490, 2003.

[40] E. Gindensperger, C. Meier, and J. A. Beswick. Mixing quantum and classical dynamics using bohmian trajectories. *J. Chem. Phys.*, 113:9369–9372, 2000.

[41] Etienne Gindensperger, Irene Burghardt, and Lorenz S. Cederbaum. Short-time dynamics through conical intersections in macrosystems. i. theory: Effective-mode formulation. *The Journal of Chemical Physics*, 124(14), 2006.

[42] Y. Goldfarb, I. Degani, and D. J. Tannor. Bohmian mechanics with complex action: A new trajectory-based formulation of quantum mechanics. *J. Chem. Phys.*, 125:231103, 2006.

[43] Bing Gu, Robert J Hinde, Vitaly A Rassolov, and Sophya Garashchuk. Estimation of the Ground State Energy of an Atomic Solid by Employing Quantum Trajectory Dynamics with Friction. *J. Chem. Theory Comput.*, 11(7):2891–2899, jul 2015.

[44] Yong-Chang Han and Joel M. Bowman. Reactant zero-point energy is needed to access the saddle point in molecular dynamics calculations of the association reaction H+C2D2âĘŠC2D2HâĹŮ. *Chemical Physics Letters*, 556:39–43, jan 2013.

[45] J. P. Hansen and E. L. Pollock. Ground-state properties of solid helium-4 and -3. *Phys. Rev. A*, 5:2651–2665, Jun 1972.

[46] Jean-Pierre Hansen and Dominique Levesqure. Ground state of solid helium-4 and -3. *Phys. Rev.*, 165:293–299, Jan 1968.

[47] G. D. Harp and B. J. Berne. Time-correlation functions, memory functions, and molecular dynamics. *Phys. Rev. A*, 2:975–996, Sep 1970.

[48] E. J. Heller. Time-dependent approach to semiclassical dynamics. *J. Chem. Phys.*, 62:1544, 1975.

[49] E. J. Heller. Frozen Gaussians: A very simple semiclassical approximation. *J. Chem. Phys.*, 75:2923, 1981.

[50] E. J. Heller. Frozen gaussians: A very simple semiclassical approximation. *J. Chem. Phys.*, 75:2923–2931, 1981.

[51] E. J. Heller. Cellular-dynamics - a new semiclassical approach to time-dependent quantum-mechanics. *J. Chem. Phys.*, 94:2723–2729, 1991.

[52] E. J. Heller, J. R. Reimers, and G. Drolshagen. *Phys. Rev. A*, 36(2613), 1987.

[53] Michael F. Herman and Edward Kluk. A semiclasical justification for the use of non-spreading wavepackets in dynamics calculations. *Chemical Physics*, 91(1):27 – 34, 1984.

[54] Robert J. Hinde. QSATS: MPI-driven quantum simulations of atomic solids at zero temperature. *Computer Physics Communications*, 182(11):2339–2349, November 2011.

[55] Martinez T. J. *J. Phys. Chem.*, 100:7884, 1996.

[56] E. Kanai. On the quantization of the dissipative systems. *Prog. Theor. Phys.*, 3:440–442, 1948.

[57] B. K. Kendrick. A new method for solving the quantum hydrodynamic equations of motion. *J. Chem. Phys.*, 119:5805–5817, 2003.

[58] E. Kluk, M.F. Herman, and H.L. Davis. *J. Chem. Phys.*, 84:326, 1995.

[59] R. Kosloff. Time-dependent quantum-mechanical methods for molecular dynamics. *J. Phys. Chem.*, 92:2087–2100, 1988.

[60] C. Leforestier, R. H. Bisselling, C. Cerjan, M. D. Feit, R. Friesner, A. Guldberg, A. Hammerich, G. Jolicard, W. Karrlein, H. D. Meyer, N. Lipkin, O. Roncero, and R. Kosloff. A comparison of different propagation schemes for the time-dependent Schrödinger equation. *J. Comp. Phys.*, 94:59–80, 1991.

[61] V. A. Levashov, S. J. L. Billinge, and M. F. Thorpe. Quantum correction to the pair distribution function. *J. Comput. Chem.*, 28:1865–1882, 2007.

[62] J. C. Light and T. Carrington, Jr. Discrete variable representations and their utilization. *Adv. Chem. Phys.*, 114:263–310, 2000.

[63] C. L. Lopreore and R. E. Wyatt. Quantum wave packet dynamics with trajectories. *Phys. Rev. Lett.*, 82:5190–5193, 1999.

[64] C. L. Lopreore and R. E. Wyatt. Quantum wave packet dynamics with trajectories. *Phys. Rev. Lett.*, 82:5190–5193, 1999.

[65] Ao Ma and Richard M. Stratt. Fifth-order Raman spectrum of an atomic liquid: simulation and instantaneous-normal-mode calculation. *Physical Review Letters*, 85(5):1004–1007, 2000.

[66] V. A. Mandelshtam and H. S. Taylor. Harmonic inversion of time signals. *J. Chem. Phys.*, 107:6756–6769, 1997.

[67] G. Mazenko, J.R. Banavar, and R. Gomer. Diffusion coefficients and the time auto-correlation function of density fluctuations. *Surface Science*, 107(2âĂŞ3):459 – 468, 1981.

[68] James Mazzuca, Sophya Garashchuk, and Jacek Jakowski. *Chemical Physics Letters*, 542:153–158, 2012.

[69] A. D. Mclachlan. *Mol. Phys.*, 8:39, 1964.

[70] D. M. Medvedev, S. K. Gray, E. M. Goldfield, M. J. Lakin, D. Troya, and G. C. Schatz. Quantum wave packet and quasiclassical trajectory studies of oh+co: Influence of the reactant channel well on thermal rate constants. *J. chem. Phys.*, 120:1231–1238, 2004.

[71] H. D. Meyer, U. Manthe, and L. S. Cederbaum. The multi-configurational time-dependent hartree approach. *Chem. Phys. Lett.*, 165(1):73 – 78, 1990.

[72] W. H. Miller. Classical path approximation for the Boltzmann density matrix. *J. Chem. Phys.*, 55:3146–3149, 1971.

[73] William H. Miller, William L. Hase, and Cynthia L. Darling. A simple model for correcting the zero point energy problem in classical trajectory simulations of polyatomic molecules. *J. Chem. Phys.*, 91(5):2863, 1989.

[74] Shinichi Miura. *Computer Physics Communications*, 182:274–276, 2011.

[75] P. M. Morse. Diatomic molecules according to the wave mechanics. II. Vibrational levels. *Phys. Rev.*, 34:57–65, 1929.

[76] W. H. Press, B. P. Flannery, S. A. Teukolsky, and W. T. Vetterling. *Numerical Recipes: The Art of Scientific Computing*. Cambridge University Press, Cambridge, 3 edition, 2007.

[77] Stewart K. Reed, Maykel L. González-Martínez, Jesús Rubayo-Soneira, and Dmitrii V. Shalashilin. Cartesian coupled coherent states simulations: Ne_nBr_2 dissociation as a test case. *J. Chem. Phys.*, 134, 2011.

[78] A. S. Sanz, R. Martinez-Casado, H. C. Penate-Rodriguez, G. Rojas-Lorenzo, and S. Miret-Artes. Dissipative bohmian mechanics within the caldirola-kanai frame-

work: A trajectory analysis of wave-packet dynamics in viscid media. *Annals of Physics*, 347:1–20, 2014.

[79] G. Schiffel and U. Manthe. Quantum dynamics of the H+CH_4 $\rightarrow$ H_2+CH_3 reaction in curvilinear coordinates: Full-dimensional and reduced dimensional calculations of reaction rates. *J. Chem. Phys.*, 132(8):3428622, 2010.

[80] Peter R. Schreiner, Hans Peter Reisenauer, David Ley, Dennis Gerbig, Chia-Hua Wu, and Wesley D. Allen. Methylhydroxycarbene: Tunneling control of a chemical reaction. *Science*, 332(6035):1300–1303, 2011.

[81] D Sewell and Donald L. Thompson. Some problems of correcting the zero-point energy problem in classical trajectories. *Chem. Phys. Lett.*, 193(6), 1992.

[82] D. V. Shalashilin and I. Burghardt. Gaussian-based techniques for quantum propagation from the time-dependent variational principle: Formulation in terms of trajectories of coupled classical and quantum variables. *J. Chem. Phys.*, 129(8):084104, 2008.

[83] Yihan Shao, Laszlo Fusti Molnar, Yousung Jung, Joerg Kussman, Christian Ochsenfeld, Shawn T. Brown, Andrew T. Gilbert, Lyudmila V. Slipchenko, Sergey Levchenko, Darragh P. O'Neill, Robert A. Distasio Jr., Rohini C. Lochan, Tao Wang, Gregory J.O. Beran, Nick A. Besley, John M. Herbert, Ching Yeh Lin, Troy Van Voorhis, Siu Hung Chien, Alex Sodt, Ryan Steele, Vitaly Rassolov, Paul Maslen, Prakashan Korambath, Ross Adamson, Brian Austin, Jon Baker, Edward F. C. Byrd, Holger Daschle, Robert J. Doerksen, Andreas Dreuw, Barry D. Dunietz, Anthony D. Dutoi, Thomas R. Furlani, Steven R. Gwaltney, Andreas Heyden, So Hirata, Chao-Ping Hsu, Gary Kedziora, Rustam Z. Khalliulin, Phil Klunzinger, Aaron Lee, Michael S. Lee, WanZhen Liang, Nikhil Nair, Baron Peters, Emil I. Proynov, Piotr Pieniazek, Young Min Rhee, Jim

Ritchie, Edina Rosta, C. David Sherrill, Andrew C. Simmonett, Joseph E. Subotnik, H. Lee Woodcock, Weimin Zhang, Alexis T. Bell, Arup K. Chakraborty, Daniel M. Chipman, Warren Hehre, Arieh Warshel, Henry F. Schaefer III, Jing Kong, Anna I. Krylov, Peter M. W. Gill, and Martin Head-Gordon. Advances in methods and algorithms in a modern quantum chemistry program package. 2006.

[84] Hiroyuki Tamura, John G. S. Ramon, Eric R. Bittner, and Irene Burghardt. Phonon-driven ultrafast exciton dissociation at donor-acceptor polymer heterojunctions. *Phys. Rev. Lett.*, 100:107402, Mar 2008.

[85] D. J. Tannor. *Introduction to Quantum Mechanics: A Time-Dependent Perspective*. University Science Books, 2006.

[86] Ivano Tavernelli. Nonadiabatic molecular dynamics simulations: Synergies between theory and experiments. *Accounts of Chemical Research*, 48(3):792–800, 2015. PMID: 25647401.

[87] C. J. Trahan, K. Hughes, and R. E. Wyatt. A new method for wave packet dynamics: Derivative propagation along quantum trajectories. *J. Chem. Phys.*, 118:9911–9914, 2003.

[88] H. B. Wang and M. Thoss. Multilayer formulation of the multiconfiguration time-dependent Hartree theory. *J. Chem. Phys.*, 119:1289–1299, 2003.

[89] Lei Wang, Jacek Jakowski, and Sophya Garashchuk. Adsorption of a hydrogen atom on a graphene flake examined with quantum trajectory/electronic structure dynamics. *The Journal of Physical Chemistry C*, 118(29):16175–16187, 2014.

[90] Ulrich Weiss. *Quantum Dissipative Systems*. World Scientific, 4 edition, 2008.

[91] G. A. Worth and I. Burghardt. Full quantum mechanical molecular dynamics using gaussian wavepackets. *Chem. Phys. Lett*, 368:502, 2003.

[92] Yinghua Wu and Victor S. Batista. Matching-pursuit for simulations of quantum processes. *J. Chem. Phys.*, 118(15):6720–6724, 2003.

[93] R. E. Wyatt. *Quantum Dynamics with Trajectories: Introduction to Quantum Hydrodynamics*. Springer-Verlag, 2005.

[94] R. E. Wyatt and W. R. Bittner. Quantum wave packet dynamics with trajectories: Implementation with adaptive lagrangian grids. *J. Chem. Phys.*, 113:8898–8907, 2000.

[95] R. E. Wyatt and K. Na. Quantum trajectory analysis of multimode subsystem-bath dynamics. *Phys. Rev. E*, 59:016702, 2002.

[96] Xunmo Yang and Eric R. Bittner. Intramolecular charge- and energy-transfer rates with reduced modes: Comparison to marcus theory for donorâĂŞbridgeâĂŞacceptor systems. *The Journal of Physical Chemistry A*, 118(28):5196–5203, 2014. PMID: 24983415.

[97] Xunmo Yang and Eric R. Bittner. Computing intramolecular charge and energy transfer rates using optimal modes. *The Journal of Chemical Physics*, 142(24), 2015.

[98] R. Zwanzig. Nonlinear generalized langevin equations. *J. Stat. Phys.*, 9:215, 1973.

Appendix A

Quantum Scattering

Quantum scattering is ubiquitous in chemical dynamics, which can be taken as a quantum description of the classical colliding model. This phenomenon can be studied in a time-independent approach which usually involves plane wave for the asymptotic Hamiltonian and also time-dependent method. Here we focus on time-dependent method which is more intuitive.

A convenient model which goes beyond the one-dimensional barrier scattering to understand quantum scattering is atom-diatom collision,

$$A + BC(\nu = 0) \rightarrow AB(\nu' = 0, 1, 2) + C, \tag{A.1}$$

If we assume the initial state has a product form $\psi(t_i) = \psi(R)\chi_r$, where R represents distance from A to the center BC, and r labels the diatomic distance between BC. For simplicity, we do not consider the angle here. The initial state will involve under the total Hamiltonian H. At long enough time, the wavefunction $\psi(t)$ will become reflective part ψ_R and transmitted part ψ_T. The transmission part represents the probability of reaction. If we measure the outgoing atom, which would be atom A or atom C, the amplitude for a particular event (say atom C has momentum p and diatom AB is in state ν will be $S_f = \langle p\phi_\nu|\psi(t)\rangle$. If we want to know the scattering probability of a particular initial state ϕ_i, then we have to divide the amplitude of initial wavefunction projected onto ϕ_i such that

$$S_{if} = \frac{\phi_f|\psi(t)}{\langle\phi_i|\psi(t_i)\rangle}$$

To get the time-invariant value, we should take the time to infinity thus the probability of observing that event is

$$P_{i\to f} = \lim_{t_f - t_i \to \infty} |\langle \phi_f | U(t_f, t_i) | \psi(t_i) \rangle|^2 / |\langle \phi_i | \psi(t_i) \rangle|^2 \tag{A.2}$$

This quantity should have no dependence of the initial wavefunction and initial time, thus we have the freedom to choose the initial wavefunction to to time-dependent quantum dynamics.

A.1 Collinear Reaction

For the purpose of computing S-matrix elements for the three inelastic exchange reactions,

$$A + BC(\nu = 0) \to AB(\nu' = 0, 1, 2) + C, \tag{A.3}$$

In the asymptotic region of reactants, labelled by $i = 1$, initial wavepacket $\Psi_{in}^{0,0}(r_1, R_1)$ is prepared by computing the product between the $\nu = 0$ vibrational eigenstate of the **BC** diatom, and a Gaussian wave packet,

$$\Psi_{in}^{0,0}(r_1, R_1) = \langle r_1 | 0 \rangle \left(\frac{2\alpha_{R_1}}{\pi} \right)^{1/4} \times \exp[-\alpha_{R_1}(R_1 - R_1^0)^2 + \imath p_{R_1}(R_1 - R_1^0)]. \tag{A.4}$$

In Eq. (A.4), $\langle r_1 | 0 \rangle$ is the normalized ground vibrational state of the **BC** diatom. R_1^0 is the initial center of the Gaussian wavepacket in the translational degree of freedom.

Reactant channel packets is constructed from plane waves with negative momentum only, while product channel packets will be constructed from plane waves with positive momentum. The probability for a reaction of this type described by Eq. (A.3) is

$$P_{\nu'\nu}(E) = |S_{+k_2\ -k_1}^{2,\nu';\ 1,\nu}| \tag{A.5}$$

where we have assumed that the reactants are entering from channel 1 and the products are exiting from channel 2. ν and ν' are quantum numbers for vibrational mode

of BC and AB separately. For a given total energy E, we need to calculate the plane wave expansion coefficients $\eta(\pm k_i)$ $(i = 1, 2)$, where i labels the channel and

$$k_i(E) = \sqrt{\frac{2\mu_i}{\hbar^2}(E - E_{\nu,i)}}, \tag{A.6}$$

where $E_{\nu,i}$ is the vibrational energy of the i-th channel packet and μ_i is the translational reduced mass in i-th channel.

$$\mu_1 = \frac{(m_A + m_B)m_C}{m_A + m_B + m_C}, \tag{A.7}$$

$$\mu_2 = \frac{m_A(m_B + m_C)}{m_A + m_B + m_C}. \tag{A.8}$$

A.2 Angular momentum

If the reaction is not collinear, the new Jacobi coordinates will be (R, r, θ), where θ is the angle between R and r. The Hamiltonian in (R, r, θ) for a given $\boldsymbol{J}$ and $j = 0$ in body-fixed frame is given by

$$\hat{\boldsymbol{H}} = -\frac{\hbar^2\partial^2}{2\mu_R\partial R^2} - \frac{\hbar^2\partial^2}{2\mu_r\partial r^2} + \frac{(\boldsymbol{J} - \boldsymbol{j})^2}{2\mu_R R^2} + \frac{\boldsymbol{j}^2}{2\mu_r r^2} + V(R, r, \theta) \tag{A.9}$$

where μ_R is the reduced mass of A with respect to BC and μ_r is the reduced mass of BC. J is the total angular momentum and j labels the initial rotational state of BC. $V(R, r, \theta)$ is the potential energy of the system. The initial wave packet is then chose as the product of of a Gaussian wave packet, $G_{k_0}(R)$, representing the translational motion of A with respect to BC, ground ro-vibrational $(\nu = 0, j = 0)$ eigenfunction $\phi_{\nu j}(r)$ for the diatom and a normalized associated Legendre polynomial $\tilde{P}_{jK}(cos\ \theta)$.

$$\Psi(R, r, \theta, t = 0) = G_{k_0}(R)\phi_{\nu j}(r)\tilde{P}_{jK}(cos\ \theta) \tag{A.10}$$

The normalized associated Legendre polynomials

$$\tilde{P}_{jK}(\cos(\theta)) = \sqrt{\frac{(2j + 1)(j - K)!}{2(j + K)!}}P_{jK}(cos\ \theta) \tag{A.11}$$

are eigenfunctions of the $\boldsymbol{j}^2$ operator with eigenvalues $j(j + 1)\hbar^2$.

Appendix B

Quantum trajectory in imaginary time

The imaginary time quantum dynamics is implemented in Cartesian coordinate using the momentum-dependent quantum potential approach. Implementation in Cartesian coordinates is important because it allows one to work with the Hamiltonian of the simplest form, to setup calculations in the molecular dynamics-compatible framework and to naturally mix quantum and classical description of particles. A nodeless wavefunction, represented in terms of quantum trajectories, is evolved in imaginary time according to in the Eulerian frame of reference. The quantum potential and its gradient are determined approximately from low order (quadratic) polynomial fit to the trajectory momenta, which makes the approach practical in high dimensions.

B.1 Formalism

The Boltzmann evolution of a wavefunction according to the diffusion equation with the Hamiltonian $\hat{H}$,

$$\hat{H}\psi(\boldsymbol{x},\tau) = -\hbar\frac{\partial}{\partial\tau}\psi(\boldsymbol{x},\tau), \quad \tau > 0 \tag{B.1}$$

is equivalent to Schrödinger equation with the real time variable t replaced by $-\imath\tau$.

This transformation, the so-called Wick rotation [**?**], is widely used staring with the path integral formulation of statistical mechanics and including , for example, recent Gaussian-based methods.

As $\tau \to \infty$, any initial wavefunction, not orthogonal with ground state wavefunction, propagated in time according to Eq. (B.1) will evolve to the lowest energy eigenfunction, since the lowest energy component is the slowest to decay. In other

words, the wavefunction energy E will converge to the ground-state energy, E_0,

$$E(\tau) = \frac{\langle\psi(\tau)|\hat{H}|\psi(\tau)\rangle}{\langle\psi(\tau)|\psi(\tau)\rangle}, \quad \lim_{\tau\to\infty} E(\tau) = E_0. \tag{B.2}$$

The imaginary time evolution can be viewed as "cooling" of a system to the temperature T, where $k_BT = 1/\beta = \hbar/\tau$, k_B is the Bolzman constant.

To obtain the classical-like equations of motion, we express a positive wavefunction via a single exponential function,

$$\psi(\boldsymbol{x},\tau) = \exp\left(-\frac{S(\boldsymbol{x},\tau)}{\hbar}\right).$$

Substituting this form of wavefunction into Eq. (**??**) gives the equivalent of Hamilton-Jabobi equation,

$$\frac{\partial S(\boldsymbol{x},\tau)}{\partial\tau} = -\frac{1}{2}\boldsymbol{\nabla}^T S\mathbf{M}^{-1}\boldsymbol{\nabla}S + V + \frac{\hbar}{2}\boldsymbol{\nabla}\mathbf{M}^{-1}\boldsymbol{\nabla}S. \tag{B.3}$$

Defining the momentum as $\boldsymbol{p}(\boldsymbol{x},\tau) = \boldsymbol{\nabla}S(\boldsymbol{x},\tau)$, the last term in Eq. (B.3) is interpreted as the momentum-dependent quantum potential (MDQP),

$$U(x,\tau) = \frac{\hbar}{2}\boldsymbol{\nabla}^T\mathbf{M}^{-1}\boldsymbol{p},$$

responsible for all QM effects. It is non-local and influences the dynamics on equal footing with the external classical potential V. As a consequence, trajectories leave the region of low potential energy causing under-sampling of the ground state wavefunction at long times in high-dimensional ground-state calculations. Thus, we consider the Eulerian frame of reference where the initial trajectory positions are stationary random grid points.

The trajectory momentum function at fixed $\boldsymbol{x}$ evolves according to the gradient of Eq. (B.3),

$$\frac{\partial p_\mu}{\partial\tau} = -v^\alpha\nabla_\alpha p_\mu + \nabla_\mu(V+U), \quad v_\alpha = \frac{p_\alpha}{m_\alpha}$$

For practical multidimensional implementation, the first and second derivatives of $\boldsymbol{p}$ are computed approximately from the global Least-Squares Fit in Taylor basis f,

$$f = (1, x_1, x_2, \cdots, x_1^2, x_2^2, \cdots)$$

The fitting coefficients C minimize the difference between the exact momenta and its fit $\tilde{\boldsymbol{p}}$, $p_\mu = \sum_{k=1}^{N_b} f_k C_{k\mu}$,

$$I = \langle \sum_{\mu} (p_\mu - \tilde{p_\mu})^2 \rangle \,, \ \nabla_{\boldsymbol{C}} I = 0. \tag{B.4}$$

The optimal values are obtained by solving a matrix equation,

$$\mathbf{MC} = \mathbf{B}, \tag{B.5}$$

where

$$M_{ij} = \langle f_i | f_j \rangle \,, \ B_{k\mu} = \langle p_\mu | f_k \rangle \tag{B.6}$$

The energy is evaluated over the trajectory ensemble,

$$E = \sum_i E(x_\tau, p_\tau) e^{-2S_\tau^i/\hbar} \delta x^i. \tag{B.7}$$

Superscript i labels the trajectory-based quantity. The weight, $\delta x^{(i)}$, accounts for the contribution of the ith trajectory to the integration and does not change with time.